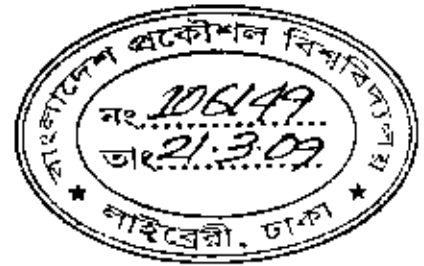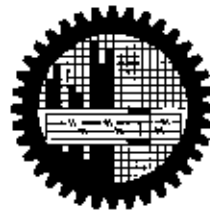# MEASUREMENT OF AIR KERMA USING DIFFERENT TYPES OF

IONIZATION CHAMBERS

by

Afia Begum
DOCTOR OF PHILOSOPHY
Department of Physics

BANGLADESH UNIVERSITY OF ENGINEERING & TECHNOLOGY
Dhaka, Bangladesh
2009

BANGLADESH UNIVERSITY OF ENGINEERING & TECHNOLOGY
DEPARTMENT OF PHYSICS

CERTIFICATION OF THESIS

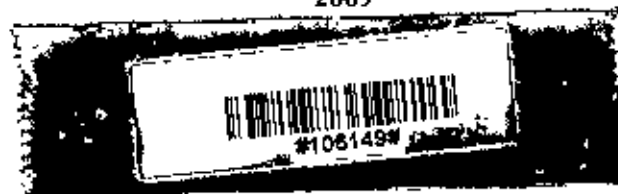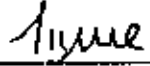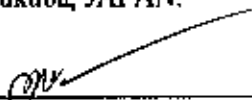The thesis titled "**MEASUREMENT OF AIR KERMA USING DIFFERENT TYPES OF IONIZATION CHAMBERS**" submitted by **AFIA BEGUM**, Roll No: P04021402P, Registration No: 93698, Session: April/2002, has been accepted as satisfactory in partial fulfillment of the requirement for the degree of **DOCTOR OF PHILOSOPHY (Ph.D.)** in Physics on 2 February, 2009

BOARD OF EXAMINERS

1. _____   Chairman
   Dr. Mominul Huq (Supervisor)
   Professor,
   Department of Physics, BUET, Dhaka.

2. _____   Member
   Dr. Nobuhisa Takata (Co-Supervisor)
   Senior Researcher, Ionizing Radiation Division, NMIJ,
   National Institute of Advanced Industrial Science & Technology,
   Tsukuba, JAPAN.

3. _____   Member
   Head,
   Department of Physics, BUET, Dhaka.

4. _____   Member
   Prof. Gias uddin Ahmad
   Vice-Chancellor, Prime Asia University, Banani, Dhaka.

5. _____   Member
   Dr. Syed Reza Husain
   Chief Medical Physicist, Delta Medical Centre Ltd.
   26/2 Darus Salam Road, Mirpur, Dhaka.

6. _____   Member
   Dr. M. A. Taher Ali
   Professor,
   Department of Mechanical Engineering, BUET, Dhaka.

7. _____   Member
   Dr. Mir Md. Akramuzzaman
   Professor,
   Department of Physics, Jahangirnagar University, Savar, Dhaka.

8. _____   Member (External)
   Dr. Badrul Alam
   Professor,
   Department of Physics, Dhaka University, Dhaka.

CANDIDATE'S DECLARATION

It is hereby declared that this thesis or any part of it has not been submitted elsewhere for the award of any degree or diploma.

Signature of the Candidate

Afia Begum

Afia Begum

Acknowledgements

A journey is easier when you travel together. Interdependence is certainly more valuable than independence. In course of preparation of this thesis, I have become obliged to a large number of wonderfully supportive individuals, only a few of whom can be mentioned here.

The first person I convey my gratitude to my supervisor Dr. Mominul Huq, Professor, Department of Physics, Bangladesh University of Engineering & Technology (BUET), Dhaka. Throughout my research. his knowledge and his logical way of thinking, detailed suggestions and stimulating support have provided a good basis for the present thesis. Not only a great mentor, my best counselor and colleague, he has also been a cornerstone in my professional development.

I would like to express my profound sense of gratitude to my co-supervisor, Dr. Nobuhisa Takata, Senior Researcher, Ionizing Radiation Section, Quantum Radiation Division, National Metrology Institute of Japan, National Institute of Advanced Industrial Science and Technology (AIST), Tsukuba, Japan whose abundant help, constructive comments, good teaching, helped me in all the time. I am obliged to his scholastic and indispensable guidance, continued support and invaluable contribution to this research work without which this work would not have been completed. His good company gave me the feeling of being at home at work. He has set a role model of a typical Japanese teacher who cares their students. I would have been lost without him.

I warmly thank Dr. Tadahiro Kurosawa, Senior Researcher, Ionizing Radiation Section, National Metrology Institute of Japan at AIST, who extended his hand in giving me a brief discussion about the Monte Carlo calculations and explain it clearly and simply. His help gave me the strength to preserve under difficult circumstances.

I am deeply indebted and grateful to Dr. Mir Md. Akramuzzaman, Professor, Department of Physics, Jahangirnagar University, for the support and encouragement provided me to complete this thesis. His lots of good ideas and tips around my work gave me a sense of direction and helped me a lot in staying at the right track.

I would like to convey my heartfelt gratitude to Dr. Abdus Sanar Mollah, Director, Nuclear Safeguard & Security Division, Bangladesh Atomic Energy Commission, from whom I was first informed about the "MEXT-The Nuclear Researchers Exchange Program", whose inspiration, sound advice, many valuable suggestions and encouragement to overcome the difficult situations during the period of my research work.

I am grateful to the concerned authority of Nuclear Safety Research Association, International Affairs and Research Department, Japan for selecting me as a fellow in the "MEXT- The Nuclear Researchers Exchange Program".

Abstract

Eight parallel-plate (pancake) and spherical ionization chambers of various volumes have been designed and fabricated at the Primary Standard Dosimetry Laboratory (PSDL), National Institute of Advanced Industrial Science and Technology (AIST), Tsukuba, Japan. These chambers are made of Poco graphite of density 1.82 g cm^{-3} and can be used for the absolute air kerma rate measurement in ^{60}Co and ^{137}Cs γ-ray fields. The air kerma rate in the γ-ray fields is obtained by measuring the signal current from the ionization chamber.

Ionization volume of each of the fabricated ionization chambers is determined using the dimensions of various parts of the chamber, the signal current measured from the chamber and that from the stem part of the chamber. Values of recombination parameters A and m^2g are obtained using a method proposed by De Almeida and Niatel and adopted by Boutillon. From the measurement it is observed that the values of recombination parameters for pancake ionization chamber are smaller than spherical ionization chambers. Using the values of A and m^2g for each of the ionization chamber, ion losses within the ionization chamber are obtained. The correction factors for the contribution of γ-rays scattered by the ionization chamber stem is determined using a dummy stem of identical size and composition placed on the side opposite to the original chamber stem. The stem scattering effect is found to be larger for smaller volume ionization chambers. Wall correction factor, k_{wall} of each of the fabricated ionization chamber is determined by Monte Carlo calculation using the EGS5 program. k_{wall} is relatively small for pancake chambers and it is close to unity. The mean mass collision stopping power ratios of graphite and air for the fabricated ionization chambers at ^{137}Cs and ^{60}Co γ-ray beam energies is also calculated using the EGS5 program. The value of $\bar{s}_{gra}/\bar{s}_{air}$ is found to depend on the cutoff energy of electrons in the calculation and also on the incident photon energy. The value of $\bar{s}_{gra}/\bar{s}_{air}$ obtained in electronic equilibrium condition for spherical chambers is used for all types of ionization chambers. Angle dependence sensitivity of each of the fabricated ionization chambers is also measured at various source-chamber distances (SCDs) in ^{137}Cs and ^{60}Co γ-ray fields. The sensitivity of these fabricated spherical ionization chambers in the present study is almost isotropic but that for parallel plate ionization chambers depends upon the angular position of the chamber with respect to the beam direction.

Two different size cylindrical ionization chambers of AIST are being used as the national standard devices for air kerma measurement, i.e. they are using for calibration of secondary standard ionization chambers and field type ionization chambers using for different radiotherapy machine output calibration and radiation protection purposes in Japan. In the present study, the air kerma rates at various SCDs in the ^{60}Co and ^{137}Cs γ-ray fields are determined by the fabricated ionization chambers. For a given SCD, the air kerma rate value measured by a fabricated ionization chamber is compared with that obtained by the cylindrical ionization chambers. It is noticed from the measurement that all the air kerma rate values obtained by the spherical ionization chambers S7A, S60A, S60B and S900A are

slightly smaller than those obtained by P9A, P9B, P60A and P60B and the relative expanded uncertainties (in % and the coverage factor $k=2$) in the air kerma rate measurement obtained by all of the fabricated ionization chambers are smaller than those by the cylindrical ionization chambers.

The E_n number which is usually used for comparison and the proficiency testing of calibration abilities of each of the fabricated ionization chambers and is obtained by choosing the air kerma rate measured by cylindrical chambers are used as the reference values. In the present study, the value of E_n number is smaller than 1 at all positions of the fabricated ionization chambers except for the air kerma rate at SCD=4 m in ^{137}Cs γ-ray field measured by S60A and P60A Ionization Chambers.

In this work a suggestion has also been given in favour of a new correction factor for the charge of photoelectrons, Compton electrons, and Auger electrons, which are included in the signal charge from an ionization chamber and are more significant for lower energy photons. Besides this, it is indicated that the definition of exposure should be made clear whether exposure includes or does not include the charge of these electrons.

Contents

Chapter V: Results and Discussion

Chapter VI: Conclusions

Published Papers

List of Figures

List of Tables

List of Symbols

Absorbed dose	D
Air Kerma	K
Atomic number	Z
Average energy spent by an electron to produce an ion pair in dry air	W
Charge-collection efficiency of an ionization chamber	f
Correction factor for change of the amount of ionization charge (or current) due to humidity	k_h
Correction factor for the contribution of γ-rays scattered by the ionization chamber stem	k_{stem}
Correction factor for the electric charge loss due to recombination and diffusion	k_{loss}
Correction factor for the non-uniformity of the γ-ray field	k_{nu}
Correction factor for wall induced attenuation and scatter of γ-rays	k_{wall}
Exposure	X
Fraction of secondary electron energy lost due to Bremsstrahlung in air	g
Initial recombination loss and diffusion loss parameter	A
Mass energy absorption coefficient for the γ-ray	$\dfrac{\mu_{en}}{\rho}$
Mean mass collision stopping power for secondary electrons	$\bar{s}$
Mass of air in the ionization volume	m
Pressure	P
Signal current from the cavity ionization chamber	I
Temperature	T
Volume recombination parameter (m and g are used for other quantities mentioned above)	m^2g

Chapter I

General Introduction

Chapter I

General Introduction

1.1 Introduction to Ionizing Radiation

The use of ionizing radiation started with the discovery of x-rays by Wilhelm Roentgen, of radioactivity by Henri Becquerel and of radium by the Curies in the 1890s. Within a very short time, both x-rays and radium became useful tools in the practice of medicine. Ionizing radiations are those, which can ionize matter. Ionizing radiations are generally characterized by their ability to excite and ionize atoms of matter with which they interact. Since the energy required to cause a valence electron to escape from an atom is of the order of 4–25 eV; radiation must carry kinetic or quantum energy in excess of this magnitude.

According to ICRU 1971 [1] (International Commission on Radiation Units and Measurements), ionizing radiation is classified as

(i) *Directly Ionizing Radiation*

Fast charged particles, which deliver their energy to matter directly through many small Coulomb-force interactions along the particle's track and produce ionization; and

(ii) *Indirectly Ionizing Radiation*

x- or γ-ray photons or neutrons (i.e., uncharged particles), which first transfer their energy to charged particles in the matter through which they pass. The resulting fast charged particles then in turn deliver their energy to the matter by Coulomb-force interaction. Thus, deposition of energy in matter by indirectly ionizing radiation is two-step process.

When an x- or γ- ray beam passes through a medium, interaction between photons and matter take place; and the energy is transferred to the medium. Ionizing photons interact with the atoms of a material or absorber and produce high-speed electrons by

three major processes: photoelectric effect, Compton effect and pair production. The relative importance of photoelectric effect, Compton effect and pair production depend on both the photon quantum energy and the atomic number Z of the absorbing medium. The photoelectric effect is dominant at the lower photon energies; the Compton effect takes over at medium energies and pair production at the higher energies. For low Z media (e.g. carbon, air, water, and human tissue) the region of Compton effect dominance is very broad, extending from 20 keV to 30 MeV. This gradually narrows with increasing Z.

Three non-stochastic quantities are useful to describe the interactions of the radiation with matter. These quantities are:

(i)   the *kerma K*, which describes the first step of energy dissipation by indirectly ionizing radiation, i.e. energy transferred to charged particles;

(ii) the *absorbed dose D*, that describes the energy imparted to matter by all kinds of ionizing radiation but delivered by the charged particles; and

(iii) the *exposure X*, which describes the ability to ionize air by x- and γ- ray.

The determination of the energy deposition in matter by the radiation is referred to as "radiation dosimetry". Radiation dosimetry deals with the measurement of absorbed dose or dose rate resulting from the interaction of ionizing radiation with matter. It refers to the determination (i.e., by measurement or calculation) of these quantities, as well as any of the other radiological relevant quantities such as exposure, kerma, fluence, dose equivalent, energy imparted and so on. One often measures one quantity (usually the absorbed dose) and derives another from it through calculations based on the standard relationships.

Dosimetry (including the field of medical dosimetry) can be classified into two categories – "in-air measurements" (or measurements under receptor free conditions) and "in-phantom measurements". Kerma is a suitable quantity for in-air measurements while for in-phantom measurements absorbed dose is the appropriate quantity. Kerma is relevant only for fields of indirectly ionizing radiations (photons or neutrons). For indirectly ionizing radiation, the first step of energy deposition in

matter is concerned with the energy dissipation by the indirect ionizing radiation . (e.g. photons), that is, energy transferred to the charged particles (i.e. electrons). The released energy by photons is called kerma (*kinetic energy released in the medium*). This is also referred as the "first collision dose". According to ICRU 1980 [2] the quantity kerma (*K*) at a point of interest in volume *V* is defined as the sum of the initial kinetic energies of all the secondary electrons emitted by photons per unit mass of a material at a point of interest,

$$K = \frac{dE_{tr}}{dm}$$

Where, dE_{tr} is the sum of the initial kinetic energy of all the charged ionizing particles (electrons and positrons) liberated by the indirectly ionizing particles (photon) in a material of mass dm. The subscript "*tr*" denotes the energy transferred from the photons to the charged particles. The statement of kerma is incomplete without a reference of the material concerned. The SI unit for kerma is the same as dose, i.e., J/kg. The unit has a specific name gray and its symbol is Gy. The relationship between kerma and absorbed dose is more subtle. The energy transfer of kerma takes place at a point, but the subsequent imparting of energy to matter which gives rise to the absorbed dose is spread over distances determined by the range of the charged particles. The mechanism of transfer of energy from a photon to the medium is shown in Fig. 1.1.
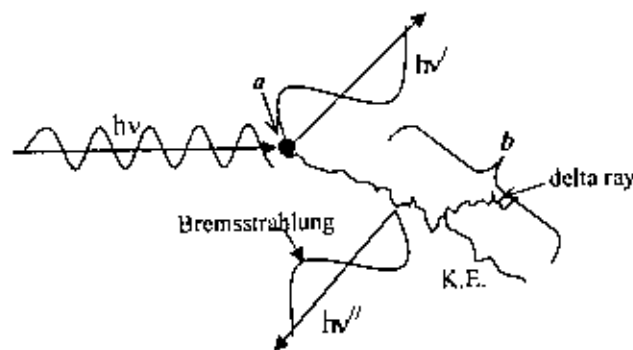
Fig. 1.1 Schematic diagram of the transfer of energy from a photon to the medium

3

According to Fig. 1.1 photon of energy $h\nu$ interacts at 'a', transferring some of the energy to an electron giving it kinetic energy (K.E.) This electron in turn gives up its energy mostly in small collisions along its track 'b'. The transfer of energy at 'a' is called kerma, and along 'b' is called absorbed dose. The photon $h\nu'$ is scattered from 'a' by Compton effect. The photon $h\nu''$ is Bremsstrahlung resulting from a collision between the electron and a nucleus. The delta ray is another electron track resulting from a relatively violent electron-electron collision. The energy absorbed, which corresponds to absorbed dose, equals the kerma less the energy carried away by Bremsstrahlung. Kerma occurs at a point, while absorbed dose occurs further down stream over a range equal to the range of the electron.

So, when a photon interacts with the electrons in the material, a part or all of its energy is converted into kinetic energy of electrons. If only a part of the photon energy is given to electrons, the photon itself is scattered with reduced energy. The scattered photon may interact again with a partial or complete transfer of energy to the electrons. Thus, a photon may experience one or multiple interactions in which the energy lost by the photon is converted into kinetic energy of electrons.

In the first step of photon interaction, when a photon traverses a material the fraction of photon energy is transferred into kinetic energy of electrons per unit thickness of absorber is given by the *energy transfer coefficient* (μ_{tr}). This coefficient is related to attenuation coefficient (μ):

$$\mu_{tr} = \frac{\overline{E}_{tr}}{h\nu}\mu \qquad\qquad (1.1)$$

where, $\overline{E}_{tr}$ is the average energy transferred into kinetic energy of electrons per interaction. Unit of energy transfer coefficient is cm^{-1}. (μ_{tr}/ρ) is the *mass energy transfer coefficient*.

In the second step of photon interaction, the kinetic energy of fast electrons may be spent in two ways:

i) Coulomb-force interaction with atomic electrons of the absorbing material, resulting in the local dissipation of the energy as ionization and excitation in or near the electron track. These are called collision interaction.

ii) Radiative interaction with the Coulomb force field of atomic nuclei, in which x-ray photons (Bremsstrahlung or "braking radiation") are emitted as the electron decelerates. These x-ray photons are relatively penetrating compared to electrons and they carry their quantum energy far away from the charged particle track.

Most of the electrons set in motion by the photons will lose their energy by inelastic collisions (ionization and excitation) with atomic electrons of the material. A few, depending on the atomic number of the material, will lose energy by Bremsstrahlung interactions with the nuclei.

Since the kerma (K) includes kinetic energy received by the electrons whether it is destined to be spent by the collision with the electrons or radiative-type interactions, so K can be subdivided into two parts according to whether the energy is spent in creating excitation and ionization (K_c) or is carried away by photons (K_r):

$$K = K_c + K_r \qquad (1.2)$$

where the subscripts c and r refer to 'collision' and 'radiative' interactions respectively. Therefore, all the photon energy transferred to kinetic energy of electrons will not be absorbed by the irradiated material. A fraction g of the electron energy is converted to photon energy (Bremsstrahlung). The Bremsstrahlung energy is radiated out of the local volume as x-rays and is not included in the calculation of locally absorbed energy. The coefficient used to derive the energy actually absorbed per unit mass in an irradiated material is the mass energy absorption coefficient (μ_{en}/ρ) and is given by

$$\frac{\mu_{en}}{\rho} = \frac{\mu_{tr}}{\rho}(1-g) \qquad (1.3)$$

For most interactions involving soft tissues or other low Z material, electrons lose energy almost entirely by ionization collisions with the Bremsstrahlung component negligible. So under these conditions, $\mu_{en} = \mu_{tr}$. These two coefficients differ appreciably when the kinetic energies of the secondary particles are high and material traversed has a high atomic number.

Exposure is the ionization equivalent to the collision kerma in-air. The exposure, X, according to ICRU 1998 [3] is defined as the quotient of dQ by dm, where dQ is the absolute value of the total charge of the ions of one sign produced in air by the secondary electrons when all electrons liberated by photons in air of mass dm are completely stopped in air. Thus,

$$X = \frac{dQ}{dm} \tag{1.4}$$

In Bangladesh, ionizing radiations are being widely used in the field of medicine, industry, research and education and guiding an important role in bringing significant social and economical benefits to mankind. When ionizing radiations are used in medicine, it is important to measure the amount of radiation delivered and to keep it within the limit. In diagnostic procedures (x-ray examinations, nuclear medicine, CT scan, PET etc) the measurement is both for the optimization of image quality and for radiation protection purposes. However, the need of accurate dosimetry is greatest in radiation therapy for cancer treatment. In radiotherapy, a large amount of radiation dose (typically 10 times the dose that would kill a person receiving this dose to his entire body) is delivered to the tumour. Modern radiotherapy relies on an accurate dose delivery to the prescribed target volume. The International Commission on Radiation Units and Measurements (ICRU) has recommended an overall accuracy in tumour dose delivery of ±5% based on an analysis of dose response data and on the evaluation of errors in dose delivery in a clinical setting. Concerning all uncertainties involved in the dose delivery to the patient, 5% accuracy recommendation is by no means easy to attain. Practical clinical dosimetry today is based on the absorbed dose quantity, and accurate measurement of absorbed dose represents one of the major responsibilities of clinical medical physicist. In order to measure the absorbed dose

in a medium, it is necessary to introduce a radiation sensitive device (dosimeter) into that medium. Generally, the sensitive medium of the dosimeter is not the same material as the medium in which it is embedded. Although there are a variety of solid-state and chemical methods for measuring radiation dose, but ionization dosimetry is the most widely used, most convenient and most accurate method for measuring either exposure or absorbed dose. This method is employed more often than any other dosimetric system because of its sensitivity and the ease of quantitative measurement compared to other methods of dosimetry.

Ionization chambers are employed as absolute or as relative dosimeters. A dosimeter that produces signal, from which the dose in its sensitive volume can be determined without requiring calibration in a known radiation field is referred to as an absolute dosimeter. Three types of ionization chambers are used as absolute dosimeters:

    (i)   Standard free air ionization chamber;

    (ii) Phantom-embedded extrapolation chamber; and

    (iii) Cavity ionization chamber

Standard free air ionization chamber measures the air-kerma in air according to its definition by collecting all ions produced by the radiation beam that results from the direct transfer of energy from photon to primary electrons in a defined volume of air. It is used as the air-kerma primary standard for photon with energy up to about 300 keV [4] and cannot function as a primary standard for ^{60}Co or ^{137}Cs beams, since the air column surrounding the sensitive volume (for establishing the electronic equilibrium condition in air) would become very long. This would make the chamber very bulky and the various required corrections and their uncertainties would become problematic.

Phantom-embedded extrapolation chamber is a variable air-volume extrapolation chamber, which is an integral part of a water-equivalent phantom in which the dose is measured. It can serve as radiation dosimeter in the measurement of absorbed dose for megavoltage photon and electron beams. Standard dosimetry protocols provide a simple linear relationship between the dose at a given point in the medium and the

ratio Q/m; where Q is the ionization charge collected in the mass of air m in the measuring cavity inside the medium. The conversion of cavity dose to the dose in the medium is based on the cavity theory.

Cavity ionization chamber measures air-kerma in the energy range from 300 keV to 3 MeV. The primary standard laboratories use the cavity ionization chamber of accurately known volume for calibration of their standard ^{60}Co and ^{137}Cs γ-ray beams. A cavity ionization chamber consists of a sensitive volume V, of radius r containing medium g, which is usually the ambient air surrounded by a wall of another medium w having a thickness t, as shown in Fig. 1.2. Therefore, a cavity ionization chamber has a cavity and its surroundings. For point-by-point measurement of the absorbed dose due to x or γ-radiation, the small-cavity ionization chamber is the chosen instrument and its reading is interpreted by Bragg-Gray cavity theory or its later refinements. This theory imposes limit on the dimension of the cavity and on the materials used in constructing the chamber wall. The cavity ionization chambers are constructed from highly pure graphite and require good insulator materials in order to minimize the leakage and polarization effects and to provide an acceptable long-term stability.
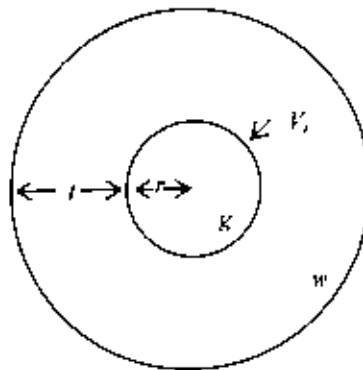
Fig. 1.2 Schematic representation of a cavity ionization chamber

The air kerma in ^{60}Co and ^{137}Cs γ-ray fields are usually measured using thick walled graphite cavity ionization chambers. Graphite walls are used at these energies to

approximate air equivalence, so that calibration can be expressed in terms of exposure rate or air kerma rate. Analogously to the free air chamber ions are collected in air, but this time inside a cavity with a known cavity volume surrounded by a graphite wall thick enough to provide full build-up of secondary electrons (charge particle equilibrium). The Bragg-Gray cavity theory relates the dose-to-air in the cavity of known volume to the dose-to-medium in which the secondary electron spectrum is being built up, i.e., in the chamber wall. The absorbed dose to the wall is related to the collision air-kerma in air through the mass energy absorption coefficient ratio of wall and air. The collision air kerma in air is related to the total air-kerma in air by correcting for the fractional energy expended in radiative interactions. In addition to the need for accurate knowledge of the sensitive air volume, knowledge on wall correction factor is required to account for the effect of photon attenuation and scattering in the chamber wall. So, in order to determine the air-kerma in air an accurate knowledge of (W/e) as well as the cavity volume and Bremsstrahlung fraction is required; where W is the average energy spent by an electron to produce an ion pair in dry air. Finally, Standard Laboratories implement additional correction factors, such as point source non-uniformity correction factor and factors that account for deviations from the Bragg-Gray cavity theory. Absolute ion chamber is, however, not usually practicable outside the National Primary Standard Laboratories.

Dosimeters requiring calibration in a known radiation field are called relative dosimeters. Ionization chambers are commercially available in a variety of designs for different applications and may be constructed in a machine shop when special designs are required. These ionization chambers are not constructed with exactly known effective volume. Hence, they require calibration and calibration of the chamber must be traceable to a standard laboratory. Since the range of application of the ionization chamber in the field of medical physics is so widespread and the requirements are so varied that a single ionization chamber would not be able to cover the whole range of application. Therefore, a chamber cannot be made energy independent over the full range of interest in medical dosimetry. Moreover, using ionization chambers of different types and sizes, the full range of application in medical field (from radiation protection survey measurements to radiotherapy

dosimetric measurements) can be covered by ionization dosimetry [5]. The highest dosimetric accuracy can be obtained in medical dosimetry using calibrated ionization chambers of good stability and a sensitive electrometer. The ionization chambers used in medical dosimetry have been carefully designed to make the various perturbations quite negligible. However, these chambers have been constructed empirically with composite wall materials (and sometimes with different materials for the wall and the central electrode) to have an energy independent response over a certain energy range. The choice of chamber materials, its dimensions and the form of cavity depend on the purpose the chamber has to serve; for example- whether it is intended to measure exposure or absorbed dose as well as the type of radiation to be measured, its intensity and its rate of change in space and time.

The success of radiation therapy depends upon the accuracy with which a dose prescription is fulfilled. Information for treatment planning, including data on depth doses and dose distribution, as supplied by the equipment manufacturer should not be used clinically without independent confirmation of the actual values [6]. Before clinical use, the output of photon and electron beams produced by external beam radiotherapy machines must be calibrated. For practical reasons, outputs of clinical photon and electron beams are usually measured with ionization chambers that have calibration coefficients (factors) either determined in air or in water traceable to a standard laboratory and are thus used as relative dosimeters. Accuracy and reliability in radiation dosimetry depends on the proper calibration and standardization of the dosimetry system and the calibration and standardization play a key role in the ultimate evaluation of radiation doses for the treatment of cancer patients. The traceability of a calibration factor to a national Primary Standard Dosimetry Laboratory (PSDL) implies that:

(i) The chamber is calibrated directly at the PSDL in terms of the air-kerma in air or absorbed dose to water; or

(ii) The chamber is calibrated directly at Secondary Standards Dosimetry Laboratory (SSDL) that traces their calibration to a PSDL; or

(iii) The chamber calibration coefficient is obtained through a cross-calibration with another ionization chamber (user's secondary standard), the calibration coefficient of which is measured directly at a PSDL or SSDL.

Before a relative dosimeter is used in radiotherapy machine output calibration, the user must identify a dosimetry protocol (code of practice) appropriate for the given radiation beam. The choice of which protocol to use is largely left to individual radiotherapy departments. A dosimetry protocol provides the formalism and the data to relate a calibration of a chamber at a standard laboratory to the measurement of absorbed dose to water under reference conditions in the clinical beam. Dosimetry protocols are issued by national or regional organizations, such as AAPM (North America), IPEMB (UK), DIN (Germany), NCS (The Netherlands and Belgium) and NACP (Scandinavia) or by international bodies such as the IAEA. This procedure ensures a high level of consistency in dose determination among different radiotherapy clinics in a given country; also between one country and another. Two types of dosimetry protocols are available:

i) Protocols based on air-kerma in air calibration coefficients and

ii) Protocols based on absorbed dose-to-water calibration coefficients.

Most current megavoltage dosimetry protocols rely on chamber calibration coefficients determined in the ^{60}Co beams at standard laboratories. Conceptually, both types of protocols are similar and based on several steps in the process of determining absorbed dose or dose rate from the charge or current measurement respectively, by an ionization chamber. The air kerma based protocol use the air-kerma in air calibration factor obtained for a local reference ionization chamber in a ^{60}Co beam at a standard laboratory. Routine ionization chambers are then cross-calibrated with the reference ionization chamber in a local ^{60}Co beam.

Generally, the air kerma in ^{60}Co or ^{137}Cs γ-ray field is obtained by measuring the ionization charge produce in the graphite-walled cavity ionization chamber. According to the Bragg Gray cavity theory, exposure

$$X = \frac{Q}{m} \frac{\bar{S}_{gra}}{\bar{S}_{air}} \frac{(\mu_{en}/\rho)_{air}}{(\mu_{en}/\rho)_{gra}} \prod k_j \qquad (1.5)$$

where Q is the signal charge from the cavity ionization chamber, m is the mass of air in the cavity of the ionization chamber. The ionization chambers are unsealed and thus allowed to communicate with the outside atmosphere. The density or mass of air in the chamber volume will depend on the atmospheric conditions. The density or mass of air in the chamber volume will increase as the temperature decreases or pressure increases and m is obtained from the relation

$$m = \rho_0 V_t \frac{273.15}{(273.15+T)} \frac{P}{101.325} \qquad (1.6)$$

Here, ρ_0 is the density of dry air at 0°C (273.15 K) and 1 atmosphere (101.325 kPa), V_t is the sensitive volume of the chamber in which ionization charge is produced, T and P are the temperature and pressure respectively at the time of measurement.

$\frac{(\mu_{en}/\rho)_{air}}{(\mu_{en}/\rho)_{gra}}$ is ratio of mass energy absorption coefficient for the γ-rays in air and graphite.

$\frac{\bar{S}_{gra}}{\bar{S}_{air}}$ is the ratio of the average mass collision stopping power of graphite and air for secondary electrons which pass through the cavity.

$\prod k_j$ is the product of several correction factors for various phenomena [7], which is required for experimental perturbations such as–

k_{wall} : Correction factor for wall induced attenuation and scatter of γ-rays.

k_{loss} : Correction factor for the electric charge loss due to recombination and diffusion.

k_{stem} : Correction factor for the contribution of γ-rays scattered by the ionization chamber stem.

k_h : Correction factor for change of the amount of ionization charge (or current) due to humidity.

k_{nu}: Correction factor for the non-uniformity of the γ-ray field.

Finally, the air kerma rate $\dot{K}$ is obtained from the exposure rate, $\dot{X}$ measurement using the following relation

$$K = \dot{X}\,\frac{(W/e)}{(1-g)}$$

So,

$$\dot{K} = \frac{I}{m}\,\frac{(W/e)}{(1-g)}\,\frac{\bar{s}_{gra}}{\bar{s}_{air}}\,\frac{(\mu_{en}/\rho)_{air}}{(\mu_{en}/\rho)_{gra}}\,\prod k, \qquad (1.7)$$

where W is the average energy spent by an electron to produce an ion pair in dry air, I is the signal current from the cavity ionization chamber and g is the fraction of secondary electron energy loss due to Bremsstrahlung in air.

1.2 Scope and Objectives of the Present Study

Two different size cylindrical ionization chambers are being used as the national standard devices for air kerma measurement at the Primary Standard Dosimetry Laboratory (PSDL), National Institute of Advanced Industrial Science and Technology (AIST), Tsukuba, Japan. These ionization chambers are used for calibration of the secondary standard ionization chambers and the field type ionization chambers used for different radiotherapy machine output calibration and radiation protection purposes in Japan. The main disadvantage of these ionization chambers is that the air kerma rate in γ-ray field is measured by setting these chambers at 45° angular position against the γ-ray beam direction so that γ-ray attenuation does not increase at the end or side walls of the chamber. But it is difficult to set the chamber at 45° angular position at a correct reference position.

In the present study eight parallel-plate (pancake) and spherical ionization chambers of various volumes have been designed and fabricated at the Primary Standard Dosimetry Laboratory (PSDL), AIST, Tsukuba, Japan. Performance of each of the

13

fabricated ionization chambers would be compared with the cylindrical ionization chambers. The absolute value of the air kerma rate at a given reference position of the ^{60}Co and ^{137}Cs γ-ray field would be determined using the fabricated ionization chambers and is compared with the air kerma rate value obtained by the cylindrical ionization chambers. When the response of the fabricated ionization chambers is comparable with that of the cylindrical ionization chambers, it is possible to use the fabricated ionization chambers for air kerma rate measurement instead of cylindrical ionization chambers. In order to achieve this goal the present study has been undertaken.

Since the photon interaction, wall attenuation etc. are energy and material dependent, so a chamber response depends on the chamber design. It is necessary to correct for various factors to obtain absolute values of the air kerma in γ-ray field using these fabricated ionization chambers. A few corrections which are usually applied to obtain absolute value of air kerma include: correction for wall attenuation and scatter of γ-rays; correction for recombination of ions within the chamber; correction for the effects of temperature, pressure and humidity; correction for the contribution of γ-rays scattered by the ionization chamber stem etc. Data on these correction factors are not available for these ionization chambers. To achieve such objectives it is planned to:

- derive the ionization volume of the fabricated ionization chambers;
- measure the correction factor for volume recombination loss and correction factor for initial recombination loss and diffusion loss within the fabricated ionization chambers;
- measure the correction factor of each of the fabricated ionization chamber for the contribution of γ-rays scattered by the ionization chamber stem;
- calculate the correction factor for wall-induced attenuation and scatter of γ-rays;
- calculate the mean mass collision stopping power ratios of graphite and air for the fabricated ionization chambers at ^{137}Cs and ^{60}Co γ-ray beam energies;
- investigate the angle dependence sensitivities of the fabricated ionization chambers.

Using the measured values of these correction factors and physical parameters of the fabricated ionization chambers the absolute value of the air kerma rate in ^{60}Co and ^{137}Cs γ-ray fields at the Primary Standard Dosimetry Laboratory (PSDL) of AIST could be determined. Based on the experimental data it would be possible to develop a method for the measurement of different correction factors and physical parameters for the parallel plate (pancake) and spherical ionization chambers. It would also be possible to propose a method for the measurement of air kerma rate accurately. In addition, it could be possible to investigate the advantages and disadvantages of different types of ionization chambers.

Chapter II

Review of the Previous Works

Chapter II

Review of the Previous Works

2.1 Introduction

In order to measure the absolute air kerma rate in the γ-ray field using the fabricated ionization chamber it is necessary to determine the various correction factors and physical parameters for these chambers. Scientists all over the world measured and calculated the various correction factors by different methods for different type of ionization chambers. Some of the previous works, which are largely relevant to the present study, are reviewed in the subsequent pages.

2.2 Studied on Ion Recombination Loss

Boutillon [8] has measured volume recombination parameter m^2 in ionization chambers which gives information about the recombination coefficient α. Two parallel-plate free air ionization chambers were used for the determination of m^2, one of them in a low-energy x-ray beam and the other in a medium-energy x-ray beam under conditions, which allows strict application of the basic theory. The method consists of measuring the ratio of ionization currents I_{v_1} and I_{v_2} obtained at two given voltages V_1 and V_2 respectively and then plotting I_{v_1}/I_{v_2} as a function of I_{v_1}. The value of m^2 was derived from the linear extrapolation to zero current. Several pairs of voltages (V_1, V_2) were used in the measurement. The value of m^2 obtained was 3.97×10^{14} sm^{-1}C^{-1}V^2, with a relative uncertainty of 1.7%. The dependence of m^2 on atmospheric conditions was also investigated.

Das and Akber [9] investigated the ion recombination (P_{ion}) and polarity (k_{pol}) effect of ionization chambers in kilovoltage x-ray exposure measurements. Six

different parallel plate ionization chambers with different volume, commonly used in diagnostic radiology, were investigated for the P_{ion} and k_{pol} effects at various exposure rates by changing the tube voltage, beam current, exposure time and distance. At a time, one parameter was changed while keeping the others constant. A mammography unit (24–35 kV peak tube voltage) and a diagnostic x-ray unit (60–125 kV peak tube voltage) were used for the measurement. The volume ion recombination correction P_{ion} was measured for each chamber using two-voltage method. Results indicate that the magnitude of P_{ion} is linearly dependent on peak tube voltage for large volume (>150 cm^3) chambers and independent for small ($\leq$150 cm^3) ones. In general, P_{ion} is higher at higher exposure rate (increasing peak tube voltage, filament current and decreasing distance); however, k_{pol} is independent of exposure rate and tube voltage but strongly depends on the sensitive volume of the ion chamber. P_{ion} and k_{pol} vary between 1–48% and 1–16% respectively, among various chambers and exposure conditions. Chambers with larger volume have higher values of P_{ion} and k_{pol}.

Takata [10] measured the ion loss due to initial recombination and back diffusion at several humidity conditions in a parallel-plate cavity ionization chamber irradiated by ^{60}Co γ-rays. It was shown from the measurements that in the range of inverse electric field strengths from 0.05 to 14 mmV^{-1}, the initial recombination took place both in clusters and columns of ions produced along the path of the secondary electrons ejected by the γ-rays. The ion loss due to recombination in clusters was found to increase with humidity, but that in columns did not. Effects of ion clustering reactions on recombination may be reduced after longer periods of ion drift, when recombination in columns takes place. Ion loss due to back diffusion was also found to have no dependence on humidity.

Takata and Matiullah [11] investigated the dependence of the value of m on the life time of ions in a parallel-plate ionization chamber which has a variable space between the polarizing electrode and collector. To do so, the chamber was exposed in ^{60}Co γ-rays at several different exposure rates. The value of m was deduced from the

17

collection efficiencies which were determined at various applied voltages. m was found to depend upon the lifetime of ions in the chamber (i.e. it increases from 17.1 to 18.5 $MVA^{-1/2}m^{-1/2}$ with a decrease in the ratio of the voltage to the square of the chamber space from 0.6 to 20 kVm^{-2})

Takata [12] determined the effects of humidity on volume recombination in ionization chambers. Saturation curves were measured with a parallel-plate ionization chamber for air with humidity in the range 0%–81%. From the curves, values of m were obtained. It was confirmed that humidity is the cause for the increase of the value of m with the lifetime of ions in the ionization chamber. Additionally it was also found that the value of m increases sharply in a range of small values of the product of the ion lifetime and the partial pressure of water vapour and increases more slowly at higher values of this parameter.

Takata et al. [13] determined the loss of ions in cavity ionization chambers. Ion losses due to initial recombination, volume recombination and back diffusion are obtained by measurement and calculations for two different-size cylindrical ionization chambers and two spherical ionization chambers. Initial recombination and volume recombination were measured using a method proposed by De Almeida and Niatel and adopted by Boutillon. The diffusion loss was obtained separately by computing electric field distributions in the ionization chambers. Diffusion loss was found to be larger than initial recombination loss for the cylindrical ionization chambers and vice versa for the spherical ionization chambers.

Takata and Sakihara [14] investigated the dependence of the m value on applied voltage of ionization chamber. Values of m were measured using a free-air ionization chamber, which has two slits for double x-ray beams. By this method, one value for m is obtained from a set of data on currents at each polarization voltage. Values obtained are for a recombination region 2.65 cm wide. It was found that these values decrease from 1.93×10^6 to 1.72×10^6 $Vs^{1/2}C^{-1/2}cm^{-1/2}$ with an increase in electric field strength from 4.8 to 48 Vcm^{-1}. This means that the value of m increases with the ion age.

Piermattei et al. [15] measured the ion recombination correction factor k_{sat} for spherical ion chambers irradiated by continuous photon beams. Three spherical ion chambers with volumes ranging from 30 to 10^4 cm^3 were irradiated by photons of ^{192}Ir source to determine the k_{sat} factors. The ionization currents of the ionization chambers as a function of the applied voltage and the air kerma rate have been analyzed to determine the contribution of the initial and general ion recombination. The k_{sat} values for large volume ionization chambers obtained by considering the general ion recombination as predominant (Almond's approach) are in disagreement with the results obtained using methods that consider both initial and general ion-recombination contributions (Niatel's approach). Such disagreement can reach 0.7% when high currents are measured for a high activity source calibration in terms of reference air-kerma rate. In this study, a new 'two-voltage' method, independent of the voltage ratio given by a dosimetry system, is proposed for practical dosimetry of continuous x- and γ-ray beams. In the case where the Almond approach is utilized, the voltage ratio V_1/V_2 should be less than 2 instead of Almond's limit of $V_1/V_2 < 5$.

Takata et al. [16] investigated the decrease in output currents due to back diffusion of ions in ionization chambers. Exact and approximate equations are derived for decreases in output current due to back diffusion of ions in parallel plate, cylindrical and spherical ionization chambers. Approximate equations are obtained under the assumption that ions are lost by back diffusion if they are produced in the electrode vicinity where the electric potential difference from the electrode is less than kT/e, where k is the Boltzmann constant, T the gas temperature and e the elementary charge. Values obtained by the corresponding exact and approximate equations agreed well except at low applied voltages. It was shown that the decrease in ion current does not depend on the electrode separation of a parallel plate ionization chamber and is independent of the size of a cylindrical or spherical ionization chamber if the ratio of the inner to outer electrodes defining the ion collection volume is constant.

Niatel [17] presented an experimental study of ion recombination in parallel plate free-air ionization chambers. Two chambers of different sizes were used for this

measurement. The results may be explained by assuming that two different types of ion recombination (initial and volume recombination) take place simultaneously. Their relative values were calculated from the results and are found to agree with theories of ion recombination. It was found that for the saturation current to be determined by extrapolation method the collection field strength should be high enough. The extrapolation is the reciprocal of ionization current against the reciprocal of collecting field strength. The results are similar for both the chambers; however, as their sizes are not the same, the space charge effects might be expected to be different.

2.3 Studied on Angular Dependence and Wall Correction Factors

Takata et al. [18] investigated the angle dependence of signal currents from cylindrical ionization chambers. Two different size graphite walled ionization chambers of volume 6.02 cm^3 and 62.7 cm^3 were used in the investigation. The signal current from the larger ionization chamber peaked when it was fixed at 0° and at 90° in ^{137}Cs and ^{60}Co γ-ray fields for source-chamber distances 1 m and 2 m. The smaller ionization chamber showed a small peak at 0° in both fields but not at 90°. However, calculations indicated that the signal current from the smaller chamber would also show a peak at 90° in a ^{137}Cs point-source γ-ray field. Peaks occur because γ-rays attenuate along the cylindrical side wall or along the end walls when a chamber is tilted slightly from 0° and 90° and the direction of the γ-ray beam agrees with the plane of one of these walls. These facts suggest the need for care in the common practice of measuring and calculating responses of cylindrical ionization chambers fixed perpendicular to γ-ray beams.

Piermattei et al. [19] measured the wall correction factor for a spherical ionization chamber used in brachytherapy source calibration. For spherical ionization chambers, the corresponding wall correction factors A_w have to be determined by a non-linear trend of the response as a function of the wall thickness. The Monte Carlo and experimental data reported here showed that the A_w factors obtained for an Exradin

A4 chamber in terms of reference air kerma rate, are up to 1.2% greater than the values obtained by the linear extrapolation method for the 250 kV peak tube voltage x-ray, ^{192}Ir and [60]Co γ-ray. Using the A_w factors derived from the EGSnrc Monte Carlo code system calculations, the accuracy of the calibration factor $N_{K,t}$ for the Exradin A4 chamber, obtained by the interpolation between two calibration factor, improves about 0.6%. The discrepancy between the new calculated factor and that obtained using the complete calibration curve of the ion chamber and the ^{192}Ir spectrum is only 0.1%.

Kurosawa et al. [20] investigated the angular dependence of wall correction factor for cylindrical cavity chamber. Attenuation correction factor was measured at several irradiation angles by extrapolation technique for cavity chamber and wall correction factor was calculated for each angle by Monte Carlo calculation using EGS4 code. From the results, it has been seen that the air kerma rate obtained by extrapolation technique is dependent on angular position but the air kerma rate obtained from wall correction factors calculated by EGS4 code has a constant value for any angle.

McCaffrey et al. [21] investigated the evidence for using Monte Carlo (MC) calculated wall attenuation and scatter correction factors of graphite-walled ionization chamber. Using the linear extrapolation method with experimental data k_{wall} was determined in this study for three different styles primary-standard-grade graphite ionization chambers: cylindrical, spherical and plane-parallel. The air kerma rates by these three chambers determined using extrapolated k_{wall} values differed by maximum 2% for measurements taken with the same ^{60}Co source. The Monte Carlo code EGSnrc was used to calculate the values of k_{wall} for these three chambers. The Monte Carlo calculated values of k_{wall} are shown to be more accurate as they provide more consistent values of air-kerma rate (within 0.3%) measured with these three chambers. Further, MC calculations were sufficiently accurate to predict the subtle structure in the response curve of a rotated plane-parallel chamber. These results add confidence to the assessment of MC as the preferred method of determining k_{wall} for ionization chambers used in ^{60}Co beams.

Büermann et al. [22] determined the wall correction factor of ionization chambers for different irradiation conditions using both linear extrapolation method and EGSnrc Monte Carlo system. A series of graphite cavity ionization chambers of different shapes and sizes was chosen for the investigation: two of cylindrical types (PTB-2 and ASMW-100) and two of the pancake types (ND-1002 and HRK-3). The chambers were irradiated in ^{137}Cs and ^{60}Co reference radiation fields of the PTB from 1 m distance from the source except the ASMW-100 chamber that was irradiated from a distance of 2 m. The ionization currents of the chambers were measured as a function of wall thickness at different incident angles of radiation. This report presents both experimental and theoretical results, which strongly support the validity of calculated wall correction factors. Moreover, it is demonstrated that, in selected cases the application of a linear extrapolation method leads to errors in the determination of the air kerma reaching up to 13%.

Takata et al. [23] determined the wall correction factors of two different size graphite cylindrical ionization chambers, which were being used at AIST for air kerma measurement in ^{60}Co and ^{137}Cs γ-ray fields. Chambers were placed at a 45° angle to γ-ray beams, so that γ-ray attenuation does not increase at end or side walls of the chamber. Correction factors for wall induced attenuation and scatter were determined by measuring the variation in chamber response as a function of wall thickness in the full build-up region, extrapolating to infer the response at zero wall thickness and applying a correction factor to account for the center of electron production. Wall correction factor was also calculated by Monte Carlo calculation using EGS4 code. Differences between values of wall correction factor obtained experimentally and by calculation for AIST ionization chambers were small, compared to the relatively large differences obtained for almost all ionization chambers at other NIMs. It is possibly because only AIST ionization chambers were placed at a 45° angle to γ-ray beams and other cylindrical ionization chambers used at many NIMS are fixed perpendicularly to γ-ray beams, i.e., at 90°.

Bielajew [24] demonstrated that wall correction factors can differ by as much as 1.0% for spherical chambers depending on whether they are obtained experimentally

by extrapolation measurements or by Monte Carlo simulation. This difference was not explained by experimental or calculational statistics, which lie in the range 0.05%-0.2%. The paper also demonstrated that, linear extrapolation of experimental data for spherical chambers are inappropriate owing to the curvature of the chamber walls. A simple nonlinear theory was constructed, that resolves the difference. The Monte Carlo calculations and the nonlinear theory were compared with extrapolation measurements for the NIST spherical chambers in ^{60}Co and ^{137}Cs γ-ray fields. It was concluded that wall correction factors should be obtained by Monte Carlo calculation for spherical chambers and that linear extrapolation techniques should be regarded with suspicion for all chambers.

Rogers and Bielajew [25] compared the measured and calculated values of wall attenuation and scatter correction factors for various ion chambers. Using the EGS4 system it has been seen that Monte Carlo calculated A_{wall} (k_{att} in IAEA terminology, K_w^{-1} in standard laboratory terminology) factors predict relative variations in detector response with wall thickness, which agrees with all available experimental data within a statistical uncertainty of less than 0.1%. However, the calculated correction factors for use in exposure and air kerma standards are different by up to 1% from those obtained by extrapolating these same measurements. Using calculated correction factors would imply increase of 0.7–1.0% in the exposure and air kerma standards based on spherical and large diameter, large length cylindrical chambers and decreases by 0.3–0.5% for standards based on large diameter pancake chambers.

Ferreira et al. [26] made Monte Carlo calculations for the ionization chamber wall correction factors for ^{192}Ir and ^{60}Co γ-rays and 250 kV x-rays used in calibration of ^{192}Ir HDR brachytherapy sources. Monte Carlo calculations were performed using EGS4 code system with the PRESTA algorithm, to calculate the wall correction factor for 51 commercial ionization chambers. The calculated A_w correction factors for ^{192}Ir and ^{60}Co and 250 kV x-rays agree very well to within 0.1% with published experimental data. For the ^{192}Ir sources A_w varied 0.973–0.993 and for the 250 kV x-rays the minimum value of A_w for all chambers studied was 0.983.

Shortt et al. [27] measured the effect of wall thickness on the response of a spherical ionization chamber. They have constructed a thin-walled spherical graphite chamber along with a series of spherical shells in order to increase the wall thickness. The change in the chamber response with wall thickness has been measured in a [137]Cs γ-ray beam and the data show that the change in response is not linear with wall thickness. A linear versus non-linear extrapolation of the measured data to zero wall thickness leads to a difference of almost 1% in the estimation of the wall correction factor K_w. The value of K_w obtained using the non-linear extrapolation for the spherical chamber is in good agreement with the result obtained using Monte Carlo techniques. This result adds support to the perspective that the Monte Carlo technique is the best approach for determining the wall correction factor for an arbitrary ionization chamber.

Laitano et al. [28] determined the k_{wall} correction factor for a cylindrical ionization chamber to measure air-kerma in [60]Co γ-ray beams. An experimental method other than the traditional extrapolation procedure was used to determine the k_{wall} correction factor. In this method, the dependence of the ionization current in a cylindrical chamber was analyzed as a function of the effective wall thickness in place of the physical (radial) wall thickness traditionally considered in this type of measurement. The wall of a cylindrical chamber consists of different regions: substantially they are the front and posterior regions and the two chamber bases. Even if having an equal physical thickness, each of these regions has a specific shape and specific position in the chamber wall with respect to beam direction. Therefore, each wall region contributes to the attenuation and scatter effects (in terms of variation of the ionization in the chamber cavity) by an amount that varies according to the wall region. A Monte Carlo calculation of attenuation and scatter effects in the different regions of the chamber wall was also made to compare calculated and measured results. The k_{wall} values experimentally determined in this work agree within 0.2% with the independent Monte Carlo calculation. The agreement of the results obtained by two totally independent methods and the appreciable deviation (up to about 1%) between the results of both these methods and those obtained by the traditional extrapolation procedure reasonably support the conclusion that the two

methods providing comparable results are correct and traditional extrapolation procedure is likely to be wrong. The method used in this study applies, however, to any other chamber of the same type.

From the literature survey, it is evident that some discrepancies exist in the value of different correction factors of ionization chambers obtained by various methods. The values of correction factors such as the wall correction factor, recombination loss, stem correction factor etc. of the ionization chamber is required to determine the absolute air kerma rate using the fabricated ionization chamber. These correction factors depend on the chamber composition, chamber material and the beam energy. Therefore, the present study has been undertaken.

Chapter III

Theoretical Aspects of Ionizing Radiation Dosimetry

Chapter III

Theoretical Aspects of Ionizing Radiation Dosimetry

3.1 Introduction

In comparison with other radiation sensitive systems for dosimetry, the ionization chamber dosimetry system is the simplest, direct and least elaborate one for high accuracy measurement in photon or electron fields. Dosimetry by ionization chamber is employed for the detection and measurement of ionizing radiation. The quantities of interest in medical dosimetry are kerma, exposure and in-phantom absorbed dose. These dosimetric quantities are well-defined point quantities, i.e. they can be defined for every point of an infinitesimal mass δm about the point. The ionization chamber usually occupies a finite volume about the point.

3.2 Ionization Chamber

An ionization chamber as shown in Fig. 3.1 generally consists of a sensitive volume filled with a given medium, surrounded by a wall of another medium. In the context of cavity theory, the sensitive volume of the dosimeter is identified as the "cavity", which may contain a gaseous, liquid or solid medium. Gas is often used as the sensitive medium, since it allows a relatively simple electrical means for collection of charges released in the sensitive medium by radiation. Ionization chamber also consists of a collecting electrode to collect the ionization current (charge), a high voltage electrode to apply the chamber voltage, an insulator to separate the collecting electrode from the high voltage electrode and a guard system to reduce the chamber leakage currents.

In order to avoid the perturbations caused by the various chamber components to an ideal Bragg-Gray cavity, the non-chamber materials (e.g. insulators) in the chamber

must be minimum and the central electrode must be of minimum practicable diameter. In addition, the chamber construction must be such that the chamber collection volume is well defined and the chamber polarity effect is negligible.

Dimensions and Form of Cavity

For point-by-point measurement of absorbed dose in a medium, an ionization chamber must satisfy certain conditions that are basic to cavity theory. These conditions impose an upper limit on the chamber dimension and particularly on the dimension of the gas cavity but do not impose a lower limit. The lower limit of the chamber dimension is set by the practical considerations of mechanical design in order to obtain adequate ionization current. To minimize the disturbance of the radiation field due to the insertion of the chamber, the chamber is made as small as is practically possible.

On the other hand, if the ionization chamber is intended for measuring low-intensity radiation, current measurement can be eased using larger volume ionization chamber. But the loss of ions by recombination is then the criterion that will set the upper limit of its size or least to the spacing of the electrodes.
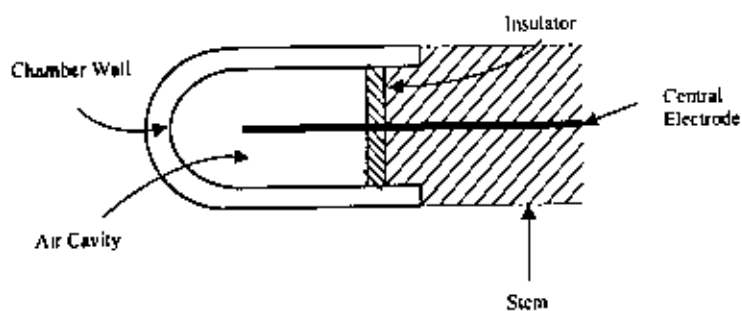
Fig. 3.1 Different parts of an ionization chamber

Bragg-Gray theory imposes no explicit restrictions on the geometrical form of the cavity: it can be spherical, cylindrical, pancake shaped or needle shaped.

Chamber Wall and the Central Electrode

For chambers (which are not parallel plate type), the outer wall usually forms the high voltage electrode and a voltage V is applied to this wall. If the wall is not conducting, a thin conductive coating is applied to the inside of the wall and the high voltage wire is connected to the inner wall. The ion-collecting rod in the cavity ionization chamber should be made of the same material as the wall if possible, as cavity theories do not deal with inhomogeneous wall media. However, the surface area of the rod is usually so much less than that of the wall that it will not have much influence unless the interaction cross-sections in the rod are much larger than in the wall. The ion-collecting rod is held at the central position of the chamber but is electrically insulated from the chamber wall.

The choice of chamber material depends primarily on the quantity to be measured. If the chamber is used to measure the exposure, it must be made by air-equivalent material that is, it must have an effective atomic number Z closely matching to that of air. If it is used to measure absorbed dose in a particular medium, both wall and gas should be matched to the medium. Two materials should be matched for a particular type of radiation so that the absorption of the radiation leads to the same flux density and energy distribution of secondary ionizing particles in one medium as in the other. This would be achieved only if the two materials have the same absorption coefficient for the primary radiation and the same atomic stopping power for the secondary particles. The thickness of the chamber wall also depends on the intended use. On one hand, adequate wall thickness is needed for electronic equilibrium. On the other hand, the wall attenuates the radiation. If the wall is too thin, enough electrons will not be generated and the chamber response will be low. If wall is too thick, chamber response is reduced due to increased attenuation. Thick walled graphite cavity ionization chambers are used by the primary standard laboratories as primary air kerma standards in ^{60}Co and ^{137}Cs γ-rays. The graphite wall should be thick enough to provide full build-up for secondary electrons. For measurements in the build-up region or for the measurement of low energy x-rays, the wall must be very thin. For the in-phantom dosimetry of ^{60}Co beams, the wall must be of equilibrium thickness, so that the chamber does not respond to the

phantom electron. The chamber material must be rigid, durable, of adequate electrical conductivity, impervious to (and free from chemical attack by) the gas; the gas must be stable in the presence of radiation. Special plastic materials closely matching with air, soft tissue or bone have been developed and appropriate mixture of stable gases have been used to match with these plastics. It is also necessary to know the W-value, which is the average energy expended in the gas by ionizing particles per ion pair formed for the particular gas mixture chosen. If air is chosen as the gas, bakelite-graphite is used as the wall material. In the calibrated ionization chambers used in radiotherapy dosimetry, the chamber wall is usually made by air-equivalent material or its composition is empirically adjusted to give a flat response over a certain energy range. In order for the chamber to be air equivalent, the effective atomic number of the wall material and the central electrode must be such that the system as a whole behaves like a free-air chamber. Commonly wall materials are made of graphite (carbon) or bakelite, or a plastic coated on the inside by a conducting layer of graphite or of a conducting mixture of bakelite and graphite. The effective atomic number of the wall is generally less than that of air because it is closer to that of carbon ($Z=6$). Consequently, such a wall should give rise to less ionization in the air cavity than in a free-air wall. Usually the greater atomic number of the central electrode, its dimensions and its placement geometry within the chamber can provide compensation for the lower atomic number of the wall. The chamber wall can serve a number of functions simultaneously:

- being the source of secondary charged particles that contribute to the dose in the air volume of the chamber and provide charged-particle equilibrium (CPE);
- protecting the air volume of the chamber from 'hostile' influences such as mechanical damage, dirt, humidity, light, electrostatic or RF fields, etc.; which may alter the chamber reading;
- serving as a container for gas medium g; and
- containing radiation filters to modify the energy dependence of the dosimeter.

Guard Electrodes

Guard electrodes serve two different purposes. The first purpose is to prevent leakage current flow from the high voltage electrode to the collector. To intercept the leakage

current, the guard electrode must surround the collector and must be maintained at the same potential in order that it may not itself become a source of leakage current. The second purpose of the guard electrodes is to define the volume within the ionization chamber from which ions can reach the collector electrode.

Insulator

The outer wall of the chamber is separated from the central electrode by an insulator. The naturally occurring substances amber, quartz and many synthetic plastics especially methyl methacrylate (Lucite), polystyrene, polyethylene, nylon, Teflon, Mylar film and polytrifluoromono-chloroethylene (Kel-F) are most suitable material for insulation in ionization chamber. Practical considerations usually govern the choice. Since the insulator has finite resistance, however large it may be, the central electrode registers a finite leakage current. For high precision measurements, the chamber leakage current must be very small.

Although the chambers differ in size and shape but the underlying principle of operation is similar for all chambers. The general succession of events, from photon to meter, is as follows:

- The photon is incident on the chamber;
- The photon interacts with the chamber wall material and emits secondary electrons, i.e. photoelectrons, Compton electrons. If the photon energy is large, positrons and electrons are also produced by pair production;
- Some of the electrons which enter into or pass through the chamber cavity interact with the gas in the cavity and produce ion pairs in proportion to the absorbed photon energy;
- The ion pairs are drawn to the collecting electrode by means of the high voltage placed across the electrodes;
- Upon reaching the collecting electrode the ion pairs are converted to current; and
- The current is then amplified and filtered to produce exposure (or exposure rate), which is measured by the electrometer.

30

3.3 The Bragg-Gray Cavity Theory

An ionization chamber actually measures dose according to the Bragg-Gray cavity theory. The Bragg-Gray cavity theory relates the absorbed dose in the sensitive medium of the dosimeter (cavity) to the absorbed dose in the surrounding medium containing the cavity; i.e. it provides a relationship between the dose in the gas and that in the wall of the ionization chamber The conditions for application of the Bragg-Gray cavity theory are:

   (i) the cavity must be small compared to the range of charged particles incident on it so that its presence does not perturb the fluence (number of particles per unit area) of charged particles in the medium;
   (ii) the absorbed dose in the cavity is deposited solely by charged particles crossing it; i.e.; photon interactions in the cavity are assumed negligible and thus ignored.

If a flunce Φ of identical charged particles with kinetic energy T passes through an interface between two media g and w (assuming Φ is continuous across the boundary) then the absorbed dose on the g side of the boundary

$$D_g = \Phi\left[\left(\frac{dT}{\rho dx}\right)_{c,g}\right]_T$$

And the absorbed dose on the w side of the boundary,

$$D_w = \Phi\left[\left(\frac{dT}{\rho dx}\right)_{c,w}\right]_T$$

where, $[(dT/\rho dx)_{c,g}]_T$ and $[(dT/\rho dx)_{c,w}]_T$ are the mass collision stopping power of the two media evaluated at energy T. So, the dose ratio D_w/D_g is equal to the corresponding ratio of mass collision stopping powers.

Suppose that a homogeneous medium *w* contain a thin layer of "cavity" filled with another medium *g* is uniformly irradiated by photons, as in Fig. 3.2(b). According to the first Bragg-Gray condition, the thickness of the *g*-layer is so small compared to the range of the charged particles striking it that its presence does not perturb the charged-particles field i.e., Φ is continuous across layer *g* and both interfaces.
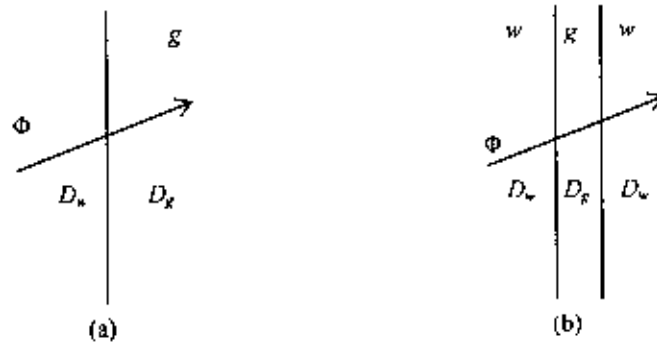
Fig. 3.2 (a) A fluence Φ of identical charged particles of kinetic energy *T* is crossing the interface between media *w* and *g*, (b) A fluence Φ of identical charged particles of kinetic energy *T* passes through a thin layer of medium *g* sandwiched between regions containing medium *w*

Again according to the second Bragg-Gray condition, the field of charged particles enter into the cavity from outside the vicinity of the cavity i.e., in the case of indirectly ionizing radiation a beam of high-energy charged particles is generated in medium *w* through interactions. It is also assumed that no interactions occur in medium *g*. All charged particles in the Bragg-Gray theory must originate elsewhere than in the cavity. Moreover, charged particles that enter the cavity are assumed not to stop in it.

Under the terms of the two Bragg-Gray conditions, the ratio of absorbed doses in the adjacent medium *w* to that in the cavity *g* for each monoenergetic component of the

spectrum of charged particles crossing g is again the same as the mass collision stopping power ratio in the two media.

$$\frac{D_w}{D_g} = \frac{(dT / \rho dx)_{c,w}}{(dT / \rho dx)_{c,g}} \tag{3.1}$$

For a differential energy distribution Φ_T (particles per cm^2 MeV), the average mass collision stopping power in the cavity medium g is

$$\overline{S}_g \equiv \frac{\int_0^{T_{max}} \Phi_T \left(\frac{dT}{\rho dx}\right)_{c,g} dT}{\int_0^{T_{max}} \Phi_T dT}$$

So,

$$\overline{S}_g = \frac{1}{\Phi} \int_0^{T_{max}} \Phi_T \left(\frac{dT}{\rho dx}\right)_{c,g} dT = \frac{D_g}{\Phi} \tag{3.2}$$

Similarly, for the thin layer of wall material w,

$$\overline{S}_w = \frac{1}{\Phi} \int_0^{T_{max}} \Phi_T \left(\frac{dT}{\rho dx}\right)_{c,w} dT = \frac{D_w}{\Phi} \tag{3.3}$$

Combining eqns. (3.2) and (3.3) gives the ratio of absorbed dose in w to that in g, which is the B-G relation in terms of absorbed dose in the cavity:

$$\frac{D_w}{D_g} = \frac{\overline{S}_w}{\overline{S}_g} \equiv \overline{S}_g^w \tag{3.4}$$

If the cavity medium g contains a gas in which a charge Q (of either sign) is produced by the radiation D_g which can be expressed (in grays) in terms of that charge as

$$D_g = \frac{Q}{m}\left(\frac{W}{e}\right)_g \qquad\qquad (3.5)$$

where, Q is the charge expressed in coulombs, m is the mass (kg) of gas in which charge Q is produced and $(W/e)_g$ is the mean energy required to produce an ion pair in the gas.

By substituting eqn. (3.5) into eqn. (3.4), the absorbed dose in the medium immediately surrounding a Bragg-Gray cavity i.e., in the chamber wall can be calculated on the basis of the charge produced in the cavity gas, provided the appropriate values of m, $(W/e)_g$ and $\bar{s}_g^w$ are known. So,

$$D_w = \frac{Q}{m}\left(\frac{W}{e}\right)_g \bar{s}_g^w \qquad\qquad (3.6)$$

Eqn. (3.6) is the Bragg-Gray relation expressed in terms of cavity ionization. Therefore, the Bragg-Gray cavity equation relates the ionization per unit mass in the small gas cavity to the energy absorbed in the wall of the chamber.

Although the cavity size is not explicitly taken into account in the Bragg-Gray cavity theory but the fulfilment of the two Bragg-Gray conditions depend on the cavity size that is based on the range of the electrons in the cavity medium, the cavity medium itself and electron energy. A cavity that qualifies as a Bragg-Gray cavity for high-energy photon beams may not behave as a Bragg-Gray cavity in a medium or low energy beams. The Bragg-Gray cavity theory does not take account of the creation of secondary (delta) electrons generated due to the slowing down of the primary electrons in the sensitive volume of the dosimeter.

3.4 Active Volume of the Ionization Chamber

In the ionization chamber the active volume, that is, the volume from which ions are drawn to the collecting electrode is the whole gas volume of the chamber. If the

chamber is totally enclosed and contains only two electrodes, the active volume is the whole volume of the gas enclosed. Whenever a guard ring is projected into the chamber to intercept any leakage current flowing from the high-potential electrode to the collector, this will affect the electric field in the chamber and some of the ions produced in the gas are drawn to the guard ring, not to the collector. The active volume is then bounded by the limiting lines of force of electric field along which ions are drifted towards the guard ring. Any change in the potential of the guard ring relative to that of the collecting electrode will cause a change in the active volume of the chamber.

3.5 Ion Chamber Saturation and Ionic Recombination

As the voltage difference between the electrodes of an ionization chamber exposed to radiation is increased from zero to a high value, the current at first increases almost linearly with voltage and then increases more slowly, until it finally approaches asymptotically the saturation current for a given radiation intensity. The curve of applied voltage V versus current for a constant dose rate or dose is called the saturation curve as shown in Fig. 3.3. The increase of ionization current is caused by incomplete ion collection at low voltages; unless the positive and negative ions are separated quickly by the electric field, they tend to recombine before they reach the collector. The recombination can be reduced by sweeping out the ions of the chamber more rapidly by increasing the field strength (V/cm) or by reducing the distance between the electrodes or by both of these measures. But it is not possible to increase the applied voltage indefinitely to eliminate recombination altogether, because of the onset of either (i) electrical breakdown of insulators, or (ii) gas multiplication, in which the free electrons gain enough kinetic energy from the electrical field within their mean free path in the gas to ionize the next atom they encounter. Thus extra ionization, not due to the ionizing radiation field, is produced. As soon as this begins to occur, a rapid multiplication of ions in the chamber takes place and the current is no longer a unique measure of the radiation intensity, but is strongly dependent on the applied voltage.
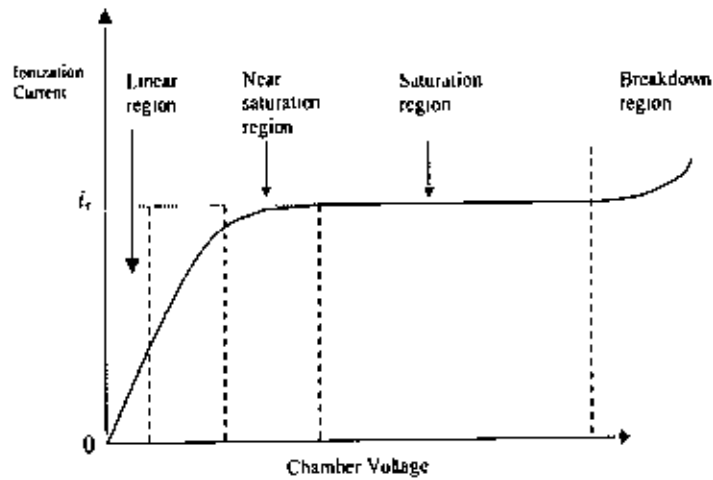
Fig. 3.3 Typical saturation curve of an ionization chamber

The collection efficiency f of an ionization chamber operating under specified conditions is the ratio of the measured current (i) to the ideal saturation current (i_s) i.e., the ratio of number of ions collected to the number of ions produced. The output current of an ionization chamber is reduced from the saturation value i_s by initial recombination, back diffusion to electrodes and volume recombination. If the losses due to these phenomena are small and do not interrupt each other, the charge collection efficiency $f(=i/i_s)$, can be expressed as

$$f = f_i f_d f_v \qquad (3.7)$$

where f_i, f_d and f_v are collection efficiencies corresponding to initial recombination, back diffusion and volume recombination respectively. In most irradiation conditions, volume recombination loss is dominant compared to the losses due to the other two processes which are usually negligible (i.e. $f_i = f_d = 1$). Ionization chambers are commonly used in the near-saturation region or even in the saturation region where $f = 1$, so that small changes in the voltage don't change the current.

Depending on the chamber design and ionization intensity, a certain amount of ion loss through ion recombination is to be expected. Especially at very high ionization

intensities, even at maximum possible chamber voltage there may be significant amount of recombination losses.

3.5.1 Mechanisms of Recombination

Recombination is usually classified as:

    i) initial recombination and

    ii) volume or general recombination.

Initial recombination occurs when the positive and negative ions formed in the track of a single ionizing particle meet and recombine. Initial recombination is an intratrack process and independent of the number of tracks formed per second, i.e., of the dose rate. Initial recombination takes place both in clusters and columns of ions produced along the path of the secondary electrons ejected by the γ-rays [29]. It occurs before ions can escape from their initial neighbors to mix with ions from other tracks in the process of general recombination. Initial recombination depends only on the initial ion density in each track and the field strength normal to the tracks which tends to pull the positive and negative ion columns apart. Although some initial recombination must always occur, it is only of importance when the ion density in the track is high such as α-particle tracks even at atmospheric pressure or in the tracks of any type of charged particle at high-pressure gas.

Volume or general recombination occurs when positive and negative ions formed by different ionizing particles meet and recombine as they drift towards the oppositely charged electrodes. Thus, the amount of volume recombination increases with the dose rate. The volume recombination sets the upper limit of the dose rate that can be measured accurately by a particular ionization chamber operating at normal atmospheric pressure.

The initial and volume recombination in a continuously irradiated chamber is distinguished by plotting the reciprocal of the observed output current (i) from an ionization chamber, against an appropriate function of the collecting field strength E,

in the chamber. If initial recombination is dominant then there will be a linear relationship between $(i)^{-1}$ and $(E)^{-1}$ in the near-saturation region:

$$1/i = 1/i_s + const/E$$

where i_s is the saturation current of the ionization chamber. But if volume recombination is dominant the relationship becomes

$$1/i = 1/i_s + const/E^2$$

To achieve a clear difference between these two effects, currents must be measured very accurately. The degree of ionic recombination depends on the geometry of the ion chamber, the applied voltage and the rate of charge production by the radiation. In the theoretical model of volume recombination, it is assumed that the current in the gas is carried entirely by positive and negative ions having fixed mobility k_1 and k_2 $(cm^2/(sV))$. It also assumed that the ions are produced uniformly throughout the gas volume in small cavity chambers and they drift along the lines of force of the electric field toward the oppositely charged electrodes. The ions formed in any part of the air volume will then remain confined to the "tube of force" within which they are formed and terminate on the two electrodes as shown in Fig. 3.4. As they drift along this tube of force, any small group of ions retains the same spatial concentration it had when formed, since any change in the cross section of the tube of force implies an inversely proportional change in the field strength and consequently in the velocity of the ions. That is, if the group of ions is compressed in an area laterally, it is extended along the length of the tube by the same factor. The volume occupied by the ions, therefore, remains constant and their concentration changes only through the loss of ions by recombination. Recombination in more complex field configuration can be evaluated by dividing the whole volume of the ionization chamber into appropriate tube of force and then assessing them separately.

The rate of recombination at any instant depends on the number of collisions between positive and negative ions per unit volume and unit time. Therefore, it is proportional to the product of their concentrations. The constant of proportionality is

the recombination coefficient, α (cm³/sec), which is the characteristic of a particular gas. If the charge density per unit volume is considered instead of number density of the ions, then the constant of proportionality in the recombination equation becomes α/e, where e is the electronic charge.
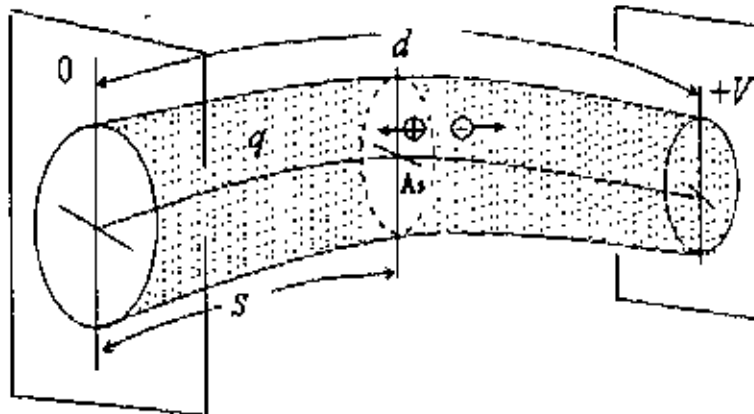
Fig. 3.4 Diagrammatic view of ions formed uniformly throughout the tube of force, within which they remain confined as they drift towards the electrodes

In a gas at atmospheric pressure, the drift velocity of an ion in an applied electric field is constant and proportional to the field strength. The constant of proportionality is called the mobility k (cm²/(sV)) and its value for positive ions k_1 is not the same, as for negative ions k_2. The field strength dV/ds is taken to be positive along the tube of force. In the absence of recombination, the charge on the negative ions crossing the section of the tube at position s in the positive direction per second must be equal to the charge on all the ions of that sign liberated in the tube per second between 0 and s, which is,

$$q \int_0^s A_s \, ds$$

Here q is the charge of ions of either sign produced by radiation per unit volume per second, and A_s is the cross-sectional area of the tube of force at position s.

The field strength at s is inversely proportional to the area of the tube of force i.e., K/A_s , where the constant K is determined by the relation

$$V = \int_o^d K(A_s)^{-1} ds$$

V is the potential difference between the electrodes of the ionization chamber. Therefore,

$$K = V \bigg/ \int_o^d (A_s)^{-1} ds$$

The velocity of negative ions with mobility k_2, at point s is therefore $k_2 K/A_s$, that is,

$$k_2 V \bigg/ A_s \int_o^d (A_s)^{-1} ds$$

So, the concentration of negative ions at position s is

$$C_s^- = \frac{q \int_o^s A_s ds}{A_s (k_2 K / A_s)}$$

$$= \frac{q}{k_2 V} \int_o^d (A_s)^{-1} ds \int_o^s A_s ds \qquad (3.8)$$

Similarly, the concentration of positive ions that crossing the plane at s in the opposite direction is

$$C_s^+ = \frac{q}{k_1 V} \int_o^d (A_s)^{-1} ds \int_s^d A_s ds \qquad (3.9)$$

The amount of charge recombination per second in the volume element $A_s ds$ is then

$$(\alpha / e) C_s^- C_s^+ A_s ds$$

and the total recombination per second throughout the tube of force is

$$
\int_0^d \frac{\alpha}{e} C_s^- C_s^+ A_s \, ds
$$

The total charge liberated per second in the tube is

$$
\int_0^d q A_s \, ds
$$

The fractional amount of recombination $(1-f)$ that occurs throughout the tube of force is

$$
1 - f = \frac{\int_0^d (\alpha/e) C_s^- C_s^+ A_s \, ds}{\int_0^d q A_s \, ds} \qquad (3.10)
$$

where f is the collection efficiency (ratio of the measured current to the ideal saturation current) of an ionization chamber under specified conditions.

This is the general formula of the fractional amount of recombination for any tube of force: the three usual cases are pancake, cylindrical and spherical geometry ionization chamber.

a. Volume Recombination in a Parallel Plate (Pancake) Ionization Chamber

When the chamber is operated at near saturation, the space-charge field due to the ions can be neglected in comparison with the collecting field strength V/d. In a parallel plate ionization chamber, the area of the tube of force is constant along its length and is denoted by A_p. Hence eqns. (3.8) and (3.9) become

$$
C_s^- = \frac{q s d}{k_2 V} \qquad \text{and} \qquad C_s^+ = \frac{q d (d - s)}{k_1 V}
$$

Now the fractional recombination becomes

$$1 - f_{para} = \frac{1}{qA_p d} \int_0^d \frac{\alpha}{e} \frac{qsd}{k_2 V} \frac{qd(d-s)}{k_1 V} A_p ds$$

$$= \frac{\alpha}{6ek_1 k_2} \left(\frac{d^4 q}{V^2} \right) \qquad (3.11)$$

By substituting

$$\xi_{para}^2 = \left(\frac{\alpha}{ek_1 k_2} \right) \left(\frac{d^4 q}{V^2} \right)$$

The factors in the first parentheses are the properties of the gaseous ions and are independent of the experimental variables. It is denoted by m^2 and is related to the volume recombination process. In the second parentheses, the experimental variables are grouped together. So,

$$\xi_{para}^2 = m^2 \frac{d^4 q}{V^2}$$

Thus for parallel plate ionization chamber containing air

$$1 - f_{para} = \frac{1}{6} \xi_{para}^2$$

Neglecting the terms of higher order

$$\frac{1}{f_{para}} = \left(1 + \frac{1}{6} \xi_{para}^2 \right)$$

or,

$$f_{para} = \frac{1}{1 + \frac{1}{6} \xi_{para}^2} \qquad (3.12)$$

This is the expression of the collection efficiency for parallel plate ionization chamber.

b. Volume Recombination in a Cylindrical Ionization Chamber

Since the cylindrical ionization chamber is symmetrical around the axis (Fig. 3.5), so the whole electric field or any part of it bounded by radial surfaces is considered as a single tube of force and the expression for A_s per unit axial length as

$$A_s = 2\pi r = 2\pi(a - s)$$
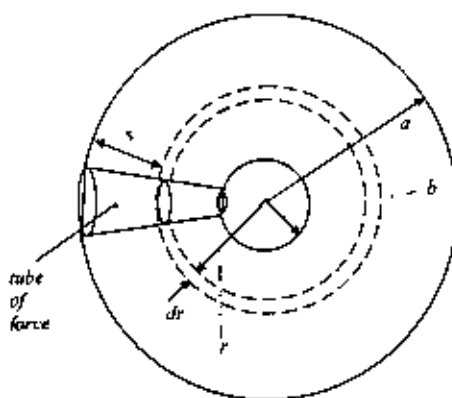
Fig. 3.5 Definition of parameters for chambers with cylindrical or spherical geometry

Therefore, eqn (3.8) and (3.9) become

$$C_r^- = \frac{q}{k_2 V} \int_b^a \frac{dp}{2\pi} \int_r^a 2\pi r dr = \frac{q \ln(a/b)}{2k_2 V}(a^2 - r^2)$$

and

$$C_r^+ = \frac{q \ln(a/b)}{2k_1 V}(r^2 - b^2)$$

where a and b are the outer and inner electrode radii of the chamber respectively.

Now, the total recombination per second throughout the whole volume is

$$\int_b^a \frac{\alpha}{e} C_r^- C_r^+ 2\pi r dr$$

43

This is equal to

$$\frac{\alpha q^2 \left[\ln(a/b)\right]^2}{4ek_1k_2V^2} \frac{\pi}{6}\left(a^2 - b^2\right)^2$$

and the charge of either sign liberated per unit time within the volume corresponding to unit axial length of the cylinder is $q\pi\left(a^2 - b^2\right)$,

So, the fractional recombination becomes

$$1 - f_{cyl} = \frac{\alpha q\left[\ln(a/b)\right]^2}{4ek_1k_2V^2} \frac{\left(a^2 - b^2\right)^2}{6}$$

or,

$$f_{cyl} = 1 - \frac{\alpha}{6ek_1k_2}\left[\frac{(a-b)^4 q}{V^2}\right]\left[\frac{(a+b)}{(a-b)}\frac{\ln(a/b)}{2}\right]^2$$

This equation has exactly the same form as that for parallel plate ionization chamber but in this case i.e., for cylindrical geometry chambers

$$\xi_{cyl}^2 = \left(\frac{\alpha}{ek_1k_2}\right)\frac{\left[(a-b)\kappa_{cyl}\right]^4 q}{V^2}$$

$$= m^2 \frac{\left[(a-b)\kappa_{cyl}\right]^4 q}{V^2}$$

where,

$$\kappa_{cyl} = \left[\frac{(a+b)}{(a-b)}\frac{\ln(a/b)}{2}\right]^{1/2}$$

So for cylindrical ionization chamber containing air the collection efficiency

$$f_{cyl} = \frac{1}{1 + \frac{1}{6}\xi_{cyl}^2}$$

c. Volume Recombination in a Spherical Ionization Chamber

In the case of spherical ionization chamber, the expression for A_s is

$$A_s = 4\pi r^2 = 4\pi(a-s)^2$$

and the fractional recombination is

$$1 - f_{sph} = \frac{\alpha}{6ek_1k_2}\left[\frac{(a-b)^4 q}{V^2}\right]\left[\frac{a^2+ab+b^2}{3ab}\right]^2$$

For spherical geometry ionization chamber

$$\xi_{sph}^2 = m^2 \frac{\left[(a-b)\kappa_{sph}\right]^4 q}{V^2}$$

The equivalent gap length in spherical geometry chamber is therefore

$$(a-b)\kappa_{sph}$$

where,

$$\kappa_{sph} = \left[\frac{1}{3}(a/b+1+b/a)\right]^{1/2}$$

and finally the expression of the collection efficiency for spherical shaped ionization chamber is

$$f_{sph} = \frac{1}{1+\frac{1}{6}\xi_{sph}^2}$$

So, the general equation for the charge-collection efficiency f of an ionization chamber containing air exposed to a continuous radiation field is

$$f = \frac{1}{1+\frac{1}{6}\xi^2}$$

3.5.2 Loss of Ions by Diffusion

If the applied voltage of the ionization chamber is low, some of the positive ions produced close to the positive plate may diffuse back and reach it and similarly for negative ions produced close to the negative plate. On this assumption, each ion reaching a plate loses its charge on the first collision. Measurements of this loss have been made by Scott and quoted by Greening [30] and found that diffusion losses will rarely need to be taken into account in practical ionization chambers.

3.6 Chamber Signal Correction for Influence Quantities

Ionization chamber reference conditions are described by a set of influence quantities which are not the subject of the measurement, but they influence the quantity being measured. The influence quantities of ionization chamber dosimetry system are chamber wall; ambient air temperature, pressure and humidity; applied voltage and polarity of the chamber; chamber leakage currents, chamber stem effect etc. If the chamber is used under conditions that differ from the reference conditions, then the measured signal of an ionization chamber must be corrected for the effect of influence quantities in order to obtain the correct signal value.

3.6.1 Chamber Wall Effect

The air kerma in ^{137}Cs and ^{60}Co γ-ray fields is usually measured by thick walled graphite cavity ionization chambers. The walls of the chamber perturb the incident beam by attenuating it and generating scattered photons. The wall correction factor k_{wall} is intended to remove the effects of attenuation of the incident primary photons in the chamber wall (and cavity air) and to remove the contribution of the recorded ionization from any photon interaction other than the first interaction in the chamber wall. So the wall correction factor corrects for attenuation and scatter in the chamber wall. The application of k_{wall} renders the measurement, that corresponds to a point in air in the absence of the chamber. In practice, wall correction factor is usually the largest and most significant correction factor applied in calculating a cavity

ionization chamber response; it can vary from 1% to 3%, depending on the design of the chamber and its wall thickness [31].

3.6.2 Air Temperature, Pressure and Humidity Effects

The mass of air contained in the sensitive volume of the chamber is equal to $\rho_a V_t$, with ρ_a being the air density and V_t is the ionization volume of the chamber. Since most ionization chambers are open to the ambient atmosphere, ρ_a is a function of the atmospheric pressure, temperature and humidity and so is the charge collected by the chamber, as both are correlated. Most standard laboratories use the value dry air density ρ_0 at standard conditions of 0°C and 101.325 kPa is 1.2930 kg/m^3. Considering air as an ideal gas, the density $\rho_a(T, P)$ at an arbitrary temperature T (in °C) and pressure P (in kPa) is given by

$$\rho_a(T, P) = \rho_0(0^\circ C, 101.325 kPa) \frac{273.15}{273.15 + T} \cdot \frac{P}{101.325}$$

Since the charge measured by an ionization chamber depends on air temperature, pressure and humidity, therefore, the absolute value of the air kerma rate must be given for stated reference values of these parameters.

The correction factor for air temperature and pressure $k_{T,P}$ is given as:

$$k_{T,P} = \frac{(273.15 + T)}{(273.15 + T_0)} \frac{P_0}{P} \qquad (3.13)$$

and it is applied to convert the measured signal to the reference conditions. Here T (in °C) and P (in kPa) are respectively the temperature and pressure of air within the chamber at the time of measurement, while T_0 (in °C) and P_0 (in kPa) are the reference conditions used in the standard laboratory.

Since the usual laboratory conditions contain a quantity of water vapour and air kerma is defined for dry air, a correction factor for the influence of humid air k_h is

required for absolute measurement of air kerma in the γ-ray field. The dependence of the inverse of the correction factor for humidity on relative humidity at 20°C and 101.325 kPa according to the data of ICRU 1979 [32] is shown in Fig. 3.6. The following polynomial is determined by fitting the data of ICRU 1979 [32] would be used for the correction factor and for the change of ionization due to humidity k_h.

$$
\begin{aligned}
1/k_h = {} & 1.0 + 4.0499 \times 10^{-4} H - 2.485 \times 10^{-5} H^2 + 8.4819 \times 10^{-5} H^3 \\
& -1.4299 \times 10^{-8} H^4 + 2.4244 \times 10^{-11} H^5 + 3.222 \times 10^{-12} H^6 \\
& -5.4071 \times 10^{-14} H^7 + 3.6796 \times 10^{-16} H^8 - 9.4258 \times 10^{-19} H^9
\end{aligned}
\tag{3.14}
$$

Here H is the relative humidity (%) at 20°C.
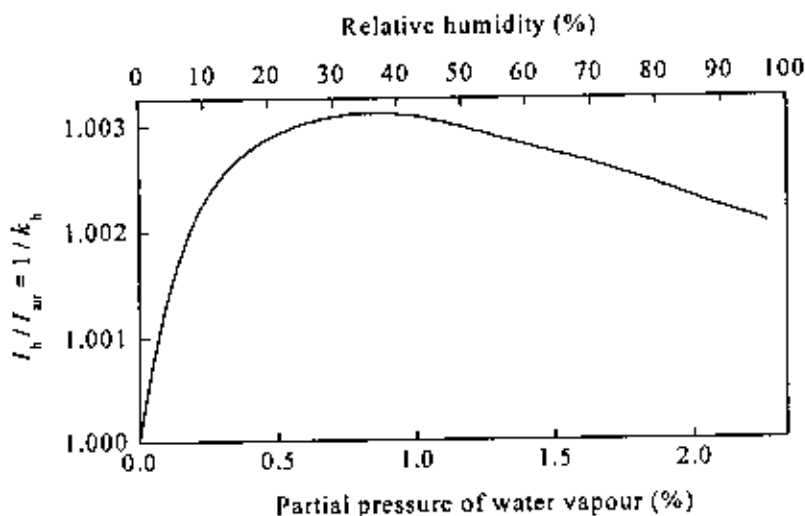
Fig. 3.6 Dependence of the inverse of the correction factor for humidity on relative humidity at 20°C and 101.325 kPa according to the data of ICRU 1979 [32]

Assuming the difference between the correction factors k_h at 20°C and at 22°C negligible, it is possible to use eqn. (3.14) without any modification as the correction factor for humidity at 22°C.

3.6.3 Chamber Stem Effect

Irradiating the chamber stem often cannot be avoided. Stem effect arises from the effect of scattered γ-rays from the stem, which reaches the chamber volume. In some case, irradiation of the chamber stem results a leakage current or extra current induced in a cavity which is formed near the cable terminal of the stem unintentionally.

3.6.4 Chamber Leakage Currents

No matter how well an ionization chamber dosimetric system is designed there will always be a small chamber leakage current. Their effects on the true radiation-induced currents are minimized by guard electrodes, low noise triaxial cables and sophisticated electrometers. The leakage currents fall into three categories:

      i)   Intrinsic leakage currents,

      ii) Radiation-induced leakage currents, and

      iii) Mechanical stress induced current and friction-induced spurious cable current.

There will always be a small, non-radiation related signal present when the system is in a ready mode to respond to radiation. This intrinsic current results from surface and volume leakage currents flowing between the polarizing and measuring electrodes of the ionization chamber. In a well designed ionization chamber dosimetry system the intrinsic leakage current are at least two orders of magnitude lower than the measured radiation induced signals and thus either negligible or can be suppressed from the actual radiation signal.

Electric leakage in the ionization chamber and electrometer may also occur because of the irradiation of insulators and chamber parts, cables and electronics of the measuring equipment. This is termed post-irradiation leakage; an effect that continues after the irradiation has ceased and decreases exponentially with time. Mechanical stress on cable insulators also causes a leakage current for which bending and twisting of the cables should be avoided.

Chapter IV

Experimental Methods

Chapter IV

Experimental Methods

4.1 Introduction

Ionization chambers used in hospitals for calibration of the radiation therapy beams must have a traceable calibration (directly or indirectly) in a standard laboratory. Absolute ionization chambers are not used for routine calibrations. The Primary Standard Dosimetry Laboratories (PSDLs) calibrate secondary standard dosimeters for Secondary Standard Dosimetry Laboratories (SSDLs) that are used for calibration of the reference instruments of users, such as therapy level ionization chambers used at hospitals. Graphite cavity ionization chambers with accurately known volume are used at primary metrology institutes for absolute measurement of air kerma in ^{60}Co and ^{137}Cs γ-ray fields. For the absolute ionization chamber, the sensitive air volume or mass is determined directly by measurement of the inner radius and the length of the volume. In addition to the need of accurate knowledge of the sensitive air volume, wall correction factors are required to account for the effect of photon attenuation and scattering in the chamber wall. An accurate knowledge of W/e value and Bremsstrahlung fraction is also required to determine the *air-kerma (rate) in air*. Finally, standard laboratories implement additional correction factors, which account for the deviations from the Bragg-Gray cavity theory.

For absolute air kerma measurement, cylindrical ionization chambers are being used at National Metrology Institute of Japan (NMIJ/AIST); recently eight spherical and parallel-plate (pancake) ionization chambers of various volumes have been constructed at the Primary Standard Dosimetry Laboratory (PSDL), AIST, Tsukuba, Japan. These ionization chambers can be used for the measurement of absolute air kerma rate in wide ranges in standard ^{60}Co and ^{137}Cs γ-ray fields. Figs. 4.1– 4.11 show the design and dimensions of different parts of the fabricated ionization chambers.

4.2 Specifications of the Fabricated Ionization Chambers

Chamber's electrode material: Poco graphite of density 1.82 g cm^{-3}

Symbols for spherical chambers: S7A, S60A, S60B, S900A

Symbols for parallel plate chambers: P9A, P9B, P60A, P60B

Chambers "xxA" are used both for ^{60}Co and ^{137}Cs γ-rays and those "xxB" are used only for ^{137}Cs γ-ray beam. This is because the walls of xxB are thick enough for electronic equilibrium for ^{137}Cs γ-rays and not for ^{60}Co. Figs.4.12 and 4.13 are the photographs of P9A and S60A ionization chambers.

S7A Ionization Chamber

Spherical wall:	Iinner φ24 mm and outer φ30.6 mm
Collector electrode:	Rod- φ2 mm and length16 mm

S60A Ionization Chamber

Spherical wall:	Inner φ50 mm and outer φ56.6mm
Collector electrode:	Rod- φ2 mm and length 15.7 mm
	Frustum- φ2 mm, φ5 mm and height 1.5 mm
	Rod- φ5 mm and length 16 mm
	Half sphere- φ5 mm

S60B Ionization Chamber

Spherical wall:	Inner φ50 mm and outer φ52.4 mm
Collector electrode:	Rod- φ2 mm and length 15.7 mm
	Frustum- φ2 mm, φ5 mm and height 1.5 mm
	Rod- φ5 mm and length 16 mm
	Half sphere (solid) - φ5 mm

S900A Ionization Chamber

Spherical wall:	Inner φ120 mm and outer φ126.6 mm
Collector electrode:	Rod- φ3 mm and length 35.7 mm
	Frustum- φ3 mm, φ12 mm and height 4.5 mm
	Pipe- inner φ8 mm, outer φ12 mm and length 37.5 mm
	Half sphere- inner φ8 mm and outer φ12 mm

P9A Ionization Chamber

Ring wall:	Inner φ50 mm, outer φ56.6 mm and length 4.8 mm
Both side disk walls:	φ56.6 mm and thickness: 3.3 mm
Collector electrode:	Rod- φ2 mm and length 3 mm
	Disk- φ44 mm and thickness 0.3 mm
	Both side comb shape electrode- φ44 mm
	(15 mm from the center to 22 mm with a slope of
	0.85/7)

P9B Ionization Chamber

Ring wall:	Inner φ50 mm, outer φ56.6 mm and length 4.8 mm
Both side disk walls:	φ56.6 mm and thickness: 1.2 mm
Collector electrode:	Rod- φ2 mm and length 3 mm
	Disk- φ44 mm and thickness 0.3 mm
	Both side comb shape electrode- φ44 mm
	(15 mm from the center to 22 mm with a slope of
	0.85/7)

P60A Ionization Chamber

Ring wall:	Inner φ100 mm, outer φ106.6 mm and length 8 mm
Both side disk walls:	φ106.6 mm and thickness 3.3 mm
Collector electrode:	Rod- φ2 mm and length 3 mm (OR with following Disk)
	Rod- φ0.5 mm and length 2 mm (2 Rods)
	Disk- φ96 mm and thickness 0.3 mm

P60B Ionization Chamber

Ring wall:	Inner φ100 mm, outer φ106.6 mm and length 8 mm
Both side disk walls:	φ106.6 mm and thickness 1.2 mm
Collector electrode:	Rod- φ2 mm and length 3 mm (OR with following Disk)
	Rod- φ0.5 mm and length 2 mm (2 Rods)
	Disk- φ96 mm and thickness 0.3 mm.

(a)   (b)
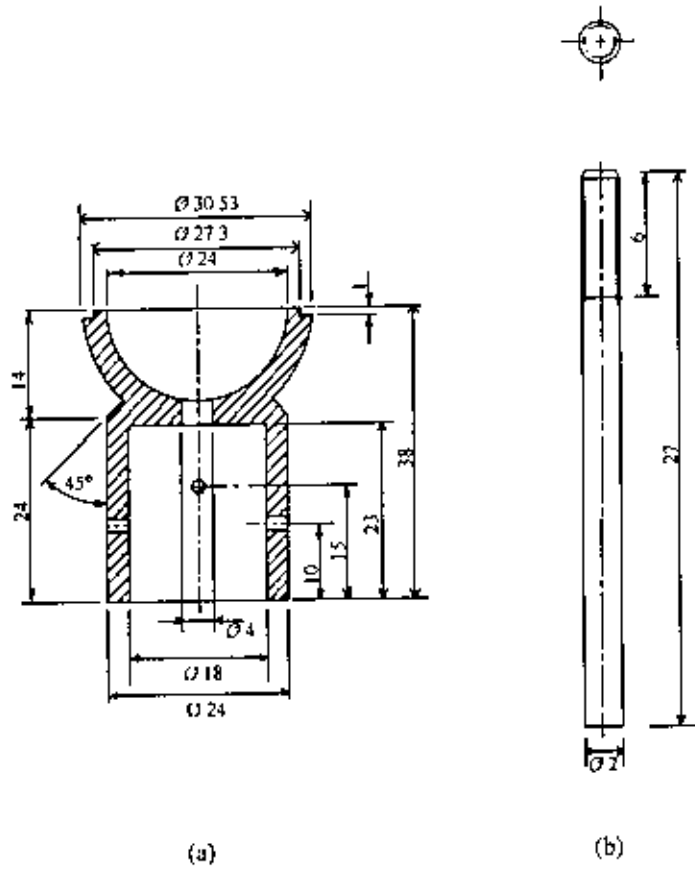
Fig. 4.1 Dimension of different parts of (a) spherical wall outer electrode and
(b) collector electrode of S7A Ionization Chamber (all dimensions
are in mm)

(a)   (b)
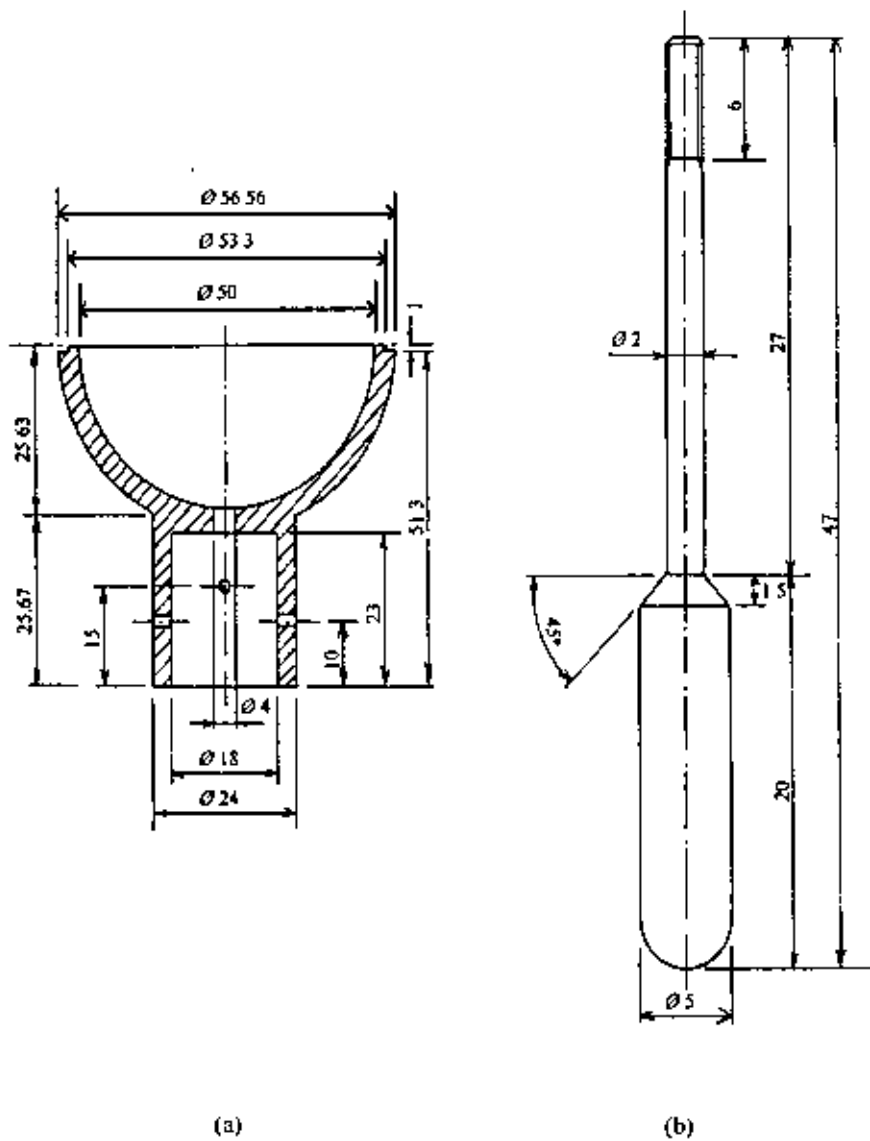
Fig. 4.2 Dimension of different parts of (a) spherical wall outer electrode and (b) collector electrode of S60A Ionization Chamber (all dimensions are in mm)

(a)   (b)
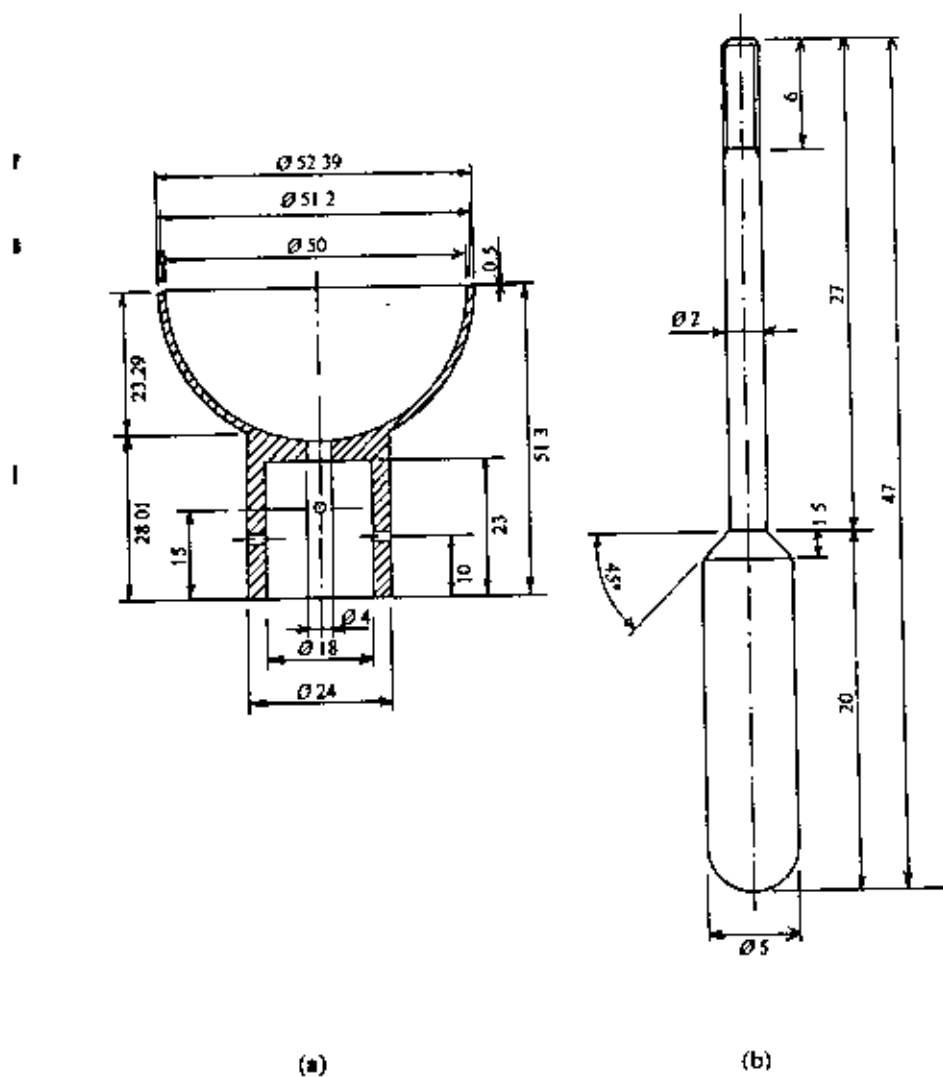
Fig. 4.3 Dimension of different parts of (a) spherical wall outer electrode and
(b) collector electrode of S60B Ionization Chamber (all dimensions
are in mm)
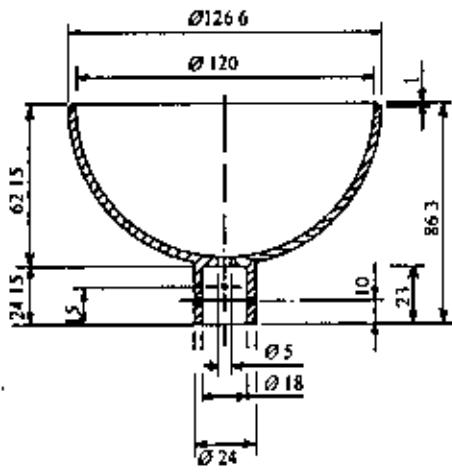
(a)
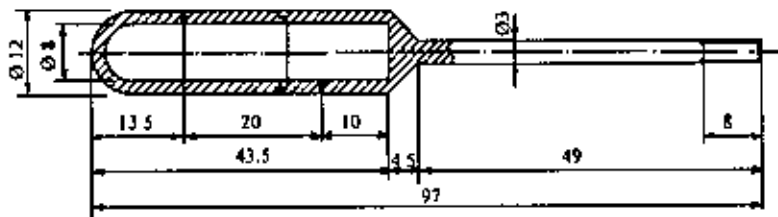
(b)

Fig. 4.4 Dimension of different parts of (a) spherical wall outer electrode and (b) collector electrode of S900A Ionization Chamber (all dimensions are in mm)

(a)

(b)
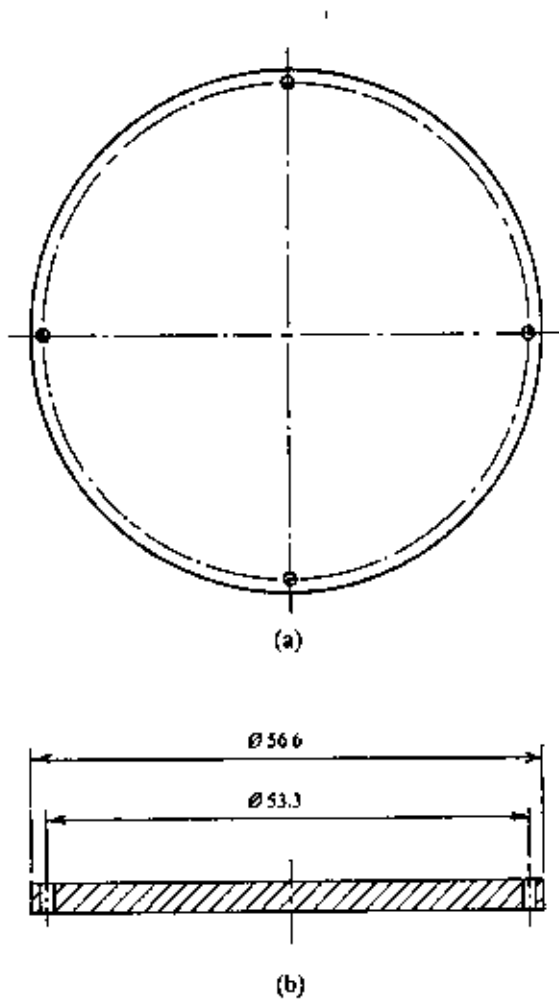
Fig. 4.5 (a) Cross-sectional view and (b) lateral view of the cover electrode
of P9A Ionization Chamber (all dimensions are in mm)
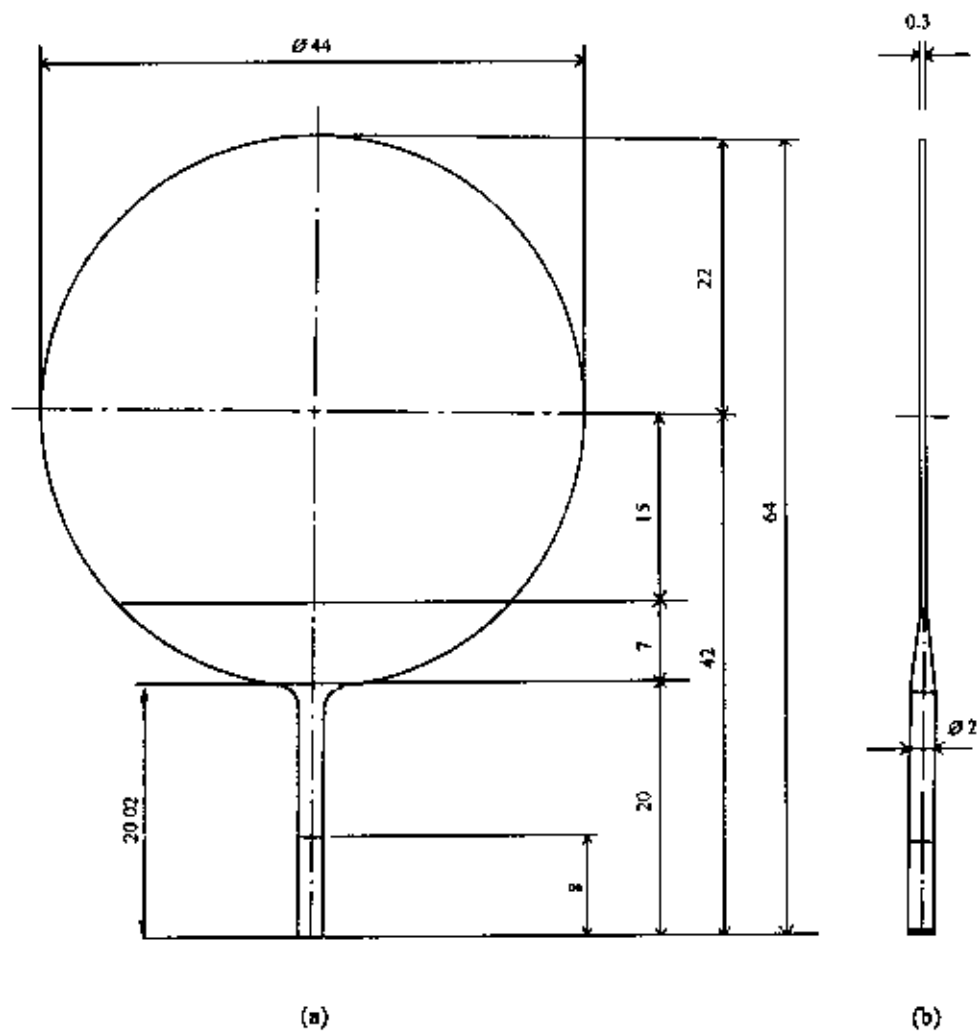
Fig. 4.6 (a) Cross-sectional view and (b) lateral view of the collector electrode
of P9A Ionization Chamber (all dimensions are in mm)

(a)   (b)
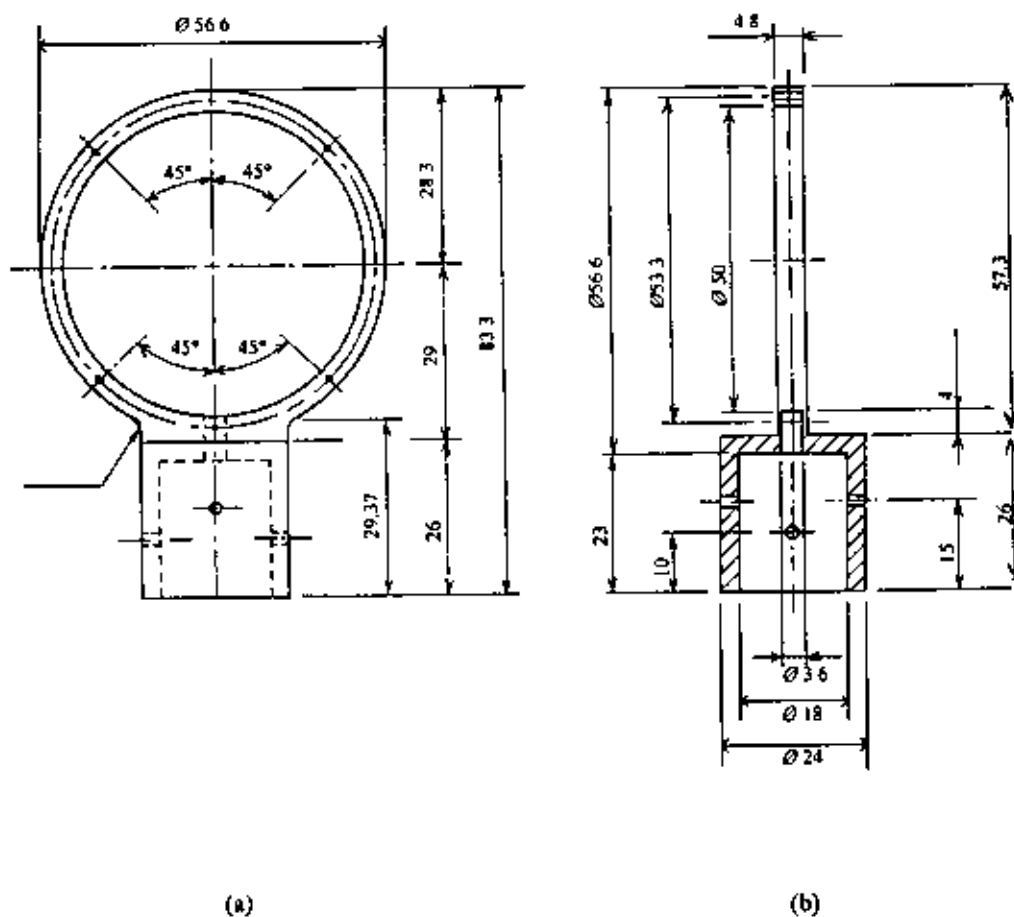
Fig. 4.7 (a) Cross- sectional view and (b) lateral view of the P9A Ionization
Chamber (all dimensions are in mm)

(a)

Ø 106.6

Ø 103 3

(b)
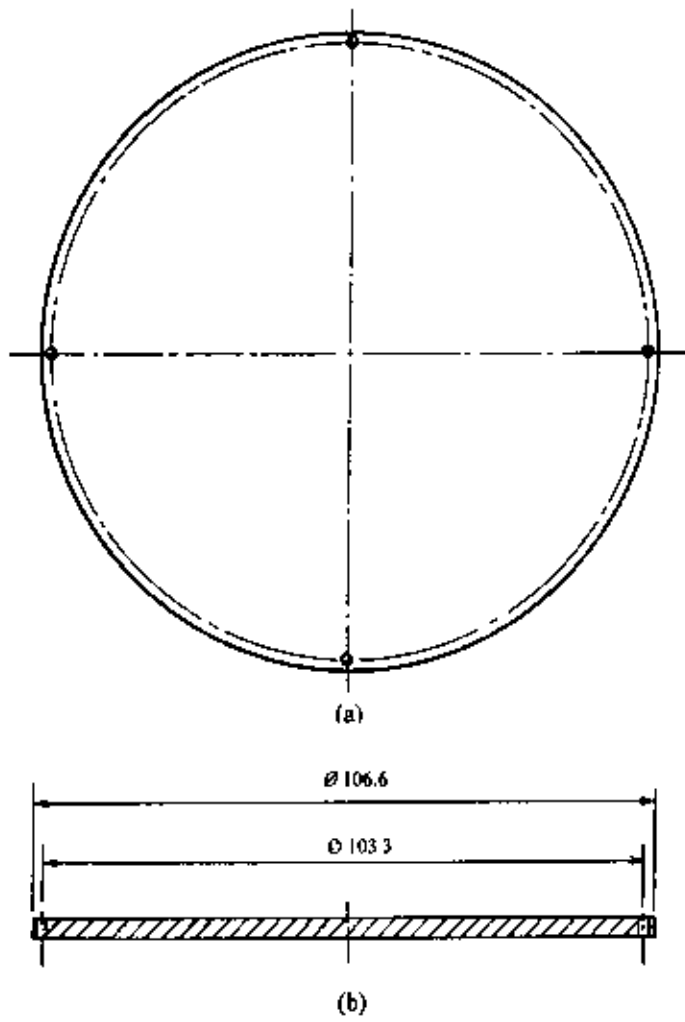
Fig. 4.8 (a) Cross-sectional view and (b) lateral view of the cover electrode of P60A Ionization Chamber (all dimensions are in mm)
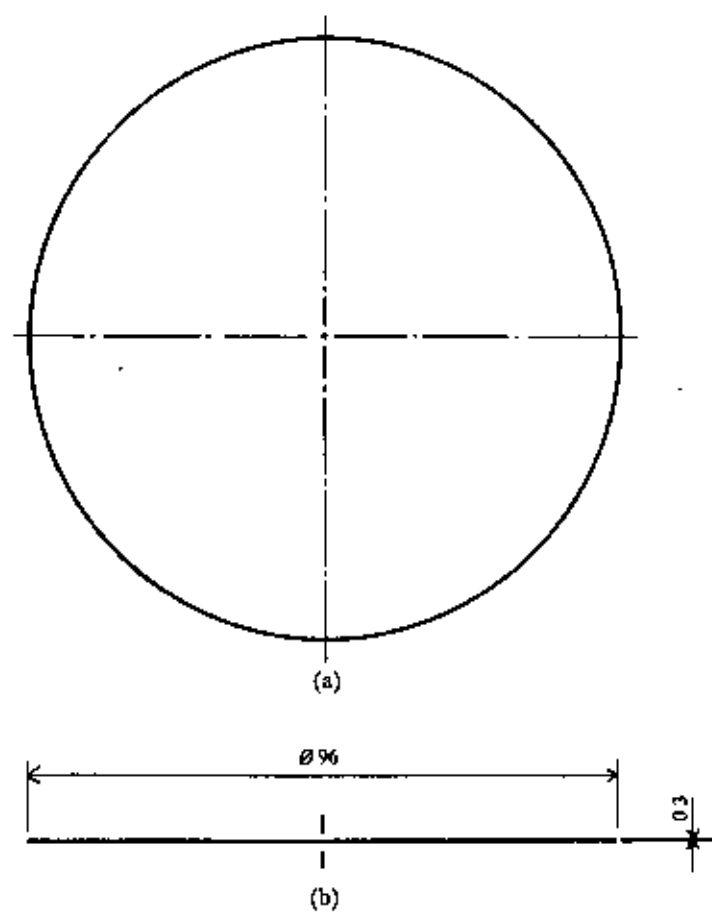
Fig. 4.9 (a) Cross-sectional view and (b) lateral view of collector electrode of the P60A Ionization Chamber (all dimensions are in mm)
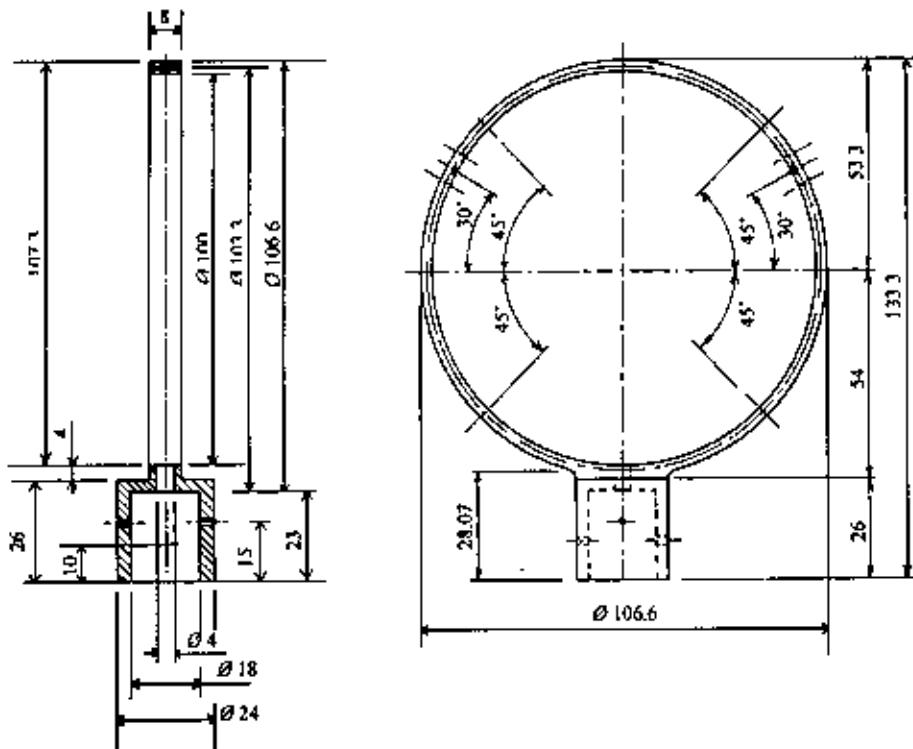
Fig. 4.10 (a) Lateral view and (b) cross-sectional view of the P60A Ionization
Chamber (all dimensions are in mm)
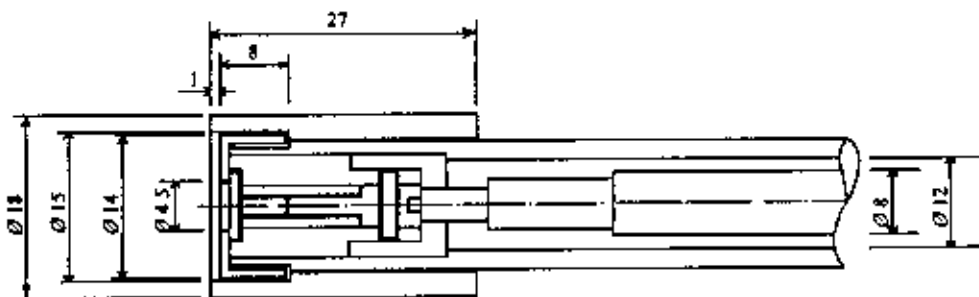
Fig. 4.11 Stem part of the fabricated ionization chambers (all dimensions are in mm)
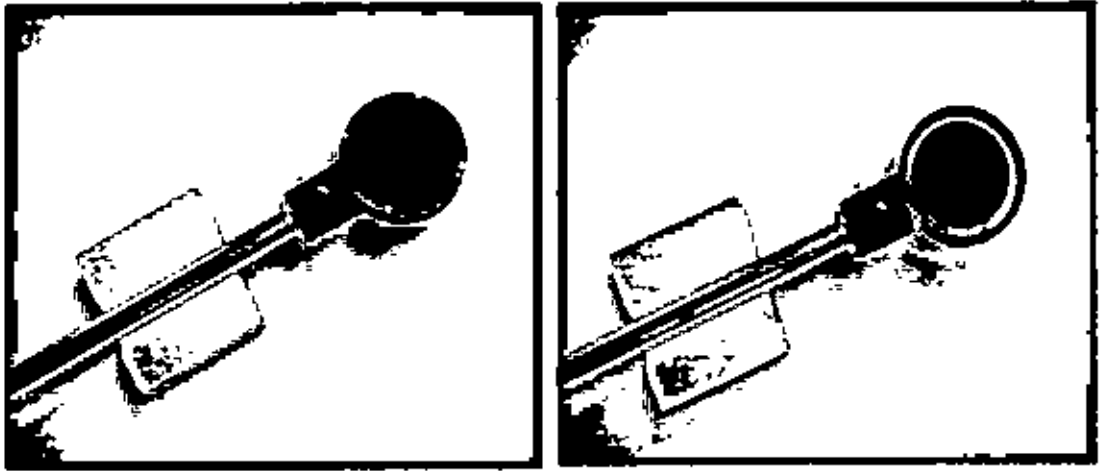
Fig. 4.12 Photograph of P9A Ionization Chamber (a) with both side disk walls and (b) without disk walls
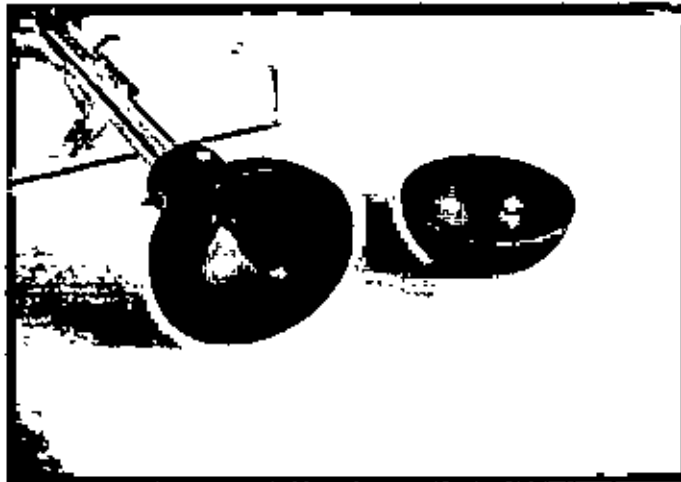
Fig. 4.13 Photograph of internal view of S60A Ionization Chamber

4.3 Ionization Chamber System

The concept of an ionization chamber system is explained in Fig. 4.14. The polarizing (i.e. usually outer) electrode of the chamber is connected to biasing (polarizing) voltage power supply. The ions produced in the ionization volume are drifted towards the biasing electrode or to the collector depending on the polarity of their charge. The signal current due to the ions is measured by an electrometer which is connected to the collector electrode.
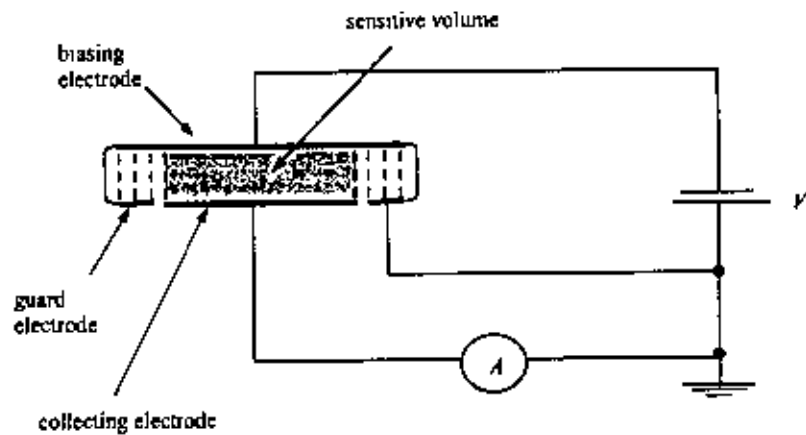
Fig. 4.14 Schematic diagram of an ionization chamber system. *A* represents the electrometer and *V* is the power supply

An ionization chamber system consists of the following components:

- An ionization chamber
- Electrometer
- Power supply
- Thermometer
- Barometer
- Hygrometer

4.4 Gamma Ray Sources

The absolute value of air kerma rate in ^{60}Co and ^{137}Cs γ-ray field with nominal activity 148 TBq and 34 TBq respectively would be measured using the fabricated ionization chambers. Fig. 4.15 shows schematically the ^{60}Co γ-ray source used in the experiment.
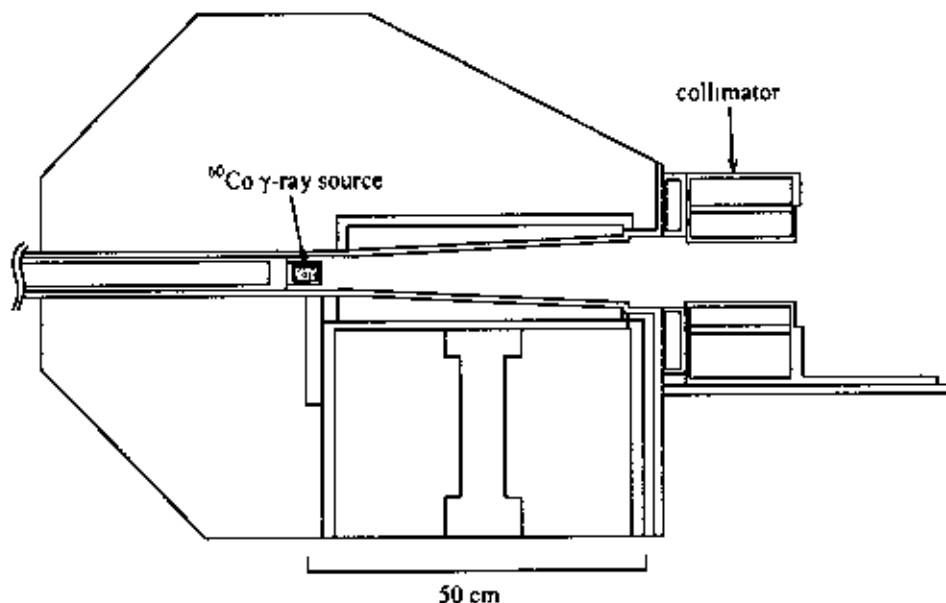
Fig. 4.15 Schematic diagram of the ^{60}Co γ-ray source used in the experiment

4.5 Setting of Ionization Chamber in γ-ray Field for the Measurement of Ionization Current

The ionization current (or charge) produced in an ionization chamber is measured by setting the mechanical center of the ionization volume of the chamber at a fixed distance from the source on the central axis of the γ-ray beam as shown in Fig 4.16. It has been done using two laser light beams, one is at the center of the γ-ray beam and the other is perpendicular to the beam. The perpendicular laser light shows a reference position at 1 m distance from the γ-ray source. For irradiation at lower air kerma rates, the chambers are placed at 2, 3, 4, 5 and 6 m from the source.

Sometimes for much lower air kerma rates, tungsten alloy disks with a thickness of 25 mm and 40 mm or both are inserted in the collimator of the ^{60}Co γ-ray irradiation container. For much lower air kerma rate of ^{137}Cs γ-ray field an iron disk is placed at the collimator of the ^{137}Cs γ-ray source. When higher air kerma rate is required, the ^{60}Co γ-ray source is pushed and placed so that source chamber distance becomes 0.6 and 0.4 m with the chamber fixed at the reference laser light position.
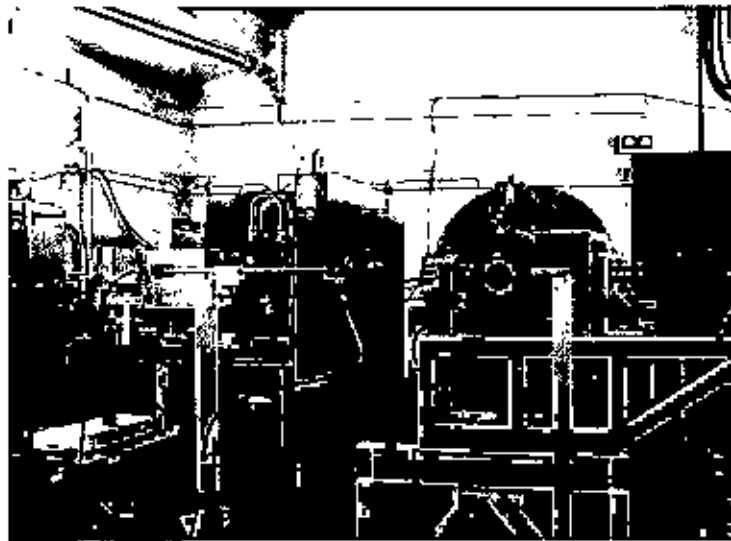
Fig. 4.16 Photograph of the setting arrangement of S60A Ionization Chamber in ^{60}Co γ-ray field for the measurement of ionization current

The ionization chamber is usually set at right angle to the γ-ray beam. Average of the absolute value of the signal current at both polarity of the applied voltage is used as the output of the chamber for absolute measurement of the air kerma rate. By using the average values, the effects of extra signal currents can be made negligible: (i) the signal current from the cavity, which could be made due to imperfect design or imperfect assembling of the chamber, in the stem or near the cable terminal, (ii) the signal current induced by irradiation of signal cables, (iii) the dark current of the electrometer. This is because all of these signals do not depend on the polarity of the applied voltage and are added to the actual signal current of the ionization chamber

when their polarities are the same as that of the actual signal current and are subtracted from the actual signal current when their polarities are different.

4.6 Measurement of Ionization Volume of the Fabricated Ionization Chambers

An ionization chamber response depends on the chamber design. In order to obtain the total ionization volume of such a chamber, for convenience, the chamber is divided into three parts:

(i)   the ionization volume in the spherical or disk part of the chamber,

(ii)   the ionization volume in the neck part of the chamber and

(iii) the ionization volume in the stem part of the chamber.

For spherical ionization chamber, the ionization volume in the spherical part of the chamber is calculated using the inner diameter of the cavity and the outer diameter and length of the central collector electrode. In the case of parallel-plate (pancake) ionization chamber, the ionization volume in the disk part is determined from the inner diameter of that part, the depth of the cavity and the outer diameter and length of the central electrode.

The ionization volume in the cylindrical shaped neck part of the chamber is calculated using the inner diameter and the length of the neck part and the outer diameter and length of the collector electrode within the neck part of the chamber. For the chamber P9A and P9B, the volume of the wedge shaped part of the collector electrode is obtained by calculation as a sum of small square pillars because it is difficult to calculate it analytically.

The ionization volume in the stem part of the chamber is measured in the following way: at first, the external cavity wall and the central electrode of the chamber are removed from the stem of the chamber and then a short central electrode is attached with the stem. The stem is then covered by a small pipe. The pipe shaped cover has the same length, inner and outer diameters as those of the stem part of the chamber.

Then a flat disk is attached in front of the pipe shaped cover. The short central electrode, the pipe shaped cover and the flat disk are made with the same material (Poco-graphite) by which the chamber is made. Another cylindrical shaped stem cover of the same dimension with a small hole at the base of the cover for passing the collector electrode through it is also used. So, two types of stem cover are used. Now each covered stem is set perpendicularly to the γ-ray beam at a distance of 1m from the source using two laser light beams. A voltage of 500V is applied to this arrangement and is irradiated by ^{60}Co or ^{137}Cs γ-ray beam. Ionization current from this arrangement using two types of stem cover is measured at both polarities of the applied voltages. Average of the absolute value of the signal current measured at both polarities in each case of this arrangement is used as the signal current from the stem part of the chamber. The ionization volume in the stem part of the chamber is obtained from an assumption that the ratio between this signal current and the signal current from the whole volume of the ionization chamber is proportional to the ratio of the effective ionization volume in the stem part and the total ionization volume of the chamber.

4.7 Correction Factors for Ion Loss in the Fabricated Ionization Chambers

The signal current from an ionization chamber at first increases with the applied voltage to the polarizing electrode and finally reaches the saturation value. The saturation characteristics are governed by three processes of ion loss in the chamber: the initial recombination, back diffusion and volume recombination. Initial recombination loss is due to the recombination of the ions created in each cluster; diffusion loss is due to the back-diffusion of positive and negative ions to anode and cathode respectively. Volume recombination loss of ions occurs when ions drift towards their respective electrodes.

Initial recombination loss and back diffusion loss both are proportional to the inverse of the applied voltage and independent of the air kerma rate. On the other hand, volume recombination loss is proportional to the inverse of the square of the applied voltage of the ionization chamber and to the air kerma rate. Volume recombination

loss can be obtained from the change of signal currents measured at several different applied voltages at high air kerma rates. Initial recombination loss and diffusion loss are obtained from signal currents measured at low air kerma rates and then it is not necessary to take into account volume recombination loss. In practice, initial recombination is generally negligible compared to the volume ion recombination for most ionization chambers. Volume ion recombination is reduced by the use of low air kerma rates and small-volume ion chambers and then the initial ion recombination is significant [17, 30].

In the present work, ion losses due to volume recombination, initial recombination and back diffusion in each of the ionization chambers are obtained using a method proposed by De Almeida and Niatel [33] and adopted by Boutillon [8]. In this method all the ion losses are obtained simultaneously by measuring signal currents at different applied voltages for different air kerma rates.

Near saturation i.e., when the ion losses due to recombination and diffusion are small, the ratio between the saturation current I_s and the ionization current I_V measured at an applied voltage V, can be obtained by the eqn. (neglecting the terms of higher order)

$$I_s/I_V = 1 + A/V + m^2\left(g/V^2\right)I_s \qquad (4.1)$$

with

$$m^2 = \alpha/\left(ek_+k_-\right) \qquad (4.2)$$

where A is constant for a particular chamber involved in the initial recombination and back diffusion;

m^2g is also constant for a particular chamber involved in the volume recombination process;

g is a factor which depends on the chamber geometry;

α is the volume recombination coefficient under continuous irradiation;

e is the charge per ion;

k_+ and k_- are the mobility of the positive and negative ions respectively.

The first variable term on the right hand side of eqn. (4.1) describes the loss of ions by initial recombination and diffusion and the second variable term describes the volume recombination loss. So, volume recombination loss depends on applied voltage, air kerma rates and the chamber geometry factor g. Ion loss due to initial recombination and diffusion within the ionization chamber are obtained from the value of A; volume recombination loss is obtained from the value of $m^2 g$ at any applied voltage and air kerma rate. Ionization chambers are used in a wide range of air kerma rates. For absolute measurements of air kerma rates, it is important to obtain accurate signal currents by correcting it for ion losses using the values of A and $m^2 g$ in each ionization chamber.

If V in eqn. (4.1) is replaced by the lower voltage V/n, a similar eqn. is obtained for the signal current $I_{V/n}$. Here n is an arbitrary value larger than 1.

Now dividing this eqn. by the eqn. (4.1) gives (neglecting the higher order terms)

$$I_V / I_{V/n} = 1 + (n-1)A/V + (n^2 - 1)m^2 (g/V^2) I_V \qquad (4.3)$$

Currents I_V and $I_{V/n}$ are measured at several different air kerma rates and then the values of $I_V / I_{V/n}$ are plotted as a function of I_V. The applied voltage must be high enough to ensure high ion collection efficiency over the whole range of measured currents.

For an ideal parallel plate ionization chamber, $g = d^4/6$, where, d is the separation between the parallel electrodes.

For an ideal spherical ionization chamber in which both the outer electrode of radius a and the central electrode of radius b are spherical shape

$$g = \frac{[(a-b) \kappa_{sph}]^4}{6}$$

with

$$\kappa_{ipk} = \left[\frac{1}{3}\left(a/b + 1 + b/a\right)\right]^{1/2}$$

However, in the present case of the fabricated ionization chambers, the chambers are not ideal one and it is not possible to obtain the value of g from the above expressions.

In the present study, in order to measure the ion loss within each of the ionization chambers signal currents are measured in ^{60}Co γ-ray field for A5, S7A, S60A, S900A, P9A and P60A ionization chambers and for S60B in ^{137}Cs γ-ray field. The applied voltages V and V/n are 600, 400, 300, 200, 150V for A5; 1000, 500, 200,100V for S7A; 1000, 600, 300, 200, 100V for S60A and S60B; 1000, 600, 400, 300V for S900A; 400, 200, 100, 50V for P9A and 700, 300, 100, 30, 10V for P60A ionization chambers. The air kerma rates are varied by placing Cu plates with the total thickness ranging from 6 to 60 mm or tungsten (W) disk of 25 mm thickness at the collimator of the ^{60}Co source or an iron disk is placed at the collimator of the ^{137}Cs γ-ray source. The measured signal current is corrected for the temperature 22°C and pressure 101.325 kPa, but no correction is made for the dependence of the signal current on humidity. Air humidity ranged from 38% to 44% throughout the ionization current measurement from all the fabricated ionization chambers in the present study at different applied voltages. Signal current is measured at least three times for a particular applied voltage in each polarity. Therefore, for a particular value of applied voltage there are six values of ionization currents at both polarities. Average of the absolute value of the signal currents measured at both polarities of the applied voltage is used as the signal current in order to obtain the effect of ion losses within the chamber.

4.8 Stem Correction Factor for the Fabricated Ionization Chambers

The stem correction factor is due to the contribution of γ-ray scattered by the ionization chamber stem. This factor (k_{stem}) is determined using a dummy stem of

identical size and composition placed on the side opposite to the original chamber stem, and the chamber is irradiated successively with and without the presence of a dummy stem; the ratio of the signal current gives the stem correction factor. In the present study, ionization currents are measured at both polarities of the applied voltages. Average of the absolute value of the ionization current measured at both polarities is used as the signal current in order to obtain the stem correction factor of the chamber. For each fabricated ionization chamber, stem correction factor is determined at various source chamber distances (SCD), i.e. at various air kerma rates in the γ-ray field. For a particular ionization chamber in a γ-ray field, average value of k_{stem} at various SCDs would be used as the stem correction factor during absolute air kerma measurement by that chamber. In the present study, stem correction factor of the fabricated ionization chambers are measured for the following source-to-chamber distances (SCDs):

S7A Ionization Chamber

$\quad$ SCD= 0.3m, 0.4m, 1m, 2m, 3m, 4m and 6m (for ^{60}Co source)

$\quad\quad$ = 1m, 2m and 4m (for ^{137}Cs source)

S60A Ionization Chamber

$\quad$ SCD= 1m, 2m, 4m and 6m (for ^{60}Co source)

$\quad\quad$ = 1m, 2m and 4m (for ^{137}Cs source)

S60B Ionization Chamber

$\quad$ SCD= 1m, 2m and 4m (for ^{137}Cs source)

S900A Ionization Chamber

$\quad$ SCD= 4m, 6m and 6m with 25mm W attenuator (for ^{60}Co source)

$\quad\quad$ = 1m, 2m, 3m and 4m (for ^{137}Cs source)

P9A Ionization Chamber

$\quad$ SCD= 0.3m, 0.4m, 1m, 2m, 4m and 6m (for ^{60}Co source)

$\quad\quad$ = 1m, 2m and 4m (for ^{137}Cs source)

P60A Ionization Chamber

SCD= 2m, 3m, 4m and 6m (for ^{60}Co source)

= 1m, 2m, 3m and 4m (for ^{137}Cs source)

4.9 Wall Correction Factor of the Fabricated Ionization Chambers

Several methods have been developed for the determination of the wall correction factor. In extrapolation techniques, k_{wall} is given by the extrapolated k_w value multiplied by k_{cep} (center of electron production). Traditionally, most standard laboratories determined k_w by extrapolation method. In this method ionization current is measured as a function of wall thickness varied by adding layers of wall materials to all sides of the chamber and then to linearly extrapolate the measured curve to zero wall thickness. The extrapolation to zero wall thickness over-corrects for wall attenuation. Some of the electrons that contribute to ionization in the cavity gas originate from photon interactions that take place within the wall at a point upstream from the cavity where the photon fluence has not been attenuated by the full wall thickness. The factor k_{cep} is introduced because the electrons set in motion by the photons have a finite range in the chamber wall i.e, k_{cep} is applied to account for the depth in the wall at which the electrons entering the cavity are produced. k_{cep} corrects for the mean center of electron production.

Starting in the mid 1980s, with newly developed codes and faster computers, it was possible to calculate directly the wall correction factor using Monte Carlo techniques, where the calculated factor k_{wall} included k_{cep}. Rogers and Bielajew [25] found that the calculated values of k_{wall} were significantly different (up to 1%) from those determined by linear extrapolation in combination with k_{cep} for spherical chambers. Bielajew [24] showed that linear extrapolation of experimental data for spherical chambers are inappropriate owing to the curvature of the chamber walls. A simple nonlinear theory was constructed for the spherical chambers. Using this nonlinear extrapolation of the measured data led to reasonable agreement with the

Monte Carlo calculations. Other recent studies [22, 27, 28] provide evidence that linear extrapolation technique is inadequate in measuring the wall correction factor. McCaffrey et al [21] explored the clear evidence that Monte Carlo calculations provide directly more consistent and accurate value of k_{wall} correction factor; and linear extrapolation techniques used to derive k_w correction factors introduce significant errors. The principle of Monte Carlo approach is illustrated in Fig. 4.17 from which the following equations become evident:
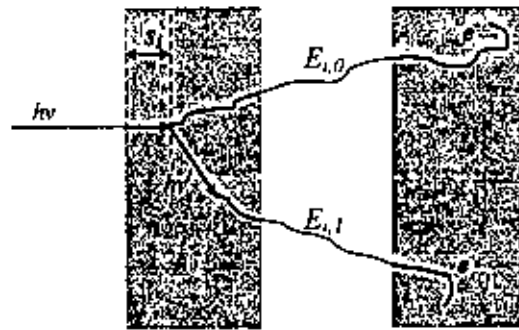
Fig 4.17 Schematic diagram of the successive events that occur if a photon of energy $h\nu$ enters in the wall of a cavity chamber

According to Fig. 4.17 a photon of energy $h\nu$ enters in the wall of a cavity chamber. After a path of length s_i, the first interaction occurs producing a scattered photon of energy $h\nu'$ and an electron, which travels through the cavity and deposits energy $E_{i,0}$ in the cavity air. The scattered photon interacts within the wall and produces an electron which travels through the cavity, thereby depositing energy $E_{i,1}$ in the cavity air.

Correction factor for attenuation of γ-rays in the chamber electrodes is

$$k_{atten} = \frac{\sum_i E_{i,0} e^{\mu_i s_i}}{\sum_i E_{i,0}} \qquad (4.4)$$

74

Correction factor for γ-rays scattered by the chamber electrodes is

$$k_{scatt} = \frac{\sum_i E_{i,0}}{\sum_i \left(E_{i,0} + E_{i,1}\right)} \tag{4.5}$$

The energy $E_{i,0}$ is the deposited energy in the cavity air by electrons generated from the ith primary photon interaction and is weighted by $e^{\mu_i s_i}$, where μ_i is the linear attenuation coefficient and s_i is the path length of the ith primary photon in the graphite wall. The weighted sum is the total energy that would be deposited in the cavity air by electrons if there is no photon attenuation in the chamber wall. The correction factor for photon attenuation in the wall is this weighted sum divided by the total energy deposited in the cavity by electrons of the first generation when photons are attenuated in the wall. The correction factor for the increase in deposited energy in the cavity air due to electrons generated from scattered photons in the wall is the total energy deposited in the cavity by first-generation electrons divided by the sum of the total energy deposited in the cavity by electrons of the first generation and those of the higher generations, expressed in eqn. (4.5). From eqn. (4.4) it is obvious that factor k_{cap} is included in the calculation of k_{atten}. The wall correction factor k_{wall} is the product of the two factors k_{atten} and k_{scan}, which are the corrections for γ-ray attenuation in the chamber walls and for scattered γ-ray contributions to chamber responses respectively. So, the wall correction factor

$$k_{wall} = k_{atten} \times k_{scan}$$

i.e.,

$$k_{wall} = \frac{\sum_i E_{i,0} e^{\mu_i s_i}}{\sum_i \left(E_{i,0} + E_{i,1}\right)} \tag{4.6}$$

The values of k_{atten}, k_{scan} and k_{wall} are calculated for spherical, cylindrical and pancake ionization chambers using the EGS5 program [34] that simulates these

different type cavities with six different sizes in ^{137}Cs and ^{60}Co γ-ray fields. Same type of chambers has the same shape but different size. The inner diameter of the cavity of the smallest spherical chamber is 20 mm; the inner diameter and the length of the smallest cylindrical chamber are 20 mm and 25 mm respectively and those of the smallest pancake chamber are 40 mm and 4 mm respectively. The size ratio between adjacent size chambers is 1.5 for spherical and cylindrical ionization chambers and is 1.4 for pancake chambers. In the calculation, the inner electrodes (i.e. the charge collector) are ignored. The chambers are made with graphite of density 1.82 gcm^{-3}. Wall thicknesses are assumed to be 1.2 mm for ^{137}Cs γ-rays (i.e. for 662 keV) and 3.3 mm for ^{60}Co γ-rays (i.e. for 1173 keV and 1332 keV). The cavity air pressure is assumed to be 101.325 kPa and temperature 22°C. It is also assumed that the flat walls of pancake ionization chambers are fixed perpendicular to parallel and uniform γ-ray beam and that of cylindrical chambers are fixed at 45° with the direction of the γ-ray beam as shown in Fig. 4.18.
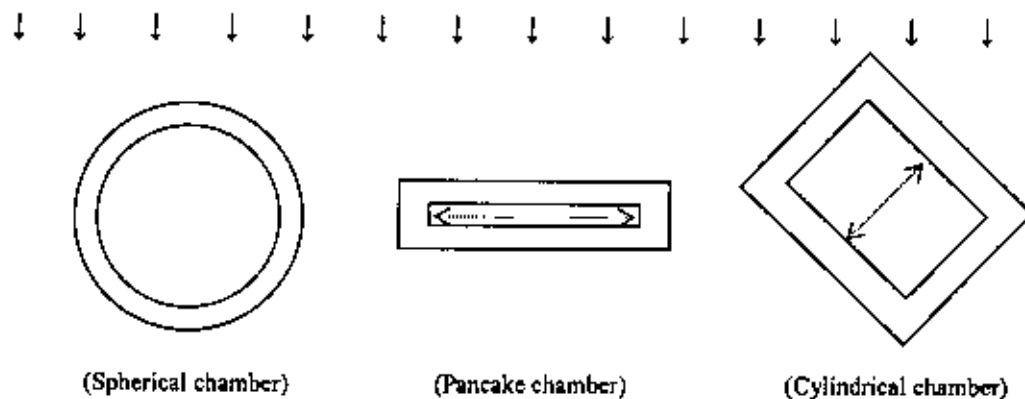
Fig. 4.18 Chamber positioning with respect to the beam direction for different types of ionization chambers

Spherical ionization chambers:

Inner diameter = 20, 30, 45, 67.5, 101.25, 151.87 mm (i.e., 1.5 time step)

Pancake (Parallel Plate) ionization chambers

Inner separation (I. S.) = 4, 5.6, 7.84, 10.97, 15.36, 21.51 mm (i.e., 1.4 time step)

Inner diameter (I.D.) = 40, 56, 78.4, 109.76, 153.66, 215.12 mm (i.e., I.D.=I. S.×10)

Cylindrical ionization chambers

Inner diameter (I.D.) = 20, 30, 45, 67.5, 101.25, 151.87 mm (i.e., 1.5 time step)

Inner length (I.L.) = 25, 37.5, 56.25, 84.375, 126.56, 189.84 mm
(i.e., I.L.=I.D.×1.25)

4.10 Average Mass Collision Stopping Power Ratio for the Ionization Chambers in ^{137}Cs and ^{60}Co γ-ray Beams

Values of the average mass collision stopping power ratio are essential for absolute air kerma rate measurement in ^{137}Cs and ^{60}Co γ-ray field. The average value of the rate of energy loss per unit path length x by a charged particle of type Y and kinetic energy T in a medium of atomic number Z is called its stopping power, $(dT/dx)_{Y,T,Z}$. Dividing the stopping power by the density ρ of the absorbing medium is the mass stopping power $(dT/\rho dx)$, in MeVcm^2/g. Total stopping power has two components:

(a) the collision stopping power, which is the average energy loss per unit path length due to inelastic Coulomb collisions with bound atomic electrons of the medium resulting in ionization and excitation;

(b) the radiative stopping power, which is the average energy loss per unit path length due to emission of Bremsstrahlung in the electric field of the atomic nucleus and the atomic electron [3].

The separation of the stopping power into these two components is useful for two reasons. First, the methods used for the evaluation of the two components are quite different. Second, the energy going into the ionization and excitation of atoms is absorbed in the medium rather close to the particle track, whereas most of the energy lost in the form of Bremsstrahlung travels far from the track before being absorbed. In the present study, values of $\bar{s}_{gra}/\bar{s}_{air}$ is obtained for secondary electrons emitted by ^{137}Cs γ-rays and ^{60}Co γ-rays using the EGS5 program [34] that simulates spherical,

pancake and cylindrical cavities of different sizes in ^{137}Cs and ^{60}Co γ-ray fields. The simulated ionization chambers and its positioning with respect to beam direction are considered same as those used to determine the values of k_{wall} .

4.11 Dependence of the Mass Energy Absorption Coefficient Ratio on the Photon Energy

In eqn. (1.7) it is assumed that all the secondary electrons are emitted from the chamber wall i.e. in the graphite. But in large cavity ionization chambers it is thought that some Compton electrons are also emitted from the air in the cavity by the incident γ-rays [35]. Consequently, the last fractional term in eqn. (1.7) should be modified to M which is

$$M = \frac{(\mu_{en}/\rho)_{air}(E_{air} + E_{gra})}{(\mu_{en}/\rho)_{air}E_{air} + (\mu_{en}/\rho)_{gra}E_{gra}}$$

So,

$$M = \frac{[(\mu_{en}/\rho)_{air}/(\mu_{en}/\rho)_{gra}](E_{air}/E_{gra} + 1)}{[(\mu_{en}/\rho)_{air}/(\mu_{en}/\rho)_{gra}](E_{air}/E_{gra}) + 1} \qquad (4.7)$$

where E_{air} and E_{gra} are the energies deposited in the cavity air by photo electrons and Compton electrons emitted from the air and from the graphite wall respectively.

In the present study, values of E_{air}/E_{gra} are also obtained using the EGS5 program [34]. The simulated ionization chambers and the chamber positioning with respect to beam direction are the same as those used for calculation of k_{wall} or average mass collision stopping power ratio in ^{137}Cs and ^{60}Co γ-ray field.

4.12 Angle Dependence Sensitivities for the Fabricated Ionization Chambers

For all the spherical and parallel plate ionization chambers, the reference direction of the chamber is along the collector, i.e. along the stem. Setting an ionization chamber

at 0° means the ionization chamber reference direction is pointing towards the γ-ray source, and at ±90° means reference direction is perpendicular to the γ-ray beam. Usually signal current from all spherical and pancake ionization chambers are measured by fixing the chamber at 90°; only cylindrical ionization chambers which are using at NMIJ/AIST are fixed at 45° during signal current measurement. In order to measure the angle dependence sensitivities of each of the fabricated ionization chambers signal currents are measured at both polarities of applied voltages at different angular positions of the chamber in a wide range of angle e.g., from -120° to +120°. The signal currents are corrected for the temperature 22°C and pressure 101.325 kPa. Sensitivities of each of the fabricated ionization chambers are measured at various source-chamber distances (SCDs) in ^{137}Cs and ^{60}Co γ-ray fields.

4.13 Correction factor to air kerma for the charge of initial ionizing electrons

Air kerma is defined as the quotient of the sum of the initial kinetic energies of all secondary electrons liberated by photons, by the mass of air from which the secondary electrons are liberated. The values of initial kinetic energies are generally obtained as the product of W-value of air for the secondary electrons and the number of ion pairs produced in the ionization chamber. The signal current from ionization chambers, however, consists of not only the charge of ion pairs but also the charge of the ionizing secondary electrons, i.e. photoelectrons, Compton electrons and Auger electrons, and the charge of positive ions which are formed by the release of these secondary electrons.

Values of the correction factor to air kerma and exposure measured by free air ionization chambers for the charge of these ionizing electrons and ions were calculated for photons with energies in the range from 1 keV to 400 keV [36]. In the calculation, the effects of an increase in the W-value of air for low-energy electrons were also taken into consideration. It was found that the correction factor for air kerma has a maximum value near photon energy of 30 keV and it was found to be 0.9951 for a spectrum with a mean energy of 7.5 keV which is the reference x-ray spectrum with the lowest mean energy in ISO 4037-1 [37]. The correction factor

increases monotonically from the minimum value 0.9977 with photon energy in the range larger than 65 keV.

Similar corrections are presumable for air kerma and exposure measured by cavity ionization chambers. In a case of a cavity ionization chamber with a very small cavity, all ionizing electrons i.e. photoelectrons, Compton electrons and Auger electrons are emitted from the wall material i.e., graphite. Some of these electrons stop in the cavity air and contribute to the signal current. As the energies and numbers of Auger electrons from graphite and air (N, O, Ar atoms) are not the same, the values of correction factors must be different for free air ionization chambers and for cavity ionization chambers. Cavity ionization chambers are used for absolute measurement of relatively high energy photons. Consequently, the ratio of the number of ionizing electrons to the total number of ion pairs produced is small and the correction factor must be very close to 1. In the present work of air kerma measurement using cavity ionization chambers, the correction for the charge of these ionizing electrons is disregarded.

4.14 Absolute Air Kerma Rate Measurement in the γ-ray Field using Different Type of Ionization Chambers

The absolute value of air kerma rate in the ^{60}Co and ^{137}Cs γ-ray fields is determined at various source-chamber-distances (SCDs) using the cylindrical, spherical and pancake ionization chambers. For this determination ionization current is measured by setting the spherical and pancake ionization chambers perpendicularly with the parallel and uniform γ-ray beam direction and the cylindrical chambers are fixed at 45° with the direction of the γ-ray beam. Ionization current is measured at both polarities of the applied voltage of the chamber and average of the absolute value of the ionization currents at both polarities of the applied voltage is used as the signal current during absolute air kerma measurement. From the signal current the absolute air kerma in the γ-ray field is obtained using eqn. (1.7).

$$\dot{K} = \frac{I}{m} \frac{(W/e)}{(1-g)} \frac{\bar{s}_{gra}}{\bar{s}_{air}} \frac{(\mu_{en}/\rho)_{air}}{(\mu_{en}/\rho)_{gra}} \prod k_j$$

Chapter V

Results and Discussion

Chapter V

Results and Discussion

5.1 Ionization Volume of the Fabricated Ionization Chambers

The ionization volume of the fabricated chambers is given in Table 5.1. The uncertainty U of the total ionization volume V_i measurement for all the fabricated ionization chamber in the present study is obtained by the following equation:

$$U = \frac{\sqrt{\left(U_m \times V\right)^2 + \left(U_s \times A_s\right)^2}}{V_i} \times 100\%$$

where U_m is the uncertainty in the ionization volume measurement of the spherical or disk part of the chamber (V) and the U_s is the uncertainty in the ionization volume measurement in the stem part of the chamber (A_s).

Table 5.1 Ionization volume in different parts of the fabricated ionization chambers

Chamber type & symbol		Ionization volume in the spherical/ disk part V (mm^3)	Ionization volume in the neck part (mm^3)	Ionization volume in the stem part of the chamber A_s (mm^3)	Total ionization volume of the chamber V_i (cm^3)	Uncertainty of total ionization volume U (%)
Spherical	S7A	7188.37	28.28	23.19	7.2398	0.01
	S60A	65038.32	31.11	25.46	65.095	0.01
	S60B	65038.32	31.10	25.46	65.095	0.06
	S900A	899608.02	57.78	16.31	899.68	0.04
Pancake	P9A	8851.82	21.11	24.69	8.8976	0.13
	P9B	8851.82	21.11	24.69	8.8976	0.13
	P60A	60651.07	28.27	22.18	60.702	0.07
	P60B	60651.07	28.27	22.18	60.702	0.07

81

In the case of spherical chambers, uncertainty U_m is estimated from the standard deviation of the measured radius of the chamber. In the case of pancake ionization chamber U_m is estimated from the standard deviation of the measured radius of the chamber and that for the height of the chamber.

The uncertainty in the measurement of ionization volume in the stem part of the chamber is less than 10% for all ionization chambers in the present study and it is obtained from the stem current measurement using two types of stem cover.

5.2 Ion Loss within the Fabricated Ionization Chambers

Figs 5.1-5.3 show the signal current ratio $I_V / I_{V/n}$ variation with I_V obtained for the ionization chambers A5, S7A and S60A respectively. A5 is a spherical ionization chamber of ionization volume about 100 cm³, which is a commercial product by Exradin. For each chamber, the value of A is obtained from the intercept on the y-axis by the lines fitted to the plotted data and the volume recombination factor $m^2 g$ is obtained from the slope of the lines. Tables 5.2–5.8 show the values of A and $m^2 g$ for various ionization chambers at different applied voltages in the present study.

Voltages for $I_V/I_{V/n}$

1: 600/150
2: 400/150
3: 300/150
4: 600/200
5: 200/150
6: 400/200
7: 300/200
8: 600/300
9: 400/300
10: 600/400
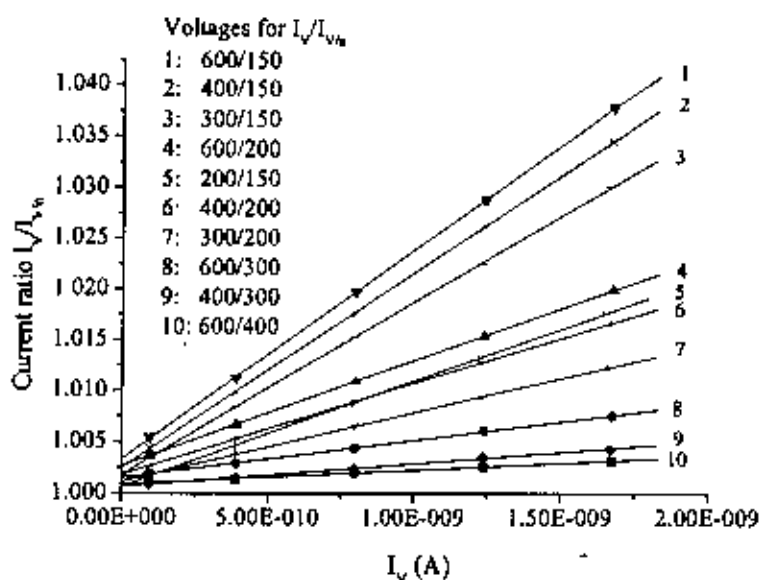
Fig. 5.1 Ratios of the signal currents measured at different applied voltages for the A5 Ionization Chamber are shown as a function of the current measured for higher applied voltages

82
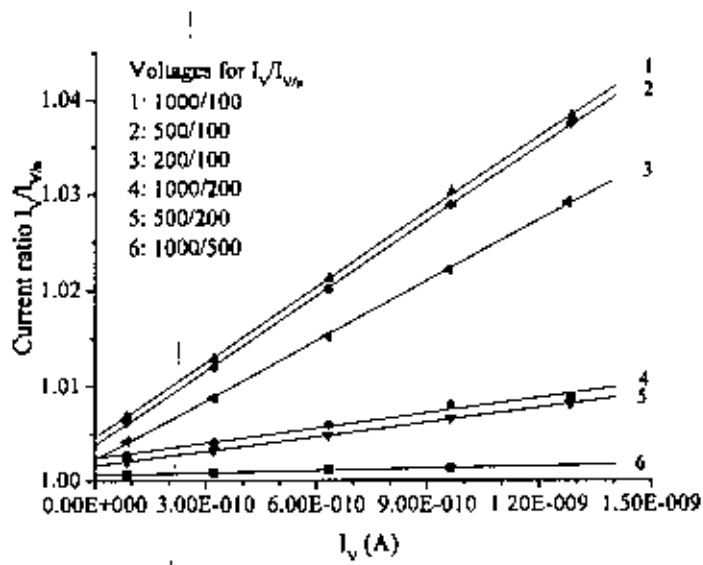
Fig 5.2 Ratios of the signal currents measured at different applied voltages for the
S7A Ionization Chamber are shown as a function of the current measured
for higher applied voltages
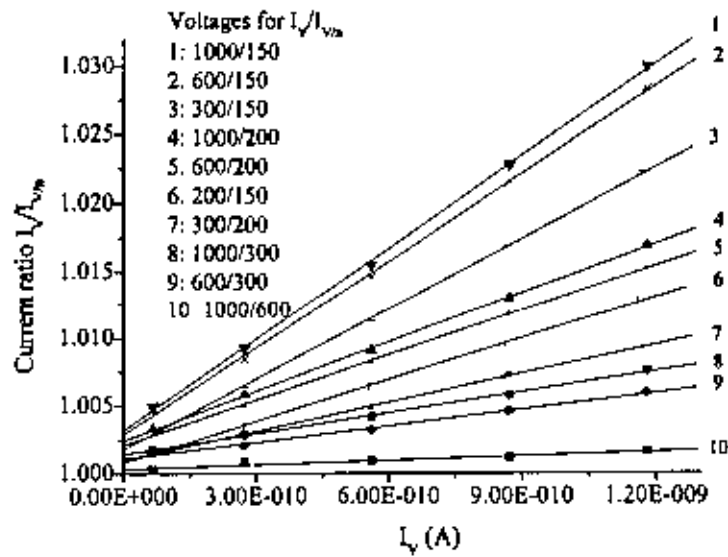
Fig. 5.3 Ratios of the signal currents measured at different applied voltages for the
S60A Ionization Chamber are shown as a function of the current measured
for higher applied voltages

83

Table 5.2 Values of A and m^2g for A5 Ionization Chamber

V (Volt)	V/n (Volt)	A(V)	m^2g (s C^{-1}V^2)
600	400	1.044±0.048	(3.975±0.114)E+11
	300	0.912±0.037	(4.324±0.072)E+11
	200	0.795±0.006	(4.635±0.009)E+11
	150	0.66±0.019	(4.937±0.023)E+11
400	300	0.78±0.085	(4.573±0.144)E+11
	200	0.712±0.017	(4.752±0.022)E+11
	150	0.583±0.019	(5.024±0.021)E+11
300	200	0.678±0.039	(4.812±0.046)E+11
	150	0.534±0.030	(5.087±0.030)E+11
200	150	0.39±0.050	(5.280±0.043)E+11

Table 5.3 Values of A and m^2g for S7A Ionization Chamber

V (Volt)	V/n (Volt)	A(V)	m^2g (s C^{-1}V^2)
1000	500	0.61±0.021	(2.568±0.118)E+11
	200	0.603±0.071	(2.227±0.151)E+11
	100	0.514±0.021	(2.655±0.025)E+11
500	200	0.53±0.016	(2.453±0.029)E+11
	100	0.476±0.021	(2.718±0.022)E+11
200	100	0.444±0.034	(2.791±0.029)E+11

Table 5.4 Values of A and m^2g for S60A Ionization Chamber

V (Volt)	V/n (Volt)	A(V)	m^2g (s C^{-1}V^2)
1000	600	0.48±0.187	(6.057±0.985)E+11
	300	0.609±0.039	(5.042±0.126)E+11
	200	0.605±0.029	(5.082±0.068)E+11
	100	0.566±0.037	(5.171±0.068)E+11
600	300	0.66±0.078	(4.825±0.218)E+11
	200	0.63±0.051	(5.002±0.107)E+11
	100	0.578±0.057	(5.132±0.096)E+11
300	200	0.594±0.033	(5.111±0.056)E+11
	100	0.534±0.046	(5.207±0.065)E+11
200	100	0.474±0.070	(5.271±0.086)E+11

Table 5.5 Values of A and m^2g for S60B Ionization Chamber

V (Volt)	V/n (Volt)	A(V)	m^2g (s C^{-1}V^2)
1000	600	0.69±0.185	(5.717±3.806)E+11
	300	0.703±0.076	(4.830±0.964)E+11
	200	0.698±0.011	(4.949±0.113)E+11
	100	0.621±0.015	(5.523±0.117)E+11
600	300	0.624±0.044	(5.453±0.539)E+11
	200	0.582±0.049	(5.725±0.454)E+11
	100	0.538±0.051	(5.944±0.375)E+11
300	200	0.54±0.080	(5.886±0.588)E+11
	100	0.489±0.061	(6.084±0.375)E+11
200	100	0.438±0.066	(6.220±0.351)E+11

Table 5.6 Values of *A* and *m²g* for S900A Ionization Chamber

V (Volt)	V/n (Volt)	A(V)	m^2g (s C^{-1}V^2)
1000	600	1.575±0.118	(1.233±0.208)E+12
	400	1.160±0.113	(1.427±0.152)E+12
	300	1.217±0.069	(1.215±0.074)E+12
600	400	0.828±0.297	(1.523±0.335)E+12
	300	1.074±0.142	(1.209±0.133)E+12
400	300	1.332±0.095	(0.980±0.077)E+12

Table 5.7 Values of *A* and *m²g* for P9A Ionization Chamber

V (Volt)	V/n (Volt)	A(V)	m^2g (s C^{-1}V^2)
400	200	0.42±0.008	(5.715±0.931)E+9
	100	0.32±0.005	(1.014±0.423)E+9
	50	0.241±0.004	(6.069±1.882)E+8
200	100	0.24±0.004	(1.063±0.201)E+8
	50	0.209±0.007	(4.118±2.868)E+8
100	50	0.182±0.007	(4.722±2.479)E+8

Table 5.8 Values of A and m^2g for P60A Ionization Chamber

V (Volt)	V/n (Volt)	A(V)	m^2g (s C^{-1}V^2)
700	30	0.134±0.003	(1.814±0.470)E+08
	10	0.111±0.002	(1.872±0.096)E+08
300	30	0.115±0.003	(1.404±0.469)E+08
	10	0.105±0.001	(1.822±0.077)E+08
100	30	0.102±0.002	(1.531±0.306)E+08
	10	0.101±0.001	(1.841±0.071)E+08
30	10	0.100±0.002	(1.879±0.104)E+08

Table 5.9 Average values of A and m^2g for various Ionization Chambers

Ionization chamber	A(V)	m^2g (s C^{-1}V^2)
A5	0.753±0.010	(4.763±0.014)E+11
S7A	0.526±0.018	(2.658±0.025)E+11
S60A	0.587±0.028	(5.136±0.053)E+11
S60B	0.655±0.016	(5.355±0.147)E+11
S900A	1.259±0.087	(1.158±0.091)E+12
P9A	0.259±0.004	(7.759±2.130)E+8
P60A	0.107±0.001	(1.838±0.082)E+8

It is observed from the results that the values of A and m^2g for a particular ionization chamber are scattered in a relatively wide range. One of the reasons is that the values of A and m^2g is not constant for a particular chamber and change depending on the lifetime of ions [11], i.e. depend on the applied voltage of the ionization chamber. Another important reason for the scattering of the values is that

these values have been obtained from very small differences of signal currents measured at different applied voltages and different air kerma rates.

In order to observe the dependence of ion loss with the chamber size of spherical chamber, let us consider a spherical ionization chamber of volume V_s with the spherical wall outer radius a and collector radius b as shown in Fig. 5.4.
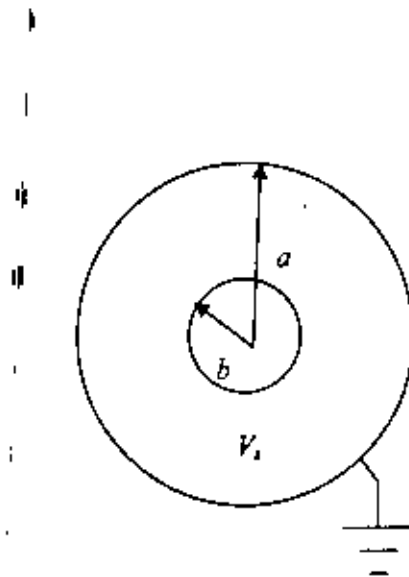
Fig. 5.4 Cross-sectional view of the spherical ionization chamber

If V is the applied voltage to the chamber then at a distance r from the center of the chamber the electric field strength E_r is

$$E_r = \frac{V}{r^2(1/b - 1/a)}$$

As the electric field strength varies with the distance r from the center of the spherical chamber, so the average electric field strength E_{avg} within the chamber volume is considered.

The average field strength E_{ava} within the spherical volume of the chamber is

$$E_{ava} = \int_b^a \frac{4\pi r^2 V}{r^2(1/b - 1/a)} dr \bigg/ \left(\frac{4\pi}{3}(a^3 - b^3)\right)$$

$$= \frac{4\pi Vab}{(a-b)} \int_b^a dr \bigg/ \left(\frac{4\pi}{3}(a^3 - b^3)\right)$$

$$= \frac{3abV}{(a^3 - b^3)}$$

If $b << a$, then neglecting b^3 in the denominator

$$E_{ava} = \frac{3bV}{a^2}$$

The initial recombination loss is inversely proportional of the electric field strength and volume recombination loss is inversely proportional to the square of the electric field strength. So, the above equation shows that both initial and volume recombination loss depends on the ratio of the outer and inner electrode radii and also the size of the spherical ionization chamber. Since average electric field strength within the spherical ionization chamber becomes smaller for larger size ionization chamber, the initial and volume recombination loss become larger for larger size spherical ionization chambers.

Ions are lost by back diffusion if they are produced near the vicinity of the electrode where the electrostatic potential difference from the electrode is less than kT/e, where e is the elementary charge, k the Boltzmann constant and T the absolute temperature of air within the chamber. Since the electric field strength near the central electrode is high, as a result the diffusion loss is negligible there and we can neglect the diffusion loss at the central electrode. So, the back diffusion loss takes place mainly at the surface of the outer electrode of the chamber.

The electric field strength at the outer electrode of the spherical chamber E_a is

$$E_a = \frac{V}{a^2(1/b - 1/a)}$$

$$= \frac{abV}{a^2(a-b)}$$

$$= \frac{bV}{a(a-b)}$$

Since for spherical ionization chamber, diffusion loss is inversely proportional to the electric field strength at the outer electrode E_a and the surface area of the outer electrode. The ion loss due to diffusion compared to the total ion-pairs produced within the ionization volume is proportional to

$$\frac{a(a-b)}{bV} 4\pi a^2 \bigg/ \left(\frac{4\pi}{3}(a^3 - b^3)\right)$$

$$= \frac{3a^3(a-b)}{bV(a^3 - b^3)}$$

$$= \frac{3a^3}{bV(a^2 + ab + b^2)}$$

If $b \ll a$ then it becomes $\dfrac{3a}{bV}$

Therefore, ion loss due to diffusion compared to the total ion pairs produced in the ionization volume of the chamber also depends on the ratio between the outer and inner electrode radii of the spherical ionization chamber.

Ion loss within an ionization chamber due to initial recombination and diffusion would be calculated by the average values of A and that by volume recombination obtained by the average value of $m^2 g$, which are presented in Table 5.9. Average

values of A and m^2g for a given ionization chamber are obtained from the values of A and m^2g at different applied voltages and n values by weighing with the inverse of uncertainties of the results. It can be observed from the table that the values of A and m^2g are larger for larger volume spherical ionization chambers, viz, in the order of S7A, S60A(B), and S900A. The reason for the increase of these values is expected due to the difference of the ratio between the outer electrode radius the collector electrode radius, (which are: 12/1=12 for S7A, 25/2.5=10 for S60A (B), and 60/6=10 for S900A) and the outer electrode radius. If the applied voltage to all the spherical chambers in the present study is same then the diffusion loss in S7A is greater than that of other spherical chambers such as S60A, S60B and S900A and the ion loss due to diffusion is same for S60A, S60B and S900A ionization chambers.

Since for larger volume spherical chamber the initial recombination loss is larger, so if the applied voltage to the chamber S60A(B) and S900A are same then the initial recombination loss in S900A Ionization Chamber is larger than S60A(B) Ionization Chambers. For this reason it has been seen from Table 5.9 that the value of A for S900A is larger than that of other spherical chambers S60A(B) in the present study.

Separation between the electrodes of pancake ionization chambers P9A and P60A is very small. For P9A Ionization Chamber separation between electrodes is (4.8-0.3)/2 = 2.25 mm and that for P60A Ionization Chamber is (8-0.3)/2 = 3.85 mm. In the case of P9A Ionization Chamber, the uncertainty in the measurement of recombination parameter is large. This is due to very small loss of signal currents from P9A Ionization Chamber. In the case of pancake ionization chambers, both the values for A and m^2g are larger for smaller chamber P9A than for larger chamber P60A. This may be due to large ion losses at the corners of the ionization volume where the electric field strength is relatively small. The percentage of the corner volume is larger for the smaller ionization chamber, P9A, than that for the larger ionization chamber P60A.

5.3 Stem Correction Factor of the Fabricated Ionization Chambers

Table 5.10 shows the stem correction factor of the fabricated ionization chambers. It is clear from the table that the stem scattering effect is larger for smaller volume ionization chambers. This is because the stem is nearer to the chamber volume for smaller volume ionization chambers than for larger volume ionization chambers and the relative effect of scattered γ-rays becomes larger due to the inverse square law.

Table 5.10 Stem correction factor of the fabricated ionization chambers

Chamber Type	γ-ray	Stem correction factor	Stem correction (%)
S7A	^{137}Cs	0.99382±0.00065	0.6181
	^{60}Co	0.99587±0.00096	0.4130
S60A	^{137}Cs	0.99687±0.00074	0.3134
	^{60}Co	0.99791±0.00027	0.2090
S60B	^{137}Cs	0.99556±0.00050	0.4445
S900A	^{137}Cs	0.99851±0.00042	0.1489
	^{60}Co	0.99929±0.00013	0.0706
P9A	^{137}Cs	0.99662±0.00041	0.3377
	^{60}Co	0.99838±0.00049	0.1617
P60A	^{137}Cs	0.99855±0.00010	0.1455
	^{60}Co	0.99909±0.00018	0.0906

5.4 Wall Correction Factors of Various Ionization Chambers

Figs. 5.5 and 5.6 show the calculated results of the correction factors k_{atten}, k_{scatt} and k_{wall} for spherical and pancake ionization chambers. It is noticed from the figures that the changes of the correction factors with the size of the chamber are relatively
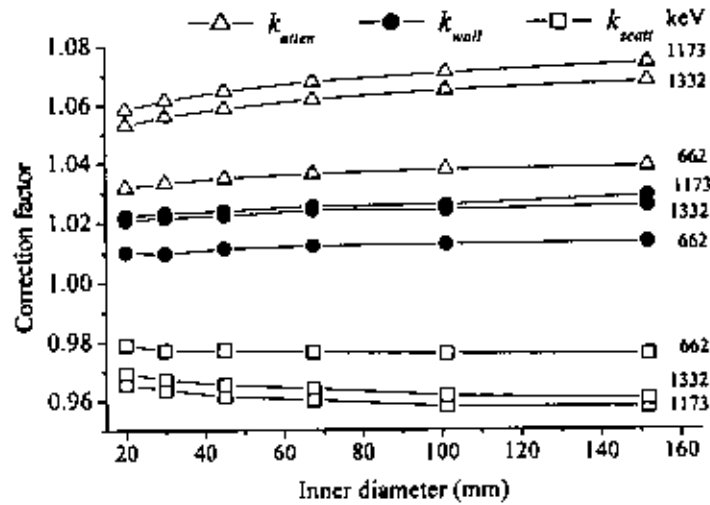
Fig. 5.5 Correction factors k_{atten}, k_{scatt} and k_{wall} for spherical ionization chambers of different sizes at various γ-ray energies. Numbers in the figure are the γ-ray energies in keV
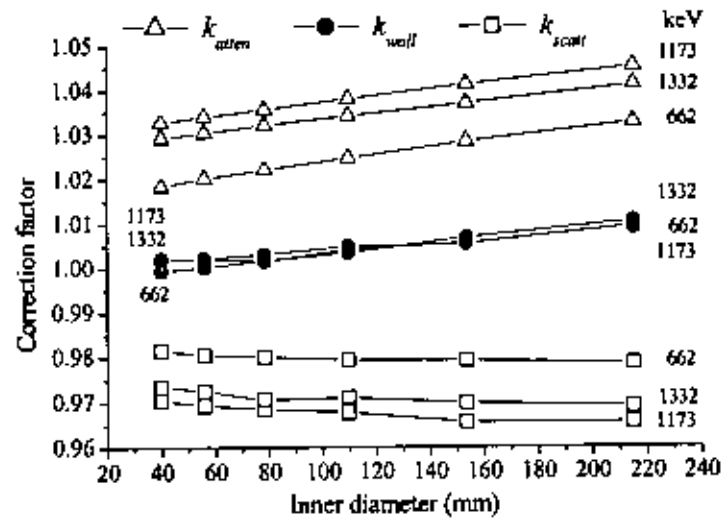
Fig. 5.6 Correction factors k_{atten}, k_{scatt} and k_{wall} for pancake ionization chambers of different sizes at various γ-ray energies. Numbers in the figure are the γ-ray energies in keV

small for pancake chambers than for spherical chambers. This is because the pass length of γ-rays in the flat walls does not change with the chamber size for pancake chambers and is shorter than that of the spherical chambers. Moreover, the correction

Table 5.11 Correction factors k_{atten}, k_{scatt} and k_{wall} of various ionization chambers

Chamber type & model		γ-rays	γ-ray energy (keV)	k_{atten}	k_{scatt}	k_{wall}
Spherical	S7A	^{137}Cs	662	1.0805	0.9551	1.0319
		^{60}Co	1173	1.0580	0.9683	1.0244
			1332	1.0526	0.9713	1.0224
	S60A	^{137}Cs	662	1.0904	0.9490	1.0348
		^{60}Co	1173	1.0690	0.9644	1.0309
			1332	1.0632	0.9675	1.0286
	S60B	^{137}Cs	662	1.0417	0.9778	1.0186
	S900A	^{137}Cs	662	1.1110	0.9440	1.0488
		^{60}Co	1173	1.0835	0.9596	1.0397
			1332	1.0768	0.9628	1.0367
Pancake	P9A	^{137}Cs	662	1.0456	0.9609	1.0047
		^{60}Co	1173	1.0303	0.9746	1.0042
			1332	1.0269	0.9771	1.0034
	P9B	^{137}Cs	662	1.0151	0.9822	0.9971
	P60A	^{137}Cs	662	1.0463	0.9598	1.0042
		^{60}Co	1173	1.0308	0.9727	1.0027
			1332	1.0274	0.9743	1.0009
	P60B	^{137}Cs	662	1.0156	0.9817	0.9970
Cylindrical	C6	^{137}Cs	662	-	-	1.0166 [7]
		^{60}Co	1225	-	-	1.0198 [7]
	C62	^{137}Cs	662	-	-	1.0192 [7]
		^{60}Co	1225	-	-	1.0209 [7]

for attenuation and scattering compensate each other and k_{wall} becomes close to 1 for both ^{137}Cs and ^{60}Co γ-ray energies in the case of pancake chambers. This is consistent with the calculated results given in reference [38]. The results for cylindrical chambers of NMIJ/AIST, which are being used as the national standard devices for air kerma measurement at the Primary Standard Dosimetry Laboratory given in reference [7], and are nearly the same as those for spherical chambers. Values of k_{atten}, k_{scatt} and k_{wall} obtained for all NMIJ/AIST chambers are listed in Table 5.11. In the calculation of these values effects of inner electrode are taken into consideration.

5.5 Average Mass Collision Stopping Power Ratio for Ionization Chambers in ^{137}Cs and ^{60}Co γ-ray Beams

Fig. 5.7 shows the results of calculation for the ratio between the average mass collision stopping powers of air and graphite for electrons entering into the cavity of each type of ionization chambers. In calculation inner electrodes i.e. the charge collector of the chamber is ignored. Only the results for the smallest and the largest size chambers for each type of ionization chamber are plotted in Fig. 5.7. The abscissa of the figure shows the lowest cutoff energy for electrons in the calculation. It is noticed from the figure that there is very little variation in the results of the different chamber sizes for all the three types of ionization chamber, i.e. the stopping power ratio does not depend on the chamber size. The figure also shows that the results for cylindrical chambers are similar to those of spherical chambers. The values for pancake chambers, however, are slightly smaller than those for the other two types. This is because more secondary electrons enter into the pancake cavity from the front wall of the chamber and the energy of these electrons are higher than those of the secondary electrons which drift perpendicular to the γ-ray direction. So it can be concluded that the energy spectra and angular distributions of secondary electrons depend on the direction of the secondary electrons and are not affected by the dimensions of the cavity. If the values of stopping power are weighted by the passlength of the secondary electrons in pancake cavities, the value of $\bar{s}_{gra}/\bar{s}_{air}$ for pancake cavities become identical to those for spherical cavities, for which the values

95

of stopping power are weighted isotropically. Consequently, the results of $\bar{s}_{gra} / \bar{s}_{air}$ obtained in electronic equilibrium condition for spherical chambers could be
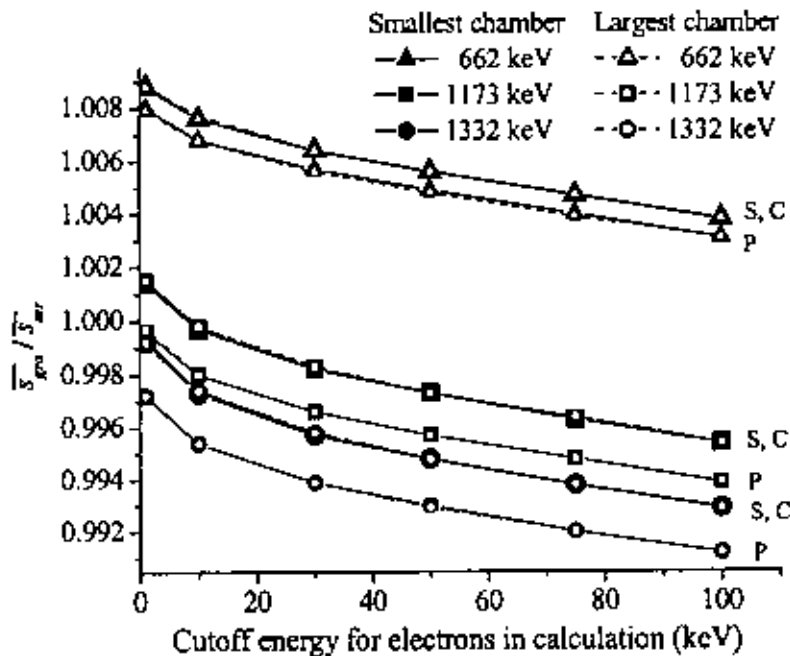
Fig. 5.7 Average mass collision stopping power ratio for electrons that enter into the cavity for each type of ionization chambers: spherical (S), cylindrical (C) and pancake (P). The results for spherical chambers, which are shown by slightly larger symbols, correspond to $\bar{s}_{gra} / \bar{s}_{air}$ for all types of ionization chambers

used for absolute air kerma measurement by any type of ionization chambers. It has also been noticed from Fig. 5.7 that $\bar{s}_{gra} / \bar{s}_{air}$ decreases with the increase of the incident photon energy viz. 662 keV, 1173 keV and 1332 keV and it also decreases as the cutoff energy for electrons in calculation increases. Rogers and Kawrakow [39] have noticed the similar type of dependence by performing calculations for a cylindrical ionization chamber in ^{60}Co γ- ray fields.

Secondary electrons having a penetration depth in air shorter than the cavity size deposit all their energies in the cavity air when they enter into the cavity. Thus, it is

reasonable to determine the value of $\bar{s}_{gra}/\bar{s}_{air}$ for an ionization chamber from the cutoff energy for which the projected range of electrons in air corresponds to the mean chord length $\bar{l}$ of the cavity. The projected range of electrons is the mean depth of the deepest points which the electrons reach in the direction of injection. The mean chord length of a volume is the mean length of randomly oriented chords in that volume and is equal to $4V/A$, where V is the volume and A is the surface area [3]. The surface of inner electrode is included in A during calculation of $\bar{l}$ for the ionization chambers constructed at NMIJ/AIST.

The projected range of electrons in air is calculated using the EGS5 program because there is no published data for low energy electrons. Also the total path length is calculated using this program. The projected range is about 47 % to 50 % of the total path length for electrons having energies in the range from 10 keV to 150 keV. The total path length corresponds to CSDA (continuous slowing down approximation) range and the total path length was about 10 % larger than the CSDA range given in reference [40].

Table 5.12 shows the values for mean chord length $\bar{l}$, the corresponding cutoff energy and $\bar{s}_{gra}/\bar{s}_{air}$ for different ionization chambers of AIST obtained from the data of spherical ionization chambers. The values of $\bar{s}_{gra}/\bar{s}_{air}$ for photons having energies of 1173 keV and 1332 keV are listed separately in the row for [60]Co γ-rays. For absolute measurement of air kerma rate in [60]Co γ-ray field, the mean value of stopping power ratios at 1173 keV and 1332 keV energies would be used because the γ-ray intensities are the same at these two energies.

Table 5.12 Mean chord length $\bar{l}$, cutoff energy and average mass collision stopping power ratio obtained for different ionization chambers

Ionization chamber		Mean $\bar{l}$	Cutoff energy	γ-rays	$\bar{s}_{gra} / \bar{s}_{air}$
Type	Model	(cm)	(keV)		
Spherical	S7A	1.50	40.3	^{137}Cs	1.0060
				^{60}Co	0.9976
					0.9952
	S60A	3.15	60.8	^{60}Co	0.9969
					0.9943
	S60B	3.15	60.8	^{137}Cs	1.0052
	S900A	7.60	101.4	^{137}Cs	1.0038
				^{60}Co	0.9954
					0.9929
Pancake	P9A	0.45	20.6	^{60}Co	0.9989
					0.9964
	P9B	0.45	20.6	^{137}Cs	1.0069
	P60A	0.74	27.2	^{60}Co	0.9983
					0.9959
	P60B	0.74	27.2	^{137}Cs	1.0066
Cylindrical	C6	1.25	36.4	^{137}Cs	1.0067
				^{60}Co	0.9979
					0.9954
	C62	2.76	56.5	^{137}Cs	1.0054
				^{60}Co	0.9970
					0.9945

5.6 Dependence of Mass Energy Absorption Coefficient Ratio on the Size of the Ionization Chamber

Fig. 5.8 shows the calculated values of E_{air}/E_{gra} obtained using EGS5 simulation program for the spherical, cylindrical and pancake ionization chambers at ^{137}Cs and ^{60}Co γ-ray beam energies.
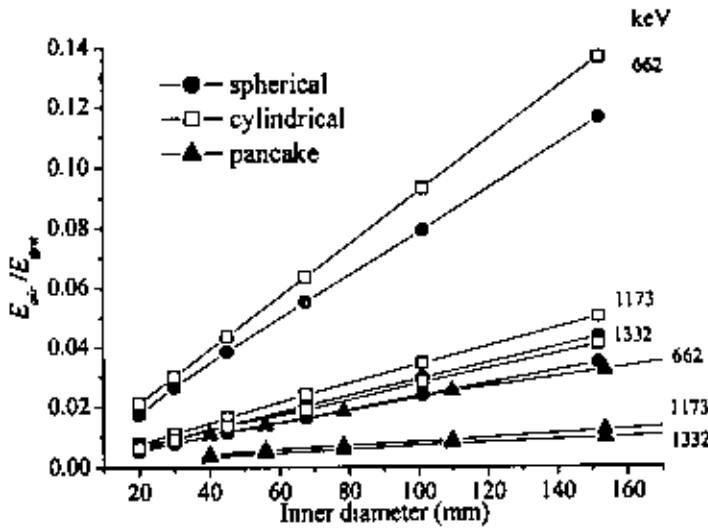
Fig. 5.8 Dependence of E_{air}/E_{gra} on the size of the ionization chamber of different type

It is found from the calculation that the value of E_{air}/E_{gra} increases as the size of the chamber increases. It also increases as the incident photon energy decreases. Lines from the top to downward are results for photons of energies 662 keV, 1173 keV and 1332 keV for each type of ionization chamber. It is known from the figure that E_{air}/E_{gra} for ^{137}Cs γ-rays is 0.09 for the spherical ionization chamber of diameter 12 cm. This chamber is the largest spherical chamber S900A that has been constructed at NMIJ/AIST in the present study.

Because the value of $(\mu_{en}/\rho)_{air}/(\mu_{en}/\rho)_{gra}$ is very close to 1 for ^{137}Cs and ^{60}Co γ-ray beam energies [41], the difference between the value of $(\mu_{en}/\rho)_{air}/(\mu_{en}/\rho)_{gra}$

and the modified factor M is less than 0.01% for $E_{air}/E_{gra} = 0.09$. In the photon with energy range from 200 keV to 3 MeV the values of $(\mu_{en}/\rho)_{air}/(\mu_{en}/\rho)_{gra}$ varies from 0.99 to 1.01; which is shown in Fig. 5.9. Consequently, eqn. (1.7) can be used without any modification if low energy scattered γ-rays are not dominant. For lower energy range photons, however, both the values of $(\mu_{en}/\rho)_{air}/(\mu_{en}/\rho)_{gra}$ and E_{air}/E_{gra} change significantly depending on the photon energy and the difference between the values of $(\mu_{en}/\rho)_{air}/(\mu_{en}/\rho)_{gra}$ and the modified factor M becomes large as shown in Fig. 5.10. On the other hand, the figure shows that the difference between the value of $(\mu_{en}/\rho)_{air}/(\mu_{en}/\rho)_{gra}$ and the modified factor M is small for γ-rays with energies larger than 100 keV. Consequently, eqn. (1.7) can be used without any modification for air kerma measurement in ^{137}Cs and ^{60}Co γ-ray field using cavity ionization chambers.
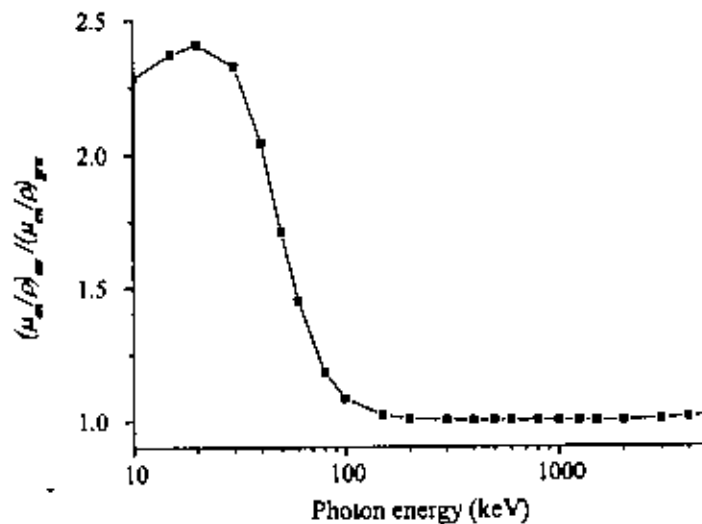
Fig. 5.9 Ratio between the mass energy absorption coefficients for air and graphite at different photon energies
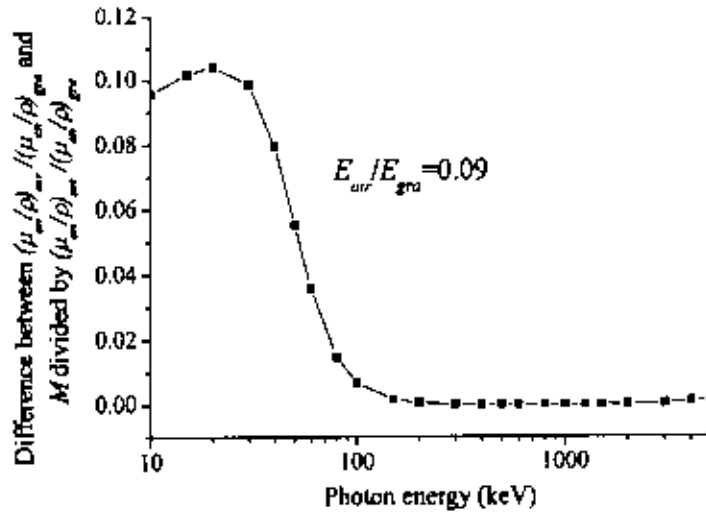
Fig. 5.10 Difference between $(\mu_{en}/\rho)_{air}/(\mu_{en}/\rho)_{gra}$ and M divided
by $(\mu_{en}/\rho)_{air}/(\mu_{en}/\rho)_{gra}$ at different photon energies

5.7 Angle Dependences of the Sensitivities of the Fabricated Ionization Chambers

Fig. 5.11 shows the signal current obtained from the pancake ionization chamber P9A at various angular positions in ^{60}Co γ-ray field at SCD=2m. The filled circular symbols are the results for applied voltage of 400 V, and the empty square symbols for -400 V. Both the results show similar type of angular dependences. The sharp decrease of signal current at 0° is due to attenuation of γ-rays by the collector electrode. In the range of ±50° angular position, the signal current decreases with the angle decreasing to about ±10°. This is due to the increase of attenuation of γ-rays by the side-walls of the chamber because the path length of γ-rays in the side wall becomes longer with the decrease of the angle. Attenuation of γ-rays by the side-walls of the chamber is maximum near ±10° because at that angular position the beam is directed along the side-walls of the chamber. This ionization chamber exhibits similar type of angular dependence in ^{137}Cs γ-ray field at SCD=1m.

Another pancake ionization chamber P60A also exhibits similar type of angular dependence to that of P9A. But in the case of P60A, a very small decrease (0.02 %) of signal current is also noticed at ±90°. This is due to the attenuation of γ-rays by the ring shaped wall electrode of the pancake chamber. For P9A this decrease of signal current is not noticed at ±90°. It is because the ring wall of P9A is short.

Figs. 5.12 and 5.13 show angle dependence sensitivities of spherical ionization chamber S7A in ^{137}Cs γ-ray field at SCD=1m and in ^{60}Co γ-ray field at SCD=2m, respectively. Filled circular symbols show signal currents for positive applied voltage of 1000V, and the empty square symbols show signal currents for negative applied voltage of -1000V. In both the γ-ray fields, signal current for positive applied voltage decreases sharply near 0°. On the other hand, for negative applied voltage signal current has a peak value at 0°. Solid lines show average of the signal currents at both the polarities. The solid lines show that signal current changes slowly about 0.6% in the ^{137}Cs γ-ray field and 0.4% in the ^{60}Co γ-ray field in the range of angle between ±100°.

Fig. 5.14 shows half of the differences between the signal currents of S7A ionization chamber for positive and negative applied voltages at various angular positions. Their values correspond to the differences between the current shown by a solid line and the current for positive or negative applied voltages; which are shown in Figs 5.12 and 5.13. It is noticed in Fig. 5.14 that both the results for ^{137}Cs and ^{60}Co γ-ray fields show sharp decrease at 0°. It is also noticed that the difference between the signals for both polarities is outstanding in the range of angle between ±75° in ^{137}Cs γ-ray field and in ^{60}Co γ-ray field it is ±25°. The diameter of the ^{137}Cs γ-ray beam is about 33cm at SCD=1m and 22cm for ^{60}Co γ-ray field at SCD=2m. It is expected from this fact that the currents shown in Fig. 5.14 are signals from the stem part of the ionization chamber. There may be a small cavity near the connector terminal of the signal cable. The signal from this cavity does not depend on the polarity of the applied voltage; and this cavity is in the γ-ray field when the chamber is at smaller angular position but it is out of the field when the chamber is set in a small diameter γ-ray field and the angle becomes large. The sharp decrease at 0° may be due to attenuation of the γ-ray beam by the stem part of the chamber. The absolute value of

signal currents due to ion pair produced in the ionization volume of the chamber is the same for both polarities of the applied voltage. If the currents shown by the solid lines in Fig. 5.12 and 5.13 correspond to the signal due to the ion pairs produced in ionization volumes, the total signal for positive applied voltage is the sum of the currents shown by the solid lines in Fig. 5.12 (or 5.13) and the current shown in Fig. 5.14. The total signal for negative applied voltage is the currents shown by the solid lines in Fig. 5.12 (or 5.13) minus the current shown in Fig. 5.14; it is because these currents have opposite polarities, since the current from the stem part does not depend on the polarity of the applied voltage. Consequently, the reasons for the sharp decreases of the signal current for positive applied voltage and the increases for negative applied voltage at 0° shown in Fig. 5.12 and 5.13 are clear.

Fig. 5.15 shows the angular dependence of the effects of scattered γ-rays from the stem part of spherical ionization chamber. It is obtained for the spherical ionization chamber S7A by fixing it vertically in ^{60}Co γ-ray field at SCD=2m and a dummy stem with a pipe shaped cover is rotated step by step in a horizontal plane around the central part of the spherical part of the S7A ionization chamber. Fig. 5.15 clearly shows that the effect of scattered γ-rays from the stem becomes maximum when the dummy stem is at ±110°. The increase of the signal with the angle from 0° is consistent with the fact that Compton scattered γ-rays are directed more strongly to the forward direction than to the backward. The signal current decreases for the angle larger than ±110°. This is due to the reason that the stem part then intercepts γ-rays which come from the γ-ray source directly to the ionization chamber head and attenuates the γ-rays. So, it is clear that the maxima of signal currents at ±95° shown in Figs. 5.12 and 5.13 are due to scattered γ-rays from the stem of the chamber S7A. A similar result is obtained for the chamber in ^{137}Cs γ-ray field at SCD=1m.

Figs 5.16 and 5.17 show respectively the angular dependence response of spherical ionization chamber S60B in ^{137}Cs γ-ray field at SCD=4m and S900A Ionization Chamber in ^{60}Co γ-ray field at SCD=6m for positive applied voltages. In the case of all spherical chambers in the present study, the decrease of the signal current at 0° could be expected partly due to the current from the small cavity near the connector terminal of ionization chamber as explained for S7A. However, the decrease of the

signal current at 0° for S60B and S900A are expected mainly due to the attenuation of γ-rays by the collector of the chamber since the decrease of these ionization chambers are much larger than that of S7A and can not be explained as a result of a small cavity near the connector.

The increase of the signal current near ±95°, which is due to scattered γ-rays from the stem of the chamber, is also noticed in Figs. 5.16 and 5.17. The signal due to scattered γ-rays from the stem is relatively large for S7A than that for S60B and S900A. It is because the distance between the stem and the ionization volume of S7A Ionization Chamber is shorter than that of S60B and S900A.
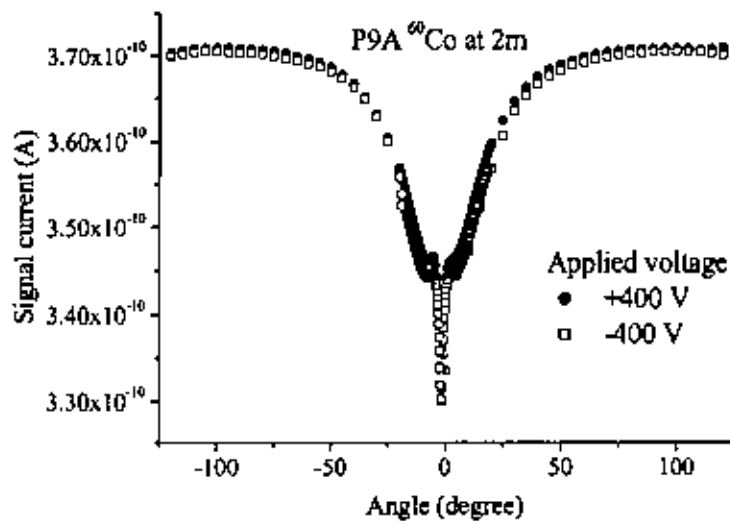
Fig. 5.11 Response of P9A Ionization Chamber at different angular positions in ^{60}Co γ-ray field at SCD = 2 m for both polarities of applied voltage
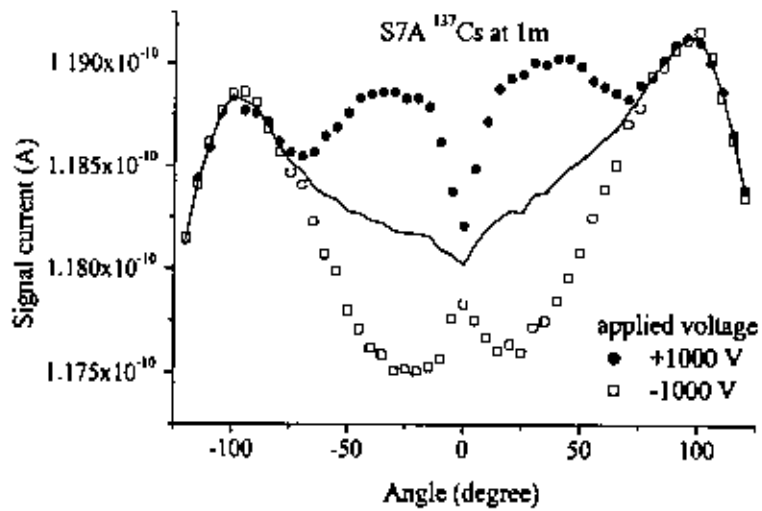
Fig 5.12 Response of S7A Ionization Chamber at different angular positions in ^{137}Cs γ-ray field at SCD = 1m for both polarities of applied voltage
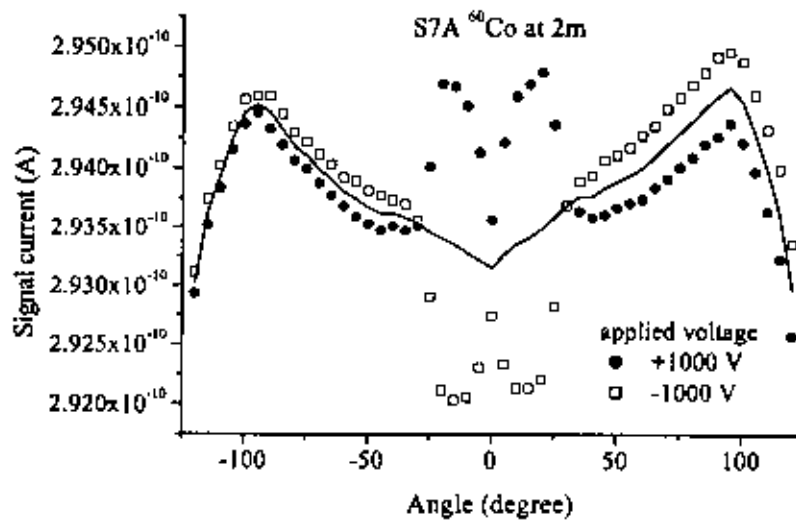
Fig. 5.13 Response of S7A Ionization Chamber at different angular positions in ^{60}Co γ-ray field at SCD = 2 m for both polarities of applied voltage
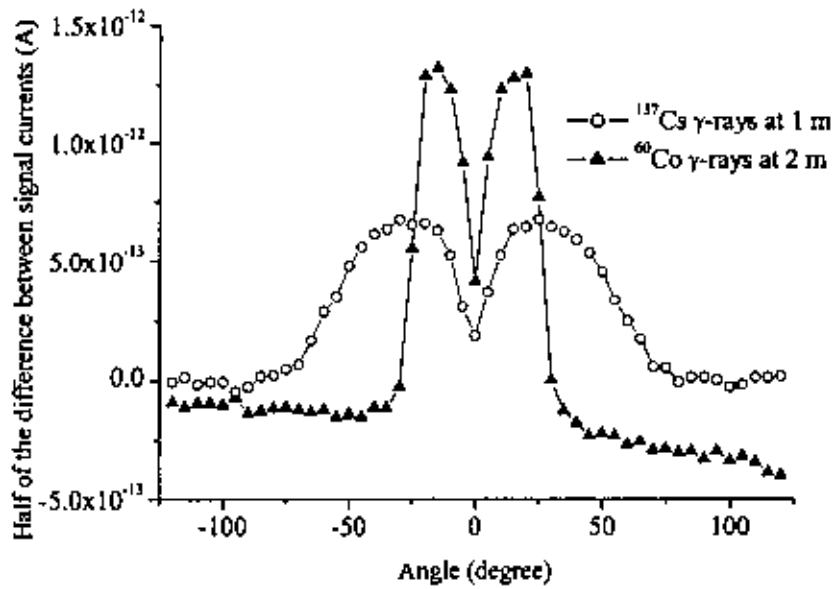
Fig. 5.14 Variation of the half of the difference between signal currents of S7A Ionization Chamber for positive and negative applied voltages in ^{137}Cs γ-ray field at SCD = 1 m and ^{60}Co γ-ray field at SCD = 2 m at different angular positions
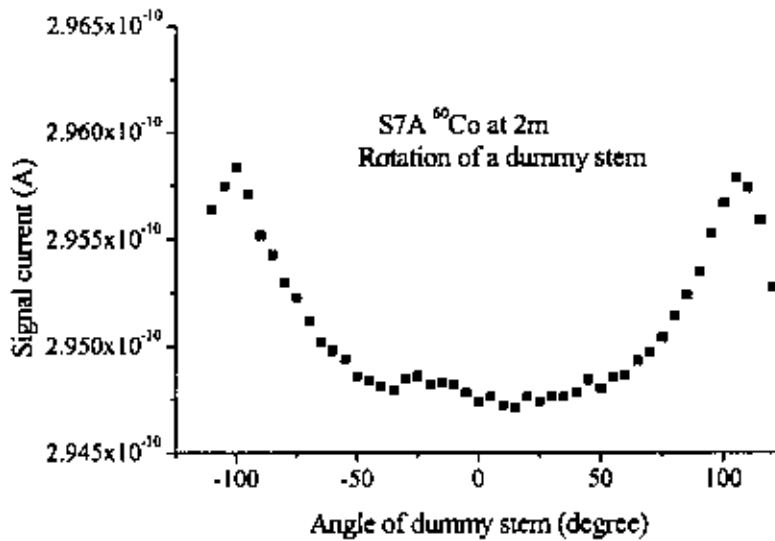
Fig. 5.15 Response of S7A Ionization Chamber which is fixed vertically in ^{60}Co γ-ray field at SCD = 2 m due to rotation of a dummy stem in a horizontal plane around the central part of the chamber

106
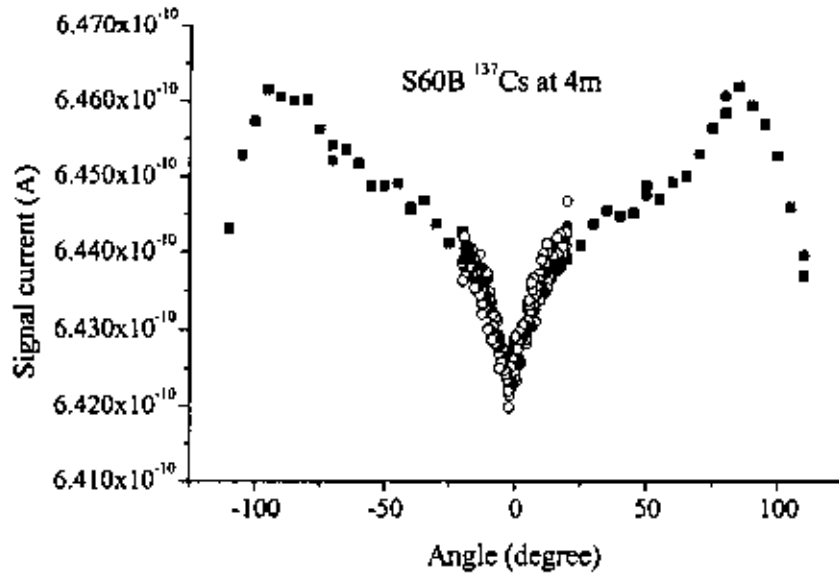
Fig. 5.16 Response of S60B Ionization Chamber at different angular positions in ^{137}Cs γ-ray field at SCD = 4 m for positive applied voltage
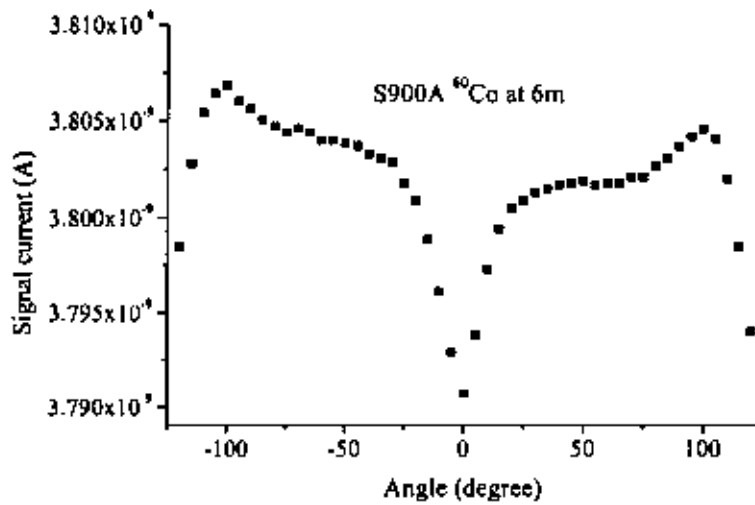
Fig. 5.17 Response of S900A Ionization Chamber at different angular positions in ^{60}Co γ-ray field at SCD = 6 m for positive applied voltage

107

5.8 Absolute Air Kerma Rate Measurement

Table 5.13 presents the absolute values of air kerma rate with their relative uncertainties at various SCDs measured by different type of ionization chambers. The values are converted to those for 25 October 2007 using half lives of 5.2714 years and 30.07 years for ^{60}Co and ^{137}Cs γ-ray sources respectively.

Table 5.13 Absolute air kerma rate measured by different ionization chambers

Chamber identification	Air kerma rate on 25 October 07 (Gy/s) [U: relative expanded uncertainty in % (k=2)] (E_n number obtained when air kerma rate by cylindrical chambers are chosen as reference values)						
	SCD from ^{60}Co source				SCD from ^{137}Cs source		
	1m	4m	6m with 25 mm W	6m with 65 mm W	1m	4m	4m with Fe disc
Cylindrical chamber	3.5440E-03 [0.88]	2.0242E-04 [0.82]	7.7751E-06 [0 86]	2.1584E-07 [0.86]	4.5164E-04 [0.66]	2.7148E-05 [0.66]	8.0020E-06 [0.66]
S7A	3.5303 E-03 [0.40] (-0.40)	2.0139E-04 [0.39] (-0.56)			4.5202E-04 [0.37] (0.11)		
S60A		2.0156E-04 [0.34] (-0.47)	7.7469E-06 [0.38] (-0 39)			2.6939E-05 [0.37] (-1.01)	
S60B						2.6978E-05 [0.39] (-0.82)	7.9488E-06 [0.37] (-0.88)
S900A			7.7738E-06 [0.39] (-0.02)	2.1736E-07 [0.51] (0.70)			7.9972E-06 [0.37] (-0.08)
P9A	3.5431E-03 [0.44] (-0.03)	2.0274E-04 [0.44] (0.17)			4.5288E-04 [0.44] (0.34)		
P9B					4.5273E-04 [0.38] (0.32)		
P60A		2.0330E-04 [0.37] (0.48)	7.7735E-06 [0 40] (-0 02)			2.7371E-05 [0 37] (1 08)	
P60B						2.7151E-05 [0.37] (0.02)	7.9846E-06 [0.38] (-0.28)

The absolute value of air kerma rates at various SCDs in the ^{60}Co and ^{137}Cs γ-ray fields are obtained using eqn. (1.7) by measuring the signal current from the ionization chambers. The chamber signal current is corrected for the temperature 22°C and pressure 101.325 kPa using eqn. (3.13). Humidity range was 27% to 30% throughout the signal current measurement by all types of ionization chambers. The chamber signal current is also corrected for the dry air (i.e. 0 % humidity) using eqn. (3.14). The signal current is corrected for humidity, pressure and temperature at each measurement by the current measuring program automatically.

For determination of absolute value of air kerma rate in the γ-ray field, values of some physical constants and correction factors for each of the fabricated ionization chamber which entered in eqn. (1.7) are required. Values of these physical constants and the correction factors with their relative uncertainties of each of the fabricated ionization chamber are mentioned in Appendix.

The value of air kerma rate obtained by the fabricated ionization chamber for each SCDs are compared with the value obtained by the cylindrical chambers, which are the national standard devices for air kerma measurement at the Primary Standard Dosimetry Laboratory of AIST, Japan. These cylindrical ionization chambers are being used for calibration of the secondary standard ionization chambers and the field type ionization chambers used for different radiotherapy machine output calibration and radiation protection purposes in Japan. It is noticed in the table that all the results obtained by the spherical ionization chambers S7A, S60A and S60B are slightly smaller than those obtained by ionization chambers P9A, P9B, P60A and P60B. It may be partly due to the fact that the collectors of ionization chambers are neglected in the calculation of k_{wall} for the fabricated ionization chambers. It may be also partly due to the fact that the values of stopping power ratio for the cylindrical ionization chambers [7], used during air kerma rate determination, are slightly larger than those shown in Table 5.12, which are obtained in the present work taking into account the chamber size and the cutoff energy for electrons in calculation. In Table 5.13, values in the square brackets show the relative expanded uncertainties (in % and the coverage factor $k=2$) for the values of the air kerma rates obtained in the

present work. It is noticed in the table that the relative uncertainties for all the results obtained by the fabricated ionization chambers are smaller than those obtained by the cylindrical ionization chambers. The value in the parentheses shows the E_n number of each result, when the air kerma rates obtained by cylindrical chambers are chosen as reference values. The E_n number is usually used for measurement comparison and the proficiency testing of calibration abilities of an ionization chamber.

The uncertainty in the air kerma rate measurement by a fabricated ionization chamber arises due to the uncertainty in the:

 -stopping power ratio determination

 - mass energy absorption coefficient ratio determination

 - non-uniformity correction factor determination

 - air temperature measurement

 - pressure measurement

 - humidity measurement

 - signal current measurement

 - chamber volume determination

 - ion loss measurement

 - stem correction factor measurement

 - ionization chamber setting positioning

 - air density measurement

 - calculation of the value of g

Typically E_n number [42] used in the measurement of comparison schemes is

$$E_n = \frac{x - X}{\sqrt{U_{lab}^2 + U_{ref}^2}}$$

where X is the value of the air kerma rate at a particular position in the γ-ray field obtained by the cylindrical ionization chamber which is considered as the reference ionization chamber in the present study and x is that obtained by a fabricated

ionization chamber. In the present study U_{ref} is the relative expanded uncertainty in air kerma rate measurement by the cylindrical ionization chamber and U_{lab} is that obtained by the fabricated ionization chamber.

If the value of E_n number for a fabricated ionization chamber is less than 1 then the response of the fabricated ionization chamber in the present study is comparable with the cylindrical ionization chamber. In the present study, the value of E_n number is smaller than 1 at all positions of the fabricated ionization chambers except for the air kerma rate at SCD=4 m in ^{137}Cs γ-ray field measured by S60A and P60A Ionization Chambers. Actually in practice the air kerma rate in ^{137}Cs γ-ray field at SCD=4 m would be measured by S60B and P60B Ionization Chambers and the results for S60A and P60A will not be used. This is because the walls of these chambers are thicker than the electronic equilibrium thickness for ^{137}Cs γ-rays and the measurement results could be deteriorated due to the large wall effect. So, it could be possible to obtain more precise air kerma rates using the fabricated ionization chambers.

Chapter VI

Conclusions

Chapter VI

Conclusions

6.1 Conclusions in General

To determine the air kerma rate in the ^{60}Co and ^{137}Cs γ-ray fields using the fabricated ionization chambers it is necessary to know various correction factors and physical parameters for the chambers. From the measurements and calculations of these parameters in the present study it has been observed that:

(i) Within spherical ionization chambers both the initial and volume recombination loss depend on the ratio of the outer and inner electrode radii and also on the size of the chamber. The diffusion loss depends on the ratio of the outer and inner electrode radii of the chamber.

(ii) Values of recombination parameters A and m^2g for pancake ionization chamber are small compared to those of spherical ionization chambers due to the small separation between the electrodes of pancake ionization chambers. Although for pancake ionization chambers the uncertainty in the values of A and m^2g is large but the uncertainty in the air kerma rates obtained by these ionization chambers are small.

(iii) The stem scattering effect is larger for smaller volume ionization chamber.

(iv) Corrections for γ-ray attenuation and scattering are relatively small for pancake ionization chambers and the value of k_{wall} is close to unity.

(v) The energy spectra and angular distributions of secondary electrons in ionization chambers are not affected by the cavity size.

(vi) The value of $\bar{s}_{gra} / \bar{s}_{air}$ depends on the cutoff energy in calculation and also on the incident photon energy.

(vii) Eqn. (1.7) is applicable for the air kerma rate calculation in ^{60}Co and [137]Cs γ-ray fields using any of these fabricated ionization chambers.

(viii) Sensitivity of these fabricated spherical ionization chambers is almost isotropic. Although there is a very small decrease of signal current at 0° which occurs due to attenuation of the γ-ray beam by the collector electrode of the chamber and partly due to the current from the small cavity near the connector terminal of ionization chamber. Also small increase of signal current near ±95° is noticed due to the effect of the scattered γ-rays from the stem part of the chamber.

(ix) Sensitivity of these fabricated parallel plate ionization chambers depends upon the angular position of the chamber with respect to the beam direction. There is a sharp decrease of signal current at 0° due to attenuation of the γ-ray beam by the collector electrode. In the range of ±50° angular position, the signal current decreases with the angle decreasing to about ±10° due to increasing of attenuation of γ-rays by the side-walls of the chamber. It is because the path length of γ-rays in the side wall becomes longer with the decrease of the angle. Attenuation of γ-rays by the side-walls of the chamber is maximum near ±10° because at that angular position the beam is directed along the side-walls of the chamber. Depending upon the size of ring shape wall electrode a very small (almost negligible) decrease of signal current at ±90° angular position is also noticed.

6.2 Advantages and Disadvantages of Different Type Ionization Chambers

From the above discussions it is seen that each type of ionization chamber has some advantages and disadvantages:

Air kerma rate in ^{60}Co and [137]Cs γ-ray fields of AIST is measured by setting the cylindrical ionization chambers at 45° angular position with respect to the γ-ray beam direction, so that γ-ray attenuation does not increase at the end or side walls of

the ionization chamber [43]. But it is difficult to set the chamber at 45° at the right reference position. The electric field strength is small at the corner side of the chamber volume. But the ionization volume of the cylindrical chambers is easy to measure.

Sensitivity of the spherical ionization chambers is almost isotropic; but the disadvantage of this type of chambers is that there is a large difference between the electric field strengths within the ionization volume.

The main advantage of pancake ionization chamber is that there is small correction for wall effect, i.e. attenuation and scattering of the γ-ray beams by the chamber wall are small. For this reason it is possible to use the pancake ionization chamber for lower energy γ-ray beams and x-rays. The other advantage of pancake ionization chamber is that less ion collecting voltage is required for this type of chamber than cylindrical and spherical types of ionization chambers. But only drawback of this type of chamber is that the sensitivity depends upon the angular position of it.

From the measured values of absolute air kerma rates at various SCDs using the fabricated ionization chambers it can be concluded that it is possible to use these fabricated spherical and pancake ionization chambers as the primary standard dosimeter for calibration purposes instead of the cylindrical ionization chambers which are now being used as the primary ionization chambers at AIST.

Appendix

Physical Parameters and Correction Factors

of the Fabricated Ionization Chambers

Physical Parameters and Correction Factors with their Estimated Uncertainties

Physical parameters and correction factors common for all the chambers are:

Physical parameters/Correction factors	Values	Uncertainty (%)
Dry air density (kg m^{-3})	: 1.2930 [44]	0.01
W/e (JC^{-1})	: 33.97 [45]	0.11
Stopping power ratio	: **	
(1-g)	: 0.9984 (^{37}Cs) [46]	0.02
	0.9970 (^{60}Co) [46]	0.02
Mass energy absorption coefficient	: 0.9996 (^{37}Cs) [41]	0.05
ratio	0.9990 (^{60}Co) [41]	0.05
Temperature	: 22 °C	0.02
Pressure	: 101.325 kPa	0.01
Humidity	: 0%	0.02

** Stopping power ratio value depends upon the chamber size.

Physical parameters and correction factors along with their uncertainties for S7A Ion Chamber

Physical parameters/Correction factors	Values	Uncertainty (%)
Ionization volume (cm^3)	: 7.2398	0.01
Stopping power ratio	: 1.0060 (^{37}Cs)	-
	0.9964 (^{60}Co)	-
k_{wall}	: 1.0319 (^{37}Cs)	0.11
	1.0234 (^{60}Co)	0.11
k_{stem}	: 0.9938 (^{37}Cs)	0.07
	0.9959 (^{60}Co)	0.10

Physical parameters and correction factors along with their uncertainties for S60A Ion Chamber

Physical parameters/Correction factors	Values	Uncertainty (%)
Ionization volume (cm^3)	: 65.0949	0.01
Stopping power ratio	: 1.0052 (^{37}Cs)	0.11
	0.9956 (^{60}Co)	0.11
k_{wall}	: 1.0348 (^{37}Cs)	0.11
	1.0298 (^{60}Co)	0.11
k_{stem}	: 0.9969 (^{37}Cs)	0.07
	0.9979 (^{60}Co)	0.03

Physical parameters and correction factors along with their uncertainties for S60B Ion Chamber

Physical parameters/Correction factors	Values	Uncertainty (%)
Ionization volume (cm^3)	: 65.0949	0.06
Stopping power ratio	: 1.0052	0.11
k_{wall}	: 1.0186	0.11
k_{stem}	: 0.9956	0.05

Physical parameters and correction factors along with their uncertainties for S900A Ion Chamber

Physical parameters/Correction factors	Values	Uncertainty (%)
Ionization volume (cm^3)	: 899.6821	0.04
Stopping power ratio	1.0038 (^{37}Cs)	0.11
	0.9942 (^{60}Co)	0.11
k_{wall}	1.0488 (^{37}Cs)	0.11
	1.0382 (^{60}Co)	0.11
k_{stem}	0.9985 (^{37}Cs)	0.04
	0.9993 (^{60}Co)	0.01

Physical parameters and correction factors along with their uncertainties for P9A Ion Chamber

Physical parameters/Correction factors	Values	Uncertainty (%)
Ionization volume (cm^3)	: 8.8976	0.13
Stopping power ratio	1.0069 (^{37}Cs)	0.11
	0.9977 (^{60}Co)	0.11
k_{wall}	1.0047 (^{37}Cs)	0.11
	1.0038 (^{60}Co)	0.11
k_{stem}	0.9966 (^{37}Cs)	0.04
	0.9984 (^{60}Co)	0.05

Physical parameters and correction factors along with their uncertainties for P9B Ion Chamber

Physical parameters/Correction factors	Values	Uncertainty (%)
Ionization volume (cm^3)	: 8.8976	0.13
Stopping power ratio	: 1.0069 (^{37}Cs)	0.11
k_{wall}	: 0.9971 (^{37}Cs)	0.11
k_{stem}	: 0.9966 (^{37}Cs)	0.04

Physical parameters and correction factors along with their uncertainties for P60A Ion Chamber

Physical parameters/Correction factors	Values	Uncertainty (%)
Ionization volume (cm^3)	: 60.7015	0.07
Stopping power ratio	: 1.0066 (^{37}Cs)	0.11
	0.9971 (^{60}Co)	0.11
k_{wall}	: 1.0042 (^{37}Cs)	0.11
	1.0018 (^{60}Co)	0.11
k_{stem}	: 0.9985 (^{37}Cs)	0.01
	0.9991 (^{60}Co)	0.02

Physical parameters and correction factors along with their uncertainties for P60B Ion Chamber

Physical parameters/Correction factors	Values	Uncertainty (%)
Ionization volume (cm^3)	: 60.7015	0.07
Stopping power ratio	: 1.0066 (^{37}Cs)	0.11
k_{wall}	: 0.9970 (^{37}Cs)	0.11
k_{stem}	: 0.9985 (^{37}Cs)	0.01

References

References

1. International Commission on Radiation Units and Measurements. Basic Concepts in Dosimetry, ICRU Report 19, Washington DC, 1971.

2. International Commission on Radiation Units and Measurements. Radiation Quantities and Units, ICRU Report 33, Washington DC, 1980.

3. International Commission on Radiation Units and Measurements. Fundamental Quantities and Units for Ionizing Radiation, ICRU Report 60, Bethesda, MD 1998.

4. Attix FH: Introduction to Radiological Physics and Radiation Dosimetry, John Wiley & Sons, New York, 1986.

5. Rajan KNG: Advanced Medical Radiation Dosimetry, Prentice-Hall of India Private Limited, New Delhi-110001, 1992.

6. ICRP publication 44. Protection of the Patient in Radiation Therapy, Pergamon Press, Oxford, Annuals of the ICRP 15(2), 1985.

7. Kurosawa T, Takata N, Koyama Y and Katou M: Establishment of gamma-ray air-kerma standard, AIST Monograph of Metrology, No. 7, 2005 (in Japanese).

8. Boutillon M: Volume recombination parameter in ionization chambers. Phys. Med. Biol. 43: 2061, 1998.

9. Das IJ and Akber FA: Ion recombination and polarity effect of ionization chambers in kilovoltage x-ray exposure measurements. Med. Phys. 25: 1751, 1998.

10. Takata N: Ion loss due to initial recombination in a parallel-plate cavity ionization chamber. Phys. Med. Biol. 39: 1037, 1994.

11. Takata N and Matiullah: Dependence of the value of m on the lifetime of ions in parallel-plate ionization chambers. Phys. Med. Biol. 36: 449, 1991.

12. Takata N: The effects of humidity on volume recombination in ionization chambers. Phys. Med. Biol. 39: 1047, 1994.

13. Takata N, Tran NT, Kim E, Marsoem P, Kurosawa T and Koyama Y: Loss of ions in cavity ionization chambers. App. Rad. Iso. 63: 805, 2005.

14. Takata N and Sakihara K: The dependence of the m value on applied voltage in the collection efficiency of ionization chambers. Phys. Med. Biol. 34: 589, 1989.

15. Piermattei A, Azario L, Arcovito G and Toni MP: Ion recombination correction factor k_{sat} for spherical ion chambers irradiated by continuous photon beams. Phys. Med. Biol. 41: 1025, 1996.

16. Takata N, Takeda N and Yin Z: Decreases in output currents due to back diffusion of ions in ionization chambers. Radiat. Protec. Dosi. 71: 309, 1997.

17. Niatel MT: An experimental study on ion recombination in parallel plate free air ionization chambers. Phys. Med. Biol. 12: 555, 1967.

18. Takata N, Kurosawa T and Tran NT: Angle dependences of signal currents from cylindrical ionization chambers. Radiat. Protec. Dosi. 107: 293, 2003.

19. Piermattei A, Azario L, Fidanzio A, Viola P, Dell'Omo C, Iadanza L, Fusco V, Lagares JI and Capote R: The wall correction factor for a spherical ionization chamber used in brachytherapy source calibration. Phys. Med. Biol. 48: 4091, 2003.

20. Kurosawa T, Takata N and Koyama Y: Angular dependence of the wall correction factor for air kerma measurements using cylindrical cavity chambers. App. Rad. Iso. 62: 805, 2005.

21. McCaffrey JP, Mainegra-Hing E, Kawrakaw I, Shortt Kr and Rogers DWO: Evidence for using Monte Carlo calculated wall attenuation and scatter correction factors for three styles of graphite-walled ion chamber. Phys. Med. Biol. 49: 2491, 2004.

22. Büermann L, Kramer HM and Csete I: Results supporting calculated wall correction factors for cavity chambers. Phys. Med. Biol. 48: 3581, 2003.

23. Takata N, Kurosawa T and Koyama Y: Ionization chamber wall correction factors in measuring air kerma for gamma rays. Jour. Met. Soc. India 18: 223, 2003.

24. Bielajew AF: On the technique of extrapolation to obtain wall correction factors for ion chambers irradiated by photon beams. Med. Phys. 17: 583, 1990.

25. Rogers DWO and Bielajew AF: Wall attenuation and scatter corrections for ion chambers: measurement versus calculations. Phys. Med. Biol. 35: 1065, 1990.

26. Ferreira IH, Almeida CE, Marre D, Marechal MH, Bridier A and Chavaudra J: Monte Carlo calculations of the ionization chamber wall correction factors for ^{192}Ir and ^{60}Co gamma rays and 250 kV x-rays for use in calibration of ^{192}Ir HDR brachytherapy sources. Phys. Med. Biol. 44: 1897, 1999.

27. Shortt KR, Bielajew AF, Ross CK, Stewart KJ, Burke JT and Corsten MJ: The effect of wall thickness on the response of a spherical ionization chamber. Phys. Med. Biol. 47: 1721, 2002.

28. Laitano RF, Toni MP, Pimpinella M and Bovi M: Determination of the k_{wall} correction factor for a cylindrical ionization chamber to measure air-kerma in ^{60}Co gamma beams. Phys. Med. Biol. 47: 2411, 2002.

29. Takata N: Ion loss due to initial recombination in a parallel-plate cavity ionization chamber. Phys. Med. Boil. 39: 1037, 1994.

30. Greening JR: Saturation characteristics of parallel-plate ionization chambers. Phys. Med. Biol. 9: 143, 1964.

31. McCaffrey JP, Mainegra-Hing E, Kawrakow I, Shortt KR and Rogers DWO: Evidence for using Monte Carlo calculated wall attenuation and scatter correction factors for three styles of graphite-walled ion chamber. Phys. Med. Biol. 49: 2491, 2004.

32. International Commission on Radiation Units and Measurements. Average energy required to produce an ion pair, ICRU Report No. 31, Washington DC, 1979.

33. De Almeida CE and Niatel MT: Comparison between IRD and BIPM exposure and air kerma standards for cobalt gamma rays. BIPM Report 12: 1, 1986.

34. Hirayama H, Namito Y, Bielajew AF, Wilderman SJ and Nelson WR: The EGS5 code system, SLAC Report 730, 2006.

35. Takata N, Kurosawa T, Begum A and Sugita T: Physical parameters and correction factors for ionization chambers for absolute measurement of air kerma in γ-ray fields. Nuclear Instruments and Methods in Physics Research A 580: 346, 2007.

36. Takata N and Begum A: Corrections to air kerma and exposure measured with free air ionization chambers for charge of photoelectrons, Compton electrons and Auger electrons. Radiat. Protec. Dosi. 130: 410, 2008.

37. International Organization for Standardization (ISO). X and gamma reference radiations for calibrating dosemeters and dose rate meters and for determining their response as a function of photon energy — Part 1: Radiation characteristics and production methods, ISO 4037-1, 1996.

38. Rogers DWO and Treurniet J: Monte Carlo calculated wall and axial non-uniformity corrections for primary standards of air kerma. NRC Report, PIRS-663, NRC, Ottawa, 1999.

39. Rogers DWO and Kawrakow I: Monte Carlo calculated correction factors for primary standards of air kerma. Med. Phys. 30: 521, 2003.

40. International Commission on Radiation Units and Measurements. Stopping powers for electrons and positrons, ICRU Report 37, Bethesda, 1984.

41. Hubbell JH and Seltzer SM: Tables of x-rays mass attenuation coefficients and mass energy absorption coefficients 1keV to 20 MeV for elements Z=1 to 92 and 48 additional substances of dosimetric interest. Gaithersburg, May 1995.

42. Proficiency testing by interlaboratory comparisons – part 1. Development and operation of proficiency testing schemes, ISO/IEC Guide 43-1:1997(E).

43. Katoh A and Yamachi I: Dependence on gamma ray incident angle of exposure rate absolutely determined by the use of cylindrical cavity chambers, Bulletin of the Electrotechnical Laboratory, 47: 862, 1983.

44. Davis RS: Equation for the determination of the density of moist air, Metrologia, 29: 67, 1992.

45. BIPM, Physical constants for radiation measurement standards, Comité Consultatif pour les Etalons de Mesure des Rayonnements Ionisants, Section I : 157,1985.

46. Takata N, Koyama Y and Kurosawa T: AIST Bulletin of Metrology, 1: 439, 2002 (in Japanese).

Published Papers

Physical parameters and correction factors for ionization chambers for absolute measurement of air kerma in γ-ray fields

N. Takata[a,*], T. Kurosawa[a], A. Begum[b], T. Sugita[c]

[a]Ionizing Radiation Section, NMIJ, AIST, Tsukuba, Ibaraki 305-8568, Japan
[b]Department of Physics, BUET, Dhaka-1000, Bangladesh
[c]Science System Laboratory, 1342-6 Tomobe, Ibaraki 309-17, Japan

Available online 18 May 2007

Abstract

Values of physical parameters and correction factors essential for the absolute measurement of air kerma in ^{137}Cs and ^{60}Co γ-ray fields were obtained using an EGS5 program for spherical, cylindrical and pancake ionization chambers. The mean mass collision stopping power ratio for graphite and air, was found to vary depending on the cutoff energy of electrons employed in calculation. The ratio between the energies deposited in cavity air due to Compton electrons emitted from the air and those from the graphite wall increases as the chamber size is increased. It also increases as the γ-ray energy is reduced and is equal to 0.09 for ^{137}Cs γ-rays in a spherical ionization chamber of cavity diameter 12 cm. Correction factors for γ-ray attenuation in chamber walls and those for the contribution of scattered γ-rays to chamber responses were obtained separately. The wall correction factor, which is equal to the product of these two factors, is close to unity for pancake chambers.

© 2007 Elsevier B.V. All rights reserved.

Keywords: Air kerma; Ionization chamber; Mean mass stopping power ratio; Wall correction factor; ^{137}Cs γ-rays; ^{60}Co γ-rays

1. Introduction

Absolute values of air kerma, K_{air}, in γ-ray fields can be obtained by using cavity ionization chambers made of pure graphite materials. They can be calculated using the equation:

$$K_{air} = \frac{Q}{m} \cdot \frac{(W/e)}{(1-g)} \cdot \frac{\bar{s}_{gra}}{\bar{s}_{air}} \cdot \frac{(\mu_{en}/\rho)_{air}}{(\mu_{en}/\rho)_{gra}} \cdot \prod k_j \qquad (1)$$

where Q is the signal charge, m is the mass of air in the cavity of the chamber, W/e is the ratio of the W-value for electrons in air to the elementary charge, g is the fraction of secondary electron energy lost due to Bremsstrahlung in air. The symbol $\bar{s}$ represents the mean mass collision stopping power for secondary electrons which pass through the cavity, and μ_{en}/ρ is the mass energy absorption coefficient for γ-rays. The suffixes "air" and "gra" indicate that the values are for air and graphite, respectively. The

symbol k_j represents the correction factors for various phenomena [1].

In large cavities it is thought that some Compton electrons are emitted from the air in the cavity by the incident γ-rays. Consequently, the last fractional term in Eq. (1) should be modified as follows:

$$\frac{(\mu_{en}/\rho)_{air}}{(\mu_{en}/\rho)_{air} \cdot E_{air} + (\mu_{en}/\rho)_{gra} \cdot E_{gra}}$$
$$= \frac{[(\mu_{en}/\rho)_{air}/(\mu_{en}/\rho)_{gra}] \cdot (E_{air}/E_{gra} + 1)}{[(\mu_{en}/\rho)_{air}/(\mu_{en}/\rho)_{gra}] \cdot (E_{air}/E_{gra}) + 1} \qquad (2)$$

where E_{air} and E_{gra} are the energies deposited in the cavity air by Compton electrons emitted from the air and from the graphite wall, respectively.

In the present study, values of $\bar{s}_{gra}/\bar{s}_{air}$ and E_{air}/E_{gra} are obtained using an EGS5 program [2] that simulates spherical, cylindrical and pancake cavities of different sizes in ^{137}Cs and ^{60}Co γ-ray fields. The values for the collision stopping power from Ref. [3] are used in the calculations. From the results for $\bar{s}_{gra}/\bar{s}_{air}$ for spherical chambers, values of $\bar{s}_{gra}/\bar{s}_{air}$ for ionization chambers at AIST are obtained.

*Corresponding author. Tel.: +81 29 861 5662; fax: +81 29 861 5673.

E-mail address: n.takata@aist.go.jp (N. Takata)

The correction factors k_{atten} and k_{scatt}, which are the corrections for γ-ray attenuation in the chamber wall and for scattered γ-ray contributions to chamber responses, respectively, are also calculated for various sizes of the three types of ionization chambers. The total correction factor for the wall effect k_{wall}, which is equal to $k_{atten} \times k_{scatt}$, is also given.

2. Ionization chambers

Calculations were performed for six different sizes for each of the three types of ionization chambers. The inner diameter of the cavity of the smallest spherical chamber was taken to be 20 mm, the inner diameter and the length of the smallest cylindrical chamber were taken to be 20 and 25 mm, respectively, while those of the smallest pancake chamber were taken to be 40 and 4 mm, respectively. The next size of chambers was produced by 1.5 times larger for spherical and cylindrical chambers and by 1.4 for pancake chambers, this process was repeated a total of five times to give six different sizes.

The wall thicknesses were taken to be 1.2 mm for ^{137}Cs γ-rays and 3.3 mm for ^{60}Co γ-rays, and the graphite density to be 1.82 g cm^{-3}. The cavity air pressure was taken to be 101.325 kPa and its temperature to be 295.15 K. The flat walls of the pancake chambers were taken to be perpendicular to the parallel and uniform γ-ray beams, while the cylindrical chambers were fixed at 45° to the γ-ray beam direction.

3. Results of calculation

3.1. Mean mass collision stopping power ratios

Fig. 1 shows the calculated results for the mean ratios of the mass collision stopping powers of graphite and air for electrons entering the cavity for each type of ionization chamber. In the calculation, the inner electrodes (i.e. the charge collectors) were ignored. Fig. 1 shows that there is very little variation in the results for the different chamber sizes for all three types of chambers. It also shows that the results for cylindrical chambers are similar to those for spherical chambers. The values for pancake chambers, however, are smaller than those for the other two types. This is because more secondary electrons enter into the pancake cavity from the front wall of the chamber, and the energies of these electrons are higher than those of the secondary electrons that drift perpendicular to the γ-ray direction. It can be concluded from these facts that the energy spectra and angular distributions of secondary electrons depend on the direction of the secondary electrons and are not affected by the dimensions of the cavity. If the values of stopping power are weighted by the path length of the secondary electrons in pancake cavities, the mean value ratios $\bar{s}_{gra}/\bar{s}_{air}$ for pancake cavities become identical to those for spherical cavities, for which the values of
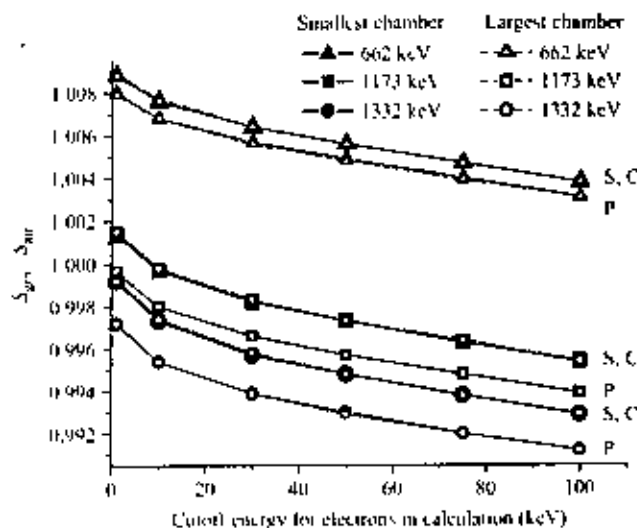

Fig. 1. Average of stopping power ratios for electron which enter the cavity for each type of ionization chambers, spherical (S) cylindrical (C) and pancake (P). The results for spherical chambers, which are shown by slightly larger symbols, correspond to $\bar{s}_{gra}/\bar{s}_{air}$ for all types of ionization chambers.

stopping power are weighted isotropically. Consequently, the results obtained for spherical chambers correspond to the values of $\bar{s}_{gra}/\bar{s}_{air}$ for secondary electrons in electronic equilibrium condition and should be used in Eq. (1) for all types of chambers.

It can be seen from Fig. 1 that $\bar{s}_{gra}/\bar{s}_{air}$ increases as the cutoff energy decreases and it also increases as the incident photon energy is reduced. Rogers and Kawrakow have shown a similar dependence by performing calculations for an ionization chamber in ^{60}Co γ-ray fields [4].

Secondary electrons having a penetration depth in air shorter than the cavity size deposit all their energies in the cavity air when they enter the cavity. Thus, it is reasonable to determine a value of $\bar{s}_{gra}/\bar{s}_{air}$ for an ionization chamber from the cutoff energy for which the projected range of electrons in air corresponds to the mean chord length $\bar{l}$ of the cavity. The mean chord length of a volume is the mean length of randomly oriented chords in that volume and is equal to $4V/A$, where V is the volume and A is the surface area [5]. The surfaces of the inner electrode are included in A for calculating $\bar{l}$ for AIST ionization chambers.

The projected range of electrons in air (i.e. the mean depth of the deepest points which the electrons reach in the direction of injection) was calculated using the EGS5 program because there are no published data for low energy electrons. The mean total path length was also calculated using the program. The projected range varied from 47% to 50% of the total path length for electrons having energies in the range from 10 to 150 keV and the total path length was about 10% larger than the CSDA (continuous slowing down approximation) range given in Ref. [3].

Table 1
Physical parameters obtained for AIST ionization chambers

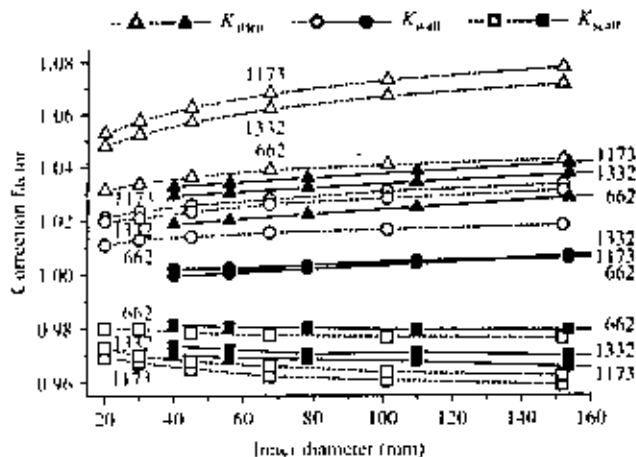| Chamber type (model)	Cavity volume (cm³)	$\bar{l}$(cm)	Cutoff energy (keV)	γ-ray $\bar{s}_{gra}/\bar{s}_{air}$
Spherical S60	64.999	3.15	60.8	^{137}Cs 1.0052
				^{60}Co 0.9969
				0.9943
Spherical S900	901.56	7.60	101.4	^{137}Cs 1.0038
				^{60}Co 0.9954
				0.9929
Cylindrical C765	62.632	2.76	56.5	^{137}Cs 1.0054
				^{60}Co 0.9970
				0.9945
Pancake P60	60.743	0.74	27.2	^{137}Cs 1.0057
				^{60}Co 0.9983
				0.9959

Fig. 2. Correction factors for spherical (empty symbols) and pancake (filled symbols) ionization chambers for various energy γ-rays. Numbers in the figure give energies in keV.

Table 1 shows the values for $\bar{l}$, the corresponding cutoff energy and $\bar{s}_{gra}/\bar{s}_{air}$ obtained for AIST ionization chambers from the data for spherical chambers shown in Fig. 1. The values of $\bar{s}_{gra}/\bar{s}_{air}$ for photons having energies of 1173–1332 keV are listed separately in the row for ^{60}Co γ-rays.

3.2. Mass energy absorption coefficient ratios

It was found from the calculation that the value of E_{air}/E_{gra} increases as the size of the chambers increases. It also increased as the incident photon energies were reduced. It had a value of 0.09 for ^{137}Cs γ-rays for the spherical ionization chamber of diameter 12 cm, which is the largest one at AIST.

Because the value of $(\mu_{en}/\rho)_{air}/(\mu_{en}/\rho)_{gra}$ is very close to unity for ^{137}Cs and ^{60}Co γ-rays, the difference between the values of $(\mu_{en}/\rho)_{air}/(\mu_{en}/\rho)_{gra}$ and those calculated using Eq. (2) was less than 0.01% for $E_{air}/E_{gra} = 0.09$. The value of $(\mu_{en}/\rho)_{air}/(\mu_{en}/\rho)_{gra}$ is in the range from 0.99 to 1.01 for photons having an energy in the range from 200 to 3000 keV; the difference between the values of $(\mu_{en}/\rho)_{air}/(\mu_{en}/\rho)_{gra}$ and those calculated using Eq. (2) is less than 0.4% even for $E_{air}/E_{gra} = 0.5$. Consequently, we can use Eq. (1) when low energy scattered γ-rays are not dominant. For lower energy photons, however, both the values of $(\mu_{en}/\rho)_{air}/(\mu_{en}/\rho)_{gra}$ and E_{air}/E_{gra} change significantly depending on the photon energy and the difference between the values of $(\mu_{en}/\rho)_{air}/(\mu_{en}/\rho)_{gra}$ and those calculated using Eq. (2) becomes large.

3.3. Wall correction factors

Fig. 2 shows the calculated values of k_{atten}, k_{scat} and k_{wall} for spherical and pancake ionization chambers. The results for cylindrical chambers were nearly the same as those for spherical chambers. It should be noted that the wall thickness is 1.2 and 3.3 mm for ^{137}Cs and ^{60}Co γ-rays, respectively.

Fig. 2 shows that the correction factor varies less with chamber size for the pancake chamber than for the spherical chamber. This is because the path length of γ-rays in the flat walls of pancake chambers does not vary with size and it is shorter than that for the spherical chamber. Moreover, the corrections for attenuation and scattering compensate each other, and k_{wall} becomes close to unity for pancake chambers. This is consistent with measured and calculated results given in Ref. [6]. Similar results were obtained for k_{atten}, k_{scat} and k_{wall} for AIST chambers. In the calculation, inner electrodes were taken into consideration.

4. Conclusions

From the calculated results it was found that:

(1) The energy spectra and angular distributions of secondary electrons in ionization chambers are not affected by the cavities considered in the present work.

(2) The value of $\bar{s}_{gra}/\bar{s}_{air}$ depends on the cutoff energy of electrons in calculation and also on the incident photon energy. Values for AIST ionization chambers were obtained.

(3) It was confirmed that Eq. (1) could be used without modification even for a 12-cm-diameter spherical ionization chamber for γ-rays.

(4) Corrections for γ-ray attenuation and scattering are relatively small for pancake chambers and the value of k_{wall} is close to unity.

References

[1] T. Kurosawa, N. Takata, Y. Koyama, M. Katou, AIST Monograph of Metrology, No. 7, 2005 (in Japanese).

[2] H. Hirayama, Y. Namito, A.F. Bielajew, S.J. Wilderman, W.R. Nelson, SLAC-Report-730, 2005.

[3] International Commission on Radiation Units and Measurements, ICRU Report 37, 1984.

[4] D.W.O. Rogers, I. Kawrakow, Med. Phys. 30 (2003) 521.

[5] International Commission on Radiation Units and Measurements, ICRU Report 60, 1998.

[6] D.W.O. Rogers, J. Treurniet, NRCC Report, PIRS-663, 1999.

CORRECTIONS TO AIR KERMA AND EXPOSURE MEASURED WITH FREE AIR IONISATION CHAMBERS FOR CHARGE OF PHOTOELECTRONS, COMPTON ELECTRONS AND AUGER ELECTRONS

N. Takata[1,*] and A. Begum[2]
[1]Ionizing Radiation Section, NMIJ, AIST, Tsukuba, Ibaraki 305-8568, Japan
[2]Department of Physics, BUET, Dhaka-1000, Bangladesh

The signal charge from a free air ionisation chamber for the measurement of air kerma and exposure consists of not only the charge of ion pairs produced by secondary electrons (i.e. photoelectrons, Compton electrons and Auger electrons), but also the charge of the secondary electrons and single and multiple charged ions formed by the release of the secondary electrons. In the present work, correction factors for air kerma and exposure for the charge of the secondary electrons and ions were calculated for photons with energies in the range from 1 to 400 keV. The effects of an increase in the W value of air for low-energy electrons were also taken into consideration. It was found that the correction factors for air kerma and exposure have a maximum value near a photon energy of 30 keV; in the lower energy region, the correction factor for exposure monotonically decreases with a decrease in photon energy except for a small dip due to K-edge absorption by argon atoms in air. The values of the correction factors were found to be 0.9951 and 0.9892, respectively, for a spectrum with a mean energy of 7.5 keV, the reference X-ray spectrum with the lowest mean energy in ISO 4037-1. The air kerma correction is smaller than that for exposure, because for air kerma the signal due to the charge of secondary electrons and ions is partly compensated by the decrease in the number of ion pairs produced by the secondary electrons due to the increase of the W value of air for lower energy electrons.

INTRODUCTION

Air kerma, K_{air}, is defined as the quotient of the sum of the initial kinetic energies of all secondary electrons liberated by photons, by the mass of air from which the secondary electrons are liberated. The value of air kerma is generally obtained by the following equation, which shows the relation between air kerma and exposure X:

$$K_{air} = \frac{X(W/e)}{1 - g} \qquad (1)$$

where W, called W value, is the mean energy of electrons expended in air per ion pair production and e is the elementary charge and g is the fraction of the energy of the secondary electrons that is lost by radiative processes in air[1].

Absolute measurement of exposure is made using a free air ionisation chamber:

$$X = \frac{Q}{m} \Pi k_i. \qquad (2)$$

Here, Q is the signal charge from the ionisation chamber and m is the mass of air in the ionisation volume at the time of measurement. The symbol k_i

corresponds to various correction factors[1,3]. Consequently, K_{air} is expressed as

$$K_{air} = \frac{Q(W/e)}{m(1 - g)} \Pi k_i. \qquad (3)$$

Most ions with an inner-shell vacancy, produced by emission of an electron due to the photoelectric effect or Compton scattering effect, undergo cascade decay emitting Auger electrons and become multiple charged ions. The photoelectrons, Compton electrons and Auger electrons (hereafter, these electrons are referred to as secondary electrons) produce ion pairs and become negative ions by attaching to molecules in air after losing their kinetic energies. The total number of the secondary electrons is the same as the total charge of the positive ions formed by the release of the secondary electrons. The signal charge from a free air ionisation chamber comprises not only the charge of the ion pairs produced by the secondary electrons but also the charge of the secondary electrons, i.e. the charge of the negative ions, and the charge of the positive ions.

In the ICRU Report 60[1] published in 1998, exposure is defined as the quotient of dQ by dm, where dQ is the absolute value of the total charge of the ions of one sign produced in air when all the electrons and positrons liberated or created by

*Corresponding author: n.takata@aist.go.jp

photons in air of mass dm are completely stopped in air. It is also noted that the ionisation produced by Auger electrons is included in dQ. It is not definite whether the charge of the secondary electrons, which include the Auger electrons contribution, should be included in dQ or not. In the Report of the ICRU[4] published in 1959, it is stated that 'the exposure dose is measured by the ion charge, ΔQ, of either sign produced in air by the secondary electrons, which are produced by X- or gamma radiation in a small mass, Δm, of air divided by Δm'. By this definition, it is clear that the charge of secondary electrons is not included in ΔQ.

In the ICRU Report 60, it is also noted that exposure can be expressed in terms of the distribution, Φ_E, of the fluence with respect to the photon energy, E, and the mass energy transfer coefficient, μ_{tr}/ρ for air, as follows:

$$X = \frac{e}{W} \int \Phi_E E \frac{\mu_{tr}}{\rho} (1 - g) dE. \qquad (4)$$

It is obvious that the charge of secondary electrons is not included in the exposure defined by Equation 4. Consequently, it should be concluded that exposure X does not include the charge of secondary electrons and hence it is necessary to correct the signal charge from a free air ionisation chamber for the signal due to the charge of the secondary electrons and positive ions to obtain accurate values of exposure and air kerma.

Usually a constant value of 33.97 J/C is used for W/e, i.e. 33.97 eV for W, to obtain air kerma[3]. The W value of air, however, increases for lower energy electrons, and less ion pairs are produced per unit energy for lower energy electrons. It is expected that some of the signal due to the charge of secondary electrons may be compensated by the decrease in the number of ion pairs produced due to the increase in the W value for lower energy electrons.

In the present work, correction factors for the charge of secondary electrons and positive ions are calculated for photons with energies in the range from 1 to 400 keV. Net values of the correction factors are also obtained for various reference X-ray spectra given in ISO 4037-1[6]. In the calculations, the energies of the photoelectrons, Compton electrons and Auger electrons emitted from air are obtained from data on photoelectric absorption cross sections, Compton scattering cross sections and electron binding energies of nitrogen, oxygen and argon atoms (hereafter denoted as N, O and Ar, respectively). The number of Auger electrons emitted is obtained from the data on mean charge states of atoms after decay of inner shell vacancies. The dependence of the W value of air on electron energy is also taken into consideration.

CALCULATION

Photoelectric absorption cross sections and Compton scattering cross sections of N, O and Ar atoms were obtained for photons with energies in the range from 1 to >400 keV with a step of 1% of each energy from the data[7,8]. In the calculations, a cubic equation was fitted to four values on a log–log scale, except for the photoelectric absorption cross section near the energy of the K shell edge of Ar atoms. For interpolation near the K edge, a quadratic equation was fitted to three values. The photoelectric absorption and Compton scattering cross sections were weighted by the relative number densities of N (0.7848), O (0.2105) and Ar (0.0047) atoms in air and the proportions of the weighted cross sections to the total cross sections were obtained. Figure 1 shows the proportions of the weighted cross sections for each atomic species as an area chart.

Photoelectric effect

Photoelectrons are emitted from the K and L shells of N, O and Ar atoms. The photoelectron emission from M shells of Ar atoms is usually negligible. The ratios between the photoelectric absorption cross sections of K and L shells were assumed to be independent of the photon energy and were obtained from the data for the K-edge absorption shift[7]. The values used in the present work for the fraction of the L shell cross section to the total (i.e. K and L shells) cross section are 0.0492 (N), 0.0535 (O) and 0.1105 (Ar). The photoelectric effect of Ar atoms for photons with energies less than the binding energy of the K shell electron is entirely due to L shell electrons. It was assumed that the photoelectric absorption cross sections for electrons belonging to L_1, L_2
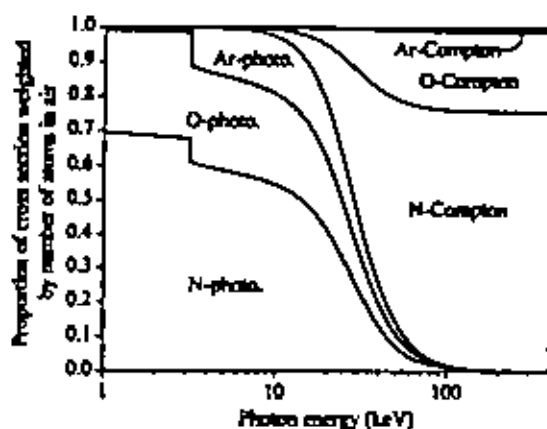

Figure 1. Normalised proportions of photoelectric and Compton scattering cross sections for N, O and Ar atoms weighted by the number density of atomic species in air.

and L_3 shells are the same. The kinetic energy of a photoelectron is equal to the photon energy minus the binding energy of the electron in the atom. The binding energy of electrons for each shell is shown in Table 1[9]. The values for L_2 and L_3 shells of N and O atoms were obtained from their first ionisation energy. In the calculation of the kinetic energy, average values of binding energy obtained by weighting with the number of electrons of each atomic shell were used for L_2 and L_3 shells of all atoms, and for M_1, M_2 and M_3 shells of Ar atoms.

The photoelectron energy was multiplied by the respective fractions of the photoelectric absorption cross sections of K and L shells relative to the total photoelectric absorption cross section, and also multiplied by the proportion of the photoelectric absorption cross section for each atomic species to the total photoelectric and Compton scattering cross sections for all atoms in air. Consequently, the values of the energy multiplied by the fractions and the proportions correspond to the energy contributions of photoelectrons emitted from each atomic species. The solid lines in Figure 2, which have a

Table 1. Electron binding energies of atomic shells (eV)[9].

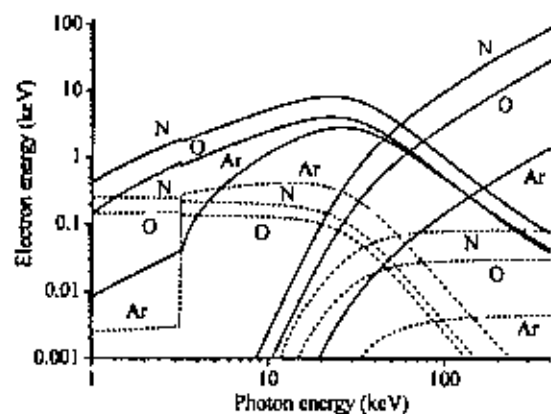| Atomic species	K	L_1	L_2	L_3	M_1	M_2	M_3
N	409.9	37.3	14.5	14.5			
O	543.1	41.6	13.6	13.6			
Ar	3205.9	326.3	250.6	248.4	29.3	15.9	15.7

Figure 2. Solid lines with maximum values near a photon energy of 20 keV show the energies of photoelectrons emitted from N, O and Ar atoms in air. The solid lines whose values increase monotonically with photon energy show the energies of Compton electrons. The dotted lines show the energies of Auger electrons emitted following the emission of photoelectrons and Compton electrons.

maximum value near a photon energy of about 20 keV, show contributions of energy of photoelectrons emitted from N, O and Ar atoms.

When an inner shell vacancy is produced by the photoelectric effect, a characteristic X-ray is emitted at a rate of fluorescence yield ω and Auger electrons are emitted with a probability of $(1 - \omega)$. In the present calculation, ω for the K shell of Ar atoms was assumed to be 0.12 and zero for all other shells of N, O and Ar atoms because they are all smaller than 0.01. Atoms become multiple charged ions by Auger electron emission. Table 2 shows average charge states after de-excitation of inner shell vacancies for N, O and Ar atoms[10,11] as well as the charge states assumed in the present calculation.

In calculations for N and O atoms, it was assumed that all atoms with a K shell vacancy emit a $K-L_{2,3}L_{2,3}$ Auger electron and become a 2+ charge state. Calculations were also made for the case of an average charge state of 2.2+ for N and O atoms to check the dependence of the correction factors on the average charge states. In this case, it was assumed that 20% of atoms with a K shell vacancy emit a $K-L_1L_{2,3}$ Auger electron and 80% emit a $K-L_{2,3}L_{2,3}$ Auger electron. The atoms with an L_1 shell vacancy produced by the emission of a $K-L_1L_{2,3}$ Auger electron subsequently emit an $L_1-L_{2,1}L_{2,3}$ Auger electron and become a 3+ charge state; consequently, the average charge state becomes 2.2+.

It was assumed that Ar atoms with an $L_{2,3}$ vacancy emit $L_{2,3}-MM$ Auger electrons and become ions with 2+ charge and Ar atoms with an L_1 vacancy emit $L_1-L_{2,3}M$ Auger electrons. The $L_{2,3}$ vacancy produced by the emission of an $L_1-L_{2,3}M$ Auger electron is de-excited by cascade emission of an $L_{2,3}-MM$ Auger electron and the Ar atom becomes an ion with 3+ charge. Ar atoms with a K shell vacancy emit K_α characteristic X-rays at a probability of 12%. An atom with a $L_{2,3}$ vacancy produced by the emission of a K_α X-ray emits an $L_{2,3}-MM$ Auger electron and becomes a 2+ charge ion. 38.6% of the residual 88% of Ar atoms with a K shell vacancy emit a $K-L_{2,3}L_{2,3}$ Auger electron and atoms with two $L_{2,3}$ vacancies are de-excited by emission of two $L_{2,3}-MM$ Auger electrons and become 4+ charge ions. 61.4% of the residual 88% of Ar atoms with a K shell vacancy emit a $K-L_1L_{2,3}$ Auger electron; the L_1 and $L_{2,3}$ vacancies undergo cascade Auger electron emission as described above and the Ar atoms become 5+ charge ions. Consequently, Ar atoms with a K shell vacancy are de-excited and become ions with a 4.3+ charge state on average (2+, 12%; 4+, 34%; 5+, 54%).

The energy of an Auger electron was assumed to be equal to the binding energy of the initial vacancy shell minus the binding energies of the two vacancy

Table 2. Average charge states of ions after de-excitation of inner atomic shell vacancy.

Atomic species	K	L₁	L₂	L₃	M	Ref.
N	1.98*	1.00				(10)
	2.21	1.00				(11)
	2.00 (2.20)	1.00 (2.00)	1.00	1.00		Present study
O	1.97	1.00				(10)
	2.20	1.00				(11)
	2.00 (2.20)	1.00 (2.00)	1.00	1.00		Present study
Ar	4.37	3.24	2.18	2.28	1.00	(10)
	4.24	3.26	2.28	2.28	1.00	(11)
	4.30	3.00	2.00	2.00	1.00	Present study

*Obtained as an average value for carbon and oxygen.

shells which are produced by the emission of the Auger electron. The energies of Auger electrons emitted from N, O and Ar atoms following photoelectron emission are shown by dotted lines in Figure 2.

Compton scattering

The Compton electron energy spectrum was calculated in 1 eV steps from 0 eV up to the maximum energy $T_{max} = h\nu/(1 + 1/2\alpha)$ for incident photons with an energy $h\nu$ using the following equation[12]:

$$\frac{d_e\sigma}{dT} = \frac{\pi r_0^2}{\alpha^2 m_0 c^2} \left\{ 2 + \left(\frac{T}{h\nu - T}\right)^2 \left[\frac{1}{\sigma^2} + \frac{h\nu - T}{h\nu} - \frac{2}{\alpha}\left(\frac{h\nu - T}{T}\right)\right] \right\} \quad (5)$$

where σ is the Compton scattering cross section for transferring energy T to an electron. The parameters $\alpha = h\nu/(m_0 c^2)$, $r_0 = e^2/(m_0 c^2)$ and $m_0 c^2$ give the electron rest mass energy. The ratio of the cross section transferring energy T within an 1 eV width to the total Compton scattering cross section was obtained and then multiplied by the proportion of the Compton scattering cross section for each atomic species N, O and Ar to the total cross section of air, (Figure 1). It was assumed that an electron is emitted with an energy of T minus the binding energy of the electron in the atom. When the value is negative, it was assumed that no emission takes place. It was also assumed that all electrons have the same Compton scattering cross section independent of the atomic shells to which the electrons belong.

When inner shell electrons (i.e. K shell electrons of N and O atoms, and K and L shell electrons of Ar atoms) are emitted by Compton scattering, an atom with an inner shell vacancy undergoes Auger electron emission as described in the previous

section, Photoelectric effect. When an electron is emitted from the K shell of an Ar atom by Compton scattering, a K_α X-ray is emitted with a probability of 12% and subsequently an $L_{2,3}$–MM Auger electron is emitted. The residual 88% of Ar atoms with K shell vacancies are de-excited by Auger electron emission. When L shell electrons of N or O atoms, or M shell electrons of Ar atoms are emitted by Compton scattering, the atoms become ions with a 1+ charge state and no Auger electron emission takes place. In calculation for an average charge state of 2.2+ for N and O atoms with a K shell vacancy, it was assumed that 20% of the atoms emit $K-L_1 L_{2,3}$ Auger electrons and that 2+ charge ions with L_1 and $L_{2,3}$ shell vacancies undergo $L_1-L_{2,3}L_{2,3}$ Auger electron emission and become ions with a 3+ charge state. The energies of Compton electrons emitted from N, O and Ar atoms and the energies of Auger electrons emitted following Compton scattering are shown by solid and dotted lines, respectively, in Figure 2.

Number of ion pairs

The number of ion pairs produced by photoelectrons, Compton electrons and Auger electrons was obtained by dividing the energy of these electrons by the W value of air corresponding to the energy. At the same time, the number of these secondary electrons was counted. The W value was calculated using the following equation, which was obtained by fitting to experimental data on a log–log scale for electron energy (e^x) and W value (e^y) (in eV):

$$y = y_0 + A_1 e^{-(x-x_0)/t_1} + A_2 e^{-(x-x_0)/t_2} + A_3 e^{-(x-x_0)/t_3} \quad (6)$$

where $y_0 = 3.51339$, $x_0 = 2.50144$, $A_1 = 2.12296$, $t_1 = 0.45155$, $A_2 = 11.34283$, $t_2 = 0.103$, $A_3 = 0.88307$, $t_3 = 1.48666$.
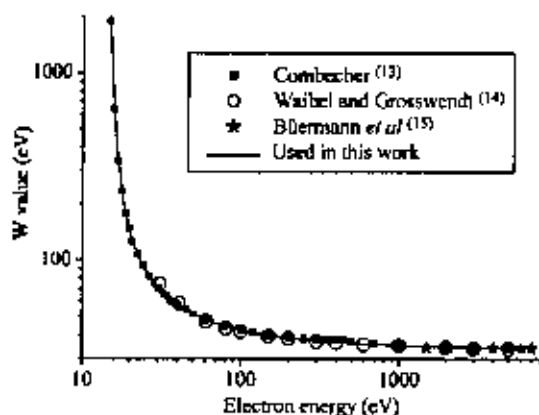
Figure 3. W value of air for electrons. The solid line shows the values used in the present calculation, assumed to be 33.97 eV for electrons with energies larger than 7195.4 eV.

In Figure 3, the solid line shows the W value obtained by the equation and the symbols show the experimental data.

Equation 6 gives a W value of 57.2 MeV for electrons with an energy of 12.2 eV, which is the ionisation potential of O_2 molecules, and gives larger values for lower energy electrons. In the calculations of the number of ion pairs, the W value was assumed to be infinite for lower energy electrons. On the other hand, Equation 6 gives a W value of 33.97 eV for electrons with an energy of 7195.4 eV and gives slightly smaller values for higher energy electrons. In the calculations of the number of ion pairs, it was assumed that the W value is constant at 33.97 eV for all electrons with an energy >7195.4 eV. This is because a value of 33.97 eV is typically used for the W value of air to obtain air kerma and/or absorbed dose[5]. The number of ion pairs produced by photoelectrons, Compton electrons and Auger electrons showed similar shapes to those for the energies of the respective secondary electrons shown in Figure 2.

RESULTS OF CALCULATIONS

The curved solid lines in Figure 4 show the energy of photoelectrons, Compton electrons and the sum of the energy of these electrons emitted from all atomic species in air. The dotted line in the figure shows the total energy of these electrons and Auger electrons emitted. The solid lines correspond, respectively, to the sum of the values for photoelectrons and Compton electrons shown by the solid lines for N, O and Ar atoms in Figure 2. The dotted line in Figure 4 corresponds to the total of all the values shown by the solid and dotted lines in Figure 2. The straight line in Figure 4 represents the relation, electron energy = photon energy. It can be
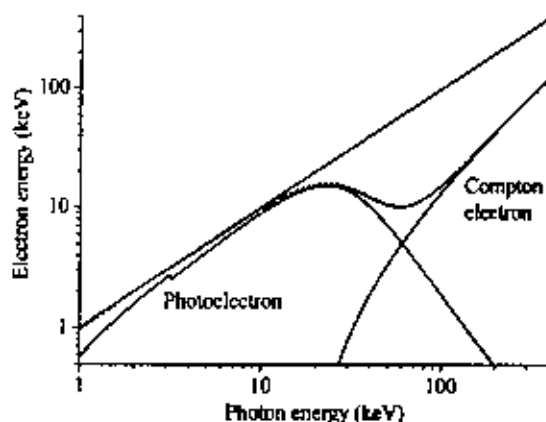

Figure 4. The curved solid lines show the energy of photoelectrons, Compton electrons and the total energy of these electrons emitted from all atoms in air. The dotted line shows the sum of the energy of these electrons and the energy of Auger electrons emitted after the emission of photoelectrons and Compton electrons. The straight line corresponds to the relation (electron energy = photon energy).

seen from Figure 4 that the total energy of secondary electrons has a local maximum value at a photon energy of 23.3 keV and a local minimum at 58.5 keV. This is due to the fact that the photoelectron energy increases and the photoelectric absorption cross section decreases with an increase in photon energy. Also, Compton scattering becomes dominant for photons with higher energies. The separation between the straight line and the solid line for the energy of photoelectrons for photon energies <10 keV corresponds to the energy expended in extracting electrons from atoms over the binding energies. In this range, the dotted line is close to the straight line. This means that most of the energy used to extract electrons over the binding energy and stored as potential energy of the remaining electrons is converted to the kinetic energy of Auger electrons. The small difference between the straight line and the dotted line corresponds to the potential energy of single and multiple charge ions, which remain as final states plus the energies of K_α X-rays emitted from Ar atoms. Most of the large difference between the straight line and the solid lines for photon energies larger than 20 keV corresponds to the energy of Compton scattered X-rays.

The curved solid lines in Figure 5 show the number of ion pairs produced by photoelectrons, Compton electrons and their sum. The dotted line in the figure shows the total number of ion pairs produced by these electrons plus those produced by Auger electrons. The straight line in the figure shows values that correspond to the number of ion pairs which is equal to the photon energy divided by 33.97 eV. Therefore, the line corresponds to the
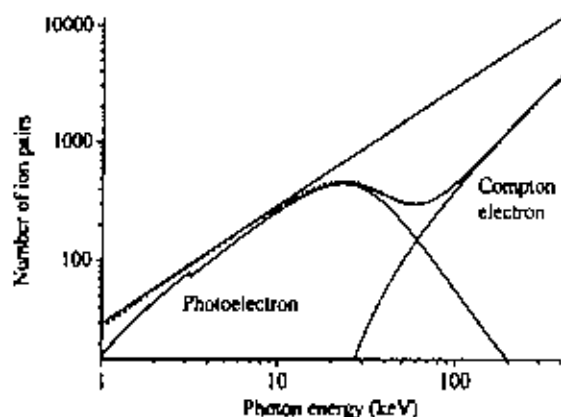
Figure 5. The curved solid lines show the numbers of ion pairs produced in air by photoelectrons, Compton electrons and the sum of these. The dotted line shows the total number of ion pairs produced by these electrons and those produced by Auger electrons. The straight line corresponds to the relation (number of ion pairs = photon energy/33.97 eV)
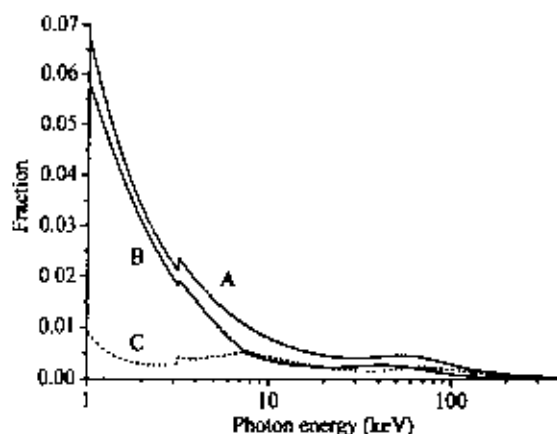

Figure 6. Line A shows the fraction of the number of secondary electrons (photoelectrons, Compton electrons and Auger electrons) relative to the total number of these electrons plus the number of ion pairs produced by these electrons. Line B shows the difference between the number of ion pairs obtained under the assumption that the W value is 33.97 eV for all electrons and the number of ion pairs obtained for the W value shown in Figure 3. The difference is represented as a fraction relative to the total number of secondary electrons plus the number of the ion pairs obtained for the W value shown in Figure 3. Line C shows the difference between the lines A and B, i.e. A − B.

number of ion pairs produced when all the photon energy was converted to kinetic energy of electrons, and ion pairs were produced by the electrons at a rate of a constant W value of 33.97 eV, independent of the electron energy. The difference between the straight line and the dotted line for low photon energies is larger than the difference between the straight line and the dotted line shown in Figure 4. This is due to the fact that the W value increases for lower energy electrons and a smaller number of ion pairs are produced per electron energy.

The solid line A in Figure 6 shows the fraction of the number of secondary electrons relative to the sum of the total number of secondary electrons and the number of ion pairs produced by these electrons. It shows the proportion of the signal due to the charge of secondary electrons in the signal from free air ionisation chambers. As is discussed in Introduction section, Q in Equation 2 should be corrected for the charge of secondary electrons to obtain the values of the exposure.

The solid line in Figure 7 shows the correction factor for exposure obtained by Equation 2. It is the correction for the charge of secondary electrons and is equal to the number of ion pairs produced by the secondary electrons divided by the sum of the number of ion pairs and the number of secondary electrons. It is also equal to 1 minus the value presented by the line A in Figure 6. The dotted line in Figure 7 shows the correction factor obtained for the average charge state of 2.2+ for N and O atoms with a K shell vacancy. The correction factor for exposure depends only slightly on the W value.

Air kerma is usually obtained from the signal charge of a free air ionisation chamber using
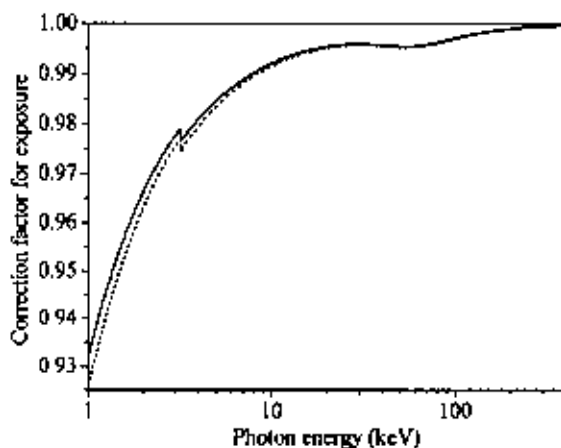

Figure 7. Correction factors for exposure due to the charge of secondary electrons (photoelectrons, Compton electrons and Auger electrons). The solid and dotted lines correspond to, respectively, the average charge states of 2.0+ and 2.2+ for N and O atoms with a K shell vacancy.

Equation 3 and a constant W value of 33.97 eV. The W value of air increases for lower energy electrons and a smaller number of ion pairs are produced per unit energy of electrons. Consequently, it is necessary to correct the signal charge for the charge of secondary electrons and for the decrease in the number of ion pairs due to the increase in the W value.

The line B in Figure 6 shows the difference between the number of ion pairs obtained under the assumption that the W value is constant at 33.97 eV for all secondary electrons and the number of ion pairs obtained for the W value shown in Figure 3. The difference is the fraction of the total number of secondary electrons plus the number of ion pairs obtained for the W value shown in Figure 3. The dotted line C in Figure 6 shows the difference between the values of the lines A and B, i.e. A − B. The difference corresponds to the rate of net increase in the total number of secondary electrons and the number of ion pairs produced by the secondary
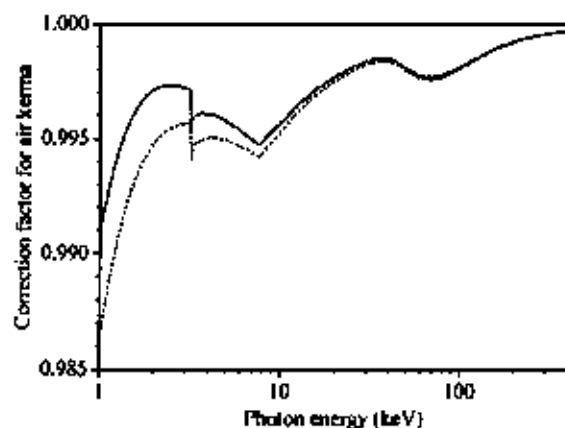

Figure 8. Correction factors for air kerma due to the charge of secondary electrons (photoelectrons, Compton electrons and Auger electrons) and the effects of the increase in W value of air for low energy electrons. The solid and dotted lines correspond to, respectively, the average charge states of 2.0+ and 2.2+ for N and O atoms with a K shell vacancy.
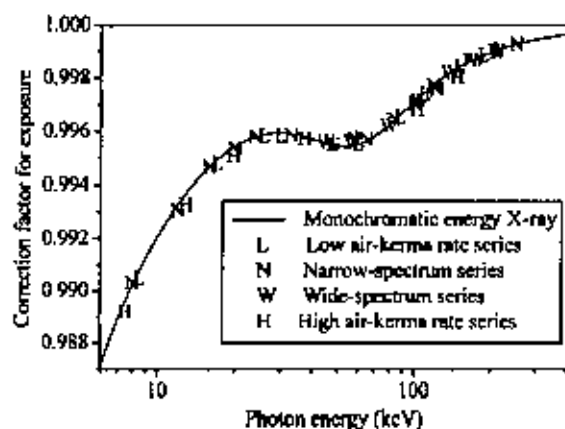

Figure 9. Correction factors for exposure due to the charge of secondary electrons (photoelectrons, Compton electrons and Auger electrons). The letters indicate values for the X-ray spectra presented in ISO 4037-1[6], presented as functions of the mean energy of the spectra
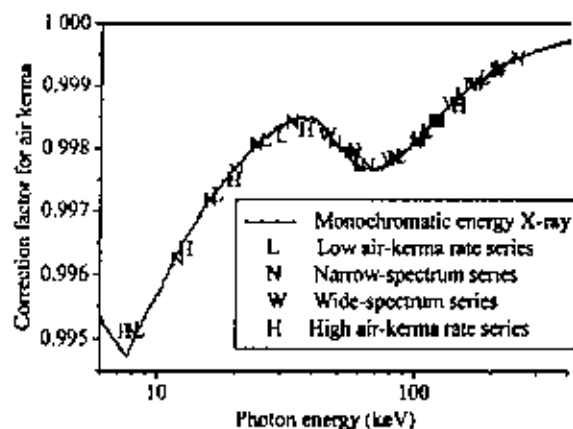

Figure 10 Correction factors for air kerma due to the charge of secondary electrons (photoelectrons, Compton electrons and Auger electrons) and the effects of the increase in W value of air for low energy electrons. The letters indicate values for the X-ray spectra presented in ISO 4037-1[6], presented as functions of the mean energy of the spectra.

electrons from the number obtained for the constant W value.

The solid line in Figure 8 shows the correction factor for air kerma obtained by Equation 3 using a constant W value of 33.97 eV. The value is equal to the total energy of secondary electrons divided by the product of 33.97 eV and the total number of the secondary electrons plus ion pairs obtained for the W value shown in Figure 3. It is also equal to 1 minus the value shown by the line C in Figure 6. The dotted line in Figure 8 shows the correction factor obtained for the average charge state of 2.2+ for N and O atoms with a K shell vacancy.

Figures 9 and 10, respectively, show the correction factors for exposure and air kerma for photons with energies larger than 6 keV. The results are for the average charge state of 2.0+ for N and O atoms with a K shell vacancy. The capital letters in the figures show the values of correction factors for spectra of reference X-rays given in ISO 4037-1; L: low air kerma rate series, N: narrow-spectrum series, W: wide-spectrum series, H: high air kerma rate series[6]. The values are plotted as functions of the mean energies of the spectra.

DISCUSSION AND CONCLUSION

Correction factors for measurement of exposure and air kerma using free air ionisation chambers were obtained. The correction factor for exposure is mainly due to the charge of secondary electrons; the correction factor for air kerma is due to the charge of secondary electrons and the decrease in the number of ion pairs caused by the increase in

the W value of air for low energy electrons. These correction factors should be added as new correction factors in Πk_i of Equations 2 and 3, respectively. Correction factors for both exposure and air kerma have a maximum value near a photon energy of about 30 keV. This is due to the fact that the energy of secondary electrons has a maximum value at a photon energy of 20 keV.

For photon energies lower than 30 keV, the correction factor for exposure decreases monotonically with decreasing photon energy except for a small dip near 3 keV, which is due to K-edge absorption by Ar atoms in air. The value of the correction factor for exposure is smaller than 0.9960 for photons with energies <74 keV. Half the number of X-ray spectra given in ISO 4037-1 have mean energies <74 keV. The value is 0.9892 for the lowest energy spectrum, which has a mean energy of 7.5 keV. The value of the correction factor decreases to 0.9323 at a photon energy of 1 keV, as shown in Figure 7.

The correction factor for air kerma is 0.9951 for the X-ray spectrum with a mean energy of 7.5 keV. The amount of correction for air kerma is smaller than that for exposure. This is because, in the case of air kerma, the signal due to the charge of secondary electrons is partly cancelled by the decrease in the number of ion pairs produced by the secondary electrons per unit energy of the electrons. The decrease occurs due to the increase in the W value of air for lower energy electrons. The correction factor for air kerma begins to increase when the photon energy decreases at 7.7 keV. This is due to the fact that the energies of photoelectrons emitted from N and O atoms become smaller than 7195.4 eV and the W value of air for these electrons becomes larger than the constant value 33.97 eV. The value of the correction factor for air kerma is very sensitive to the difference of the W values for low-energy electrons from the constant value for high-energy electrons.

It is clear from the results above that exposure and air kerma are not rigorously proportional to each other even for low-energy photons, for which the factor $(1 - g)$ in Equation 1 can be assumed to be 1. It can also be deduced that under electronic equilibrium condition the value of air kerma is slightly smaller than that of the absorbed dose of air due to the potential energies of single and multiple charged ions remaining after emission of all secondary electrons.

Büermann et al[15] obtained mass energy-absorption coefficient of air from signal charge of free air ionisation chambers for photons with energies in a range from 3 to 10 keV. In that work, the effective W value for secondary electrons (i.e. photoelectrons and Auger electrons) was used and the signal charge was corrected by subtracting the fraction of a single charge, which corresponds to the charge of

photoelectrons and single charged ions, relative to the charge of ion pairs produced by the secondary electrons. No correction was made, however, for the charge of Auger electrons and multiple charged ions remaining after emission of secondary electrons.

Figures 7 and 8 show that the correction factors for both exposure and air kerma are slightly smaller for the average charge state of 2.2+ than for 2.0+. We found no conclusive data on the average charge states of atoms with an inner shell vacancy. Also, we found no data showing the energy spectra of Auger electrons in connection with the charge state distributions of atoms after de-excitation of inner shell vacancies. The Auger cascade branches assumed in the present work were deduced to give the average charge states shown in Table 2 for each atomic species. In the present work, the energies of all secondary electrons were obtained from the values of the binding energies of electrons in the atoms assuming that the values are the same for any charge state. Differences in electron binding energies between atoms and molecules for N_2 and O_2 were ignored. The effects of dissociation of N_2 and O_2 molecules by ionisation were also ignored.

If exposure is defined such that it includes the charge of secondary electrons, the correction factors shown in Figures 7 and 9 are not needed. On the other hand, the exposure can not be expressed by Equation 4. Moreover, Equation 1, which shows the relation between air kerma and exposure, has to be modified as follows:

$$K_{air} = \frac{X(dQ - dq)(W/e)}{dQ(1 - g)} \tag{7}$$

where $X = dQ/dm$, dq is the sum of the absolute values of the charge of all secondary electrons, including Auger electrons, liberated by photons in air of mass dm, and dQ is the absolute value of the total charge of one sign of ion pairs produced in air by the secondary electrons plus dq. Here, the effect of pair production is neglected. Equation 3 must also be modified as follows:

$$K_{air} = \frac{(Q - q)(W/e)}{m(1 - g)} \Pi k_i \tag{8}$$

where q is the signal charge due to secondary electrons emitted from the air in the ionisation volume of a free air ionisation chamber and the positive ions which are formed by the release of the secondary electrons.

Exposure should be defined clearly and unambiguously to show that it does not include the charge of secondary electrons. If exposure were defined to include these electrons, the relation between exposure and other physical values such as air kerma and mass energy transfer coefficient would become complicated and the physical concept

of exposure would be vague. The effects of the charge of secondary electrons on the measurement of air kerma and exposure have been ignored under the assumption that their contribution to the signal charge from free air ionisation chambers is small.

It is important to make an international agreement on the values of the correction factors for the charge of secondary electrons and for the W value of air for low-energy electrons, to obtain consistent and reliable absolute measurements of exposure and air kerma. The values of the correction factors are universal and are independent on the type and size of free air ionisation chambers used for measurement.

ACKNOWLEDGEMENTS

REFERENCES

1. International Commission on Radiation Units and Measurements. *Fundamental quantities and units for ionizing radiation*. ICRU Report 60 (ICRU, Bethesda, MD) (1998).
2. Burns, D. T. and O'Brien, M. *Comparison of the NIST and BIPM standards for air kerma in medium-energy X-rays*. J Res. NIST **111**, 385–391 (2006).
3. Grimbergen, T. W. M., van Dijk, E. and de Vries, W. *Correction factors for the NMi free-air ionization chamber for medium-energy X-rays calculated with the Monte Carlo method*. Phys. Med. Biol. **43**, 3207–3224 (1998).
4. International Commission on Radiological Units and Measurements. *Report of the International Commission on Radiological Units and Measurements (ICRU) 1959*. NBS Handbook 78 (National Bureau of Standards) (1961)
5. Comité Consultatif pour les Étalons de Mesure des Rayonnements Ionisants. *Report of the Comité Consultatif pour les Étalons de Mesure des Rayonnements Ionisants 11th Meeting–1985*. R p157–158 (1985).
6. International Organization for Standardization (ISO). *X and gamma reference radiations for calibrating dosemeters and dose rate meters and for determining their response as a function of photon energy—Part 1: Radiation characteristics and production methods*. ISO 4037-1 (1996).
7. Chantler, C. T., Olsen, K., Dragoset, R. A., Chang, J., Kishore, A R., Kotochigova, S. A. and Zucker, D. S. *X-Ray form factor, attenuation, and scattering tables, Detailed tabulation of atomic form factors, photoelectric absorption and scattering cross section, and mass attenuation coefficients for Z = 1–92 from E = 1–10 eV to E = 04–1.0 MeV* NIST Physical Reference Data. Available on http://physics.nist.gov/PhysRefData/FFast/Text/cover.html (Last update: August 2005).
8. Berger, M. J., Hubbell, J. H., Seltzer, S. M., Chang, J., Coursey, J. S., Sukumar, R. and Zucker, D. S. *XCOM: Photon cross sections database, NIST Standard Reference Database 8 (XGAM)*. NIST Physical Reference Data. Available on http://www.physics.nist.gov/PhysRefData/Xcom/Text/XCOM.html (Last update: August 2005).
9. Winter, M. *Links to binding energy data data*. WebElements Periodic Table (http://www.webelements.com/webelements/elements/text/periodic-table/bind.html) (Document served: 27 March 2007).
10. El-Shemi, A. M., Ghoneim, A. A. and Lotfy, Y. A. *Multiply charged ions produced after deexcitation processes for important elements in astrophysics* Turk J. Phys. **27**, 51–59 (2003).
11. Carlson, T. A., Hunt, W. E. and Krause, M. O. *Relative abundances of ions formed as the result of inner-shell vacancies in atoms*. Phys. Rev. **151**, 37–78 (1966).
12. Davisson, C. M. *Chapter II Interaction of γ-radiation with matter, in Alpha-, beta- and gamma-ray spectroscopy*. Vol. 1, Siegbahn, K. ed. (Amsterdam: North-Holland Publishing Co, Amsterdam) (1968).
13. Combecher, D. *Measurement of W values of low-energy electrons in several gases*. Radiat Res. **84**, 189–218 (1980).
14. Waibel, E. and Grosswendt, B. *Determination of W values and backscatter coefficients for slow electrons in air*. Radiat. Res. **76** 241–249 (1978).
15. Büermann, L., Grosswendt, B, Kramer, H. M., Selbach, H. J., Gerlach, M., Hoffmann, M. and Krumrey, M. *Measurement of the X-ray mass energy-absorption coefficient of air using 3 keV to 10 keV synchrotron radiation*. Phys. Med. Biol. **51**, 5125–5150 (2006).